BOLT BERANEK AND NEWMAN INC

CONSULTING • DEVELOPMENT • RESEARCH

Report No. 2484

A MANUAL CONTROL THEORY ANALYSIS OF VERTICAL SITUATION DISPLAYS FOR STOL AIRCRAFT

Final Report

Contract No. NAS2-6652

Sheldon Baron

William H. Levison

April 1973

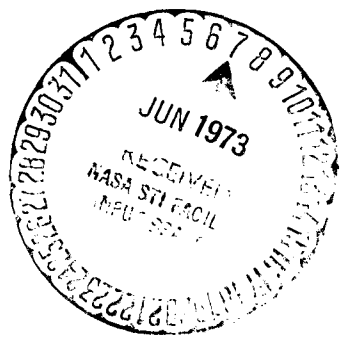

Submitted to:

National Aeronautics and Space Administration
Ames Research Center
Moffett Field, California 94035

Attention: Mr. Everett Palmer

A MANUAL CONTROL THEORY ANALYSIS OF VERTICAL SITUATION DISPLAYS FOR STOL AIRCRAFT

Sheldon Baron
William H. Levison

Final Report

Contract No. NAS2-6652

April 1973

Submitted to:

National Aeronautics and Space Administration
Ames Research Center
Moffett Field, California 94035

Attention: Mr. Everett Palmer

TABLE OF CONTENTS

LIST OF ILLUSTRATIONS

LIST OF ILLUSTRATIONS
(Continued)

LIST OF TABLES

LIST OF TABLES
(Continued)

LIST OF SYMBOLS

a	**threshold value; wind shear gradient m/s/s.**
$\underline{A}$, $\underline{B}$, $\underline{C}$, $\underline{D}$, $\underline{E}$	general "system" matrices.
d	displacement normal to glideslope in vertical plane containing glide slope, m.
f_i	fraction of attention devoted to i^{th} display.
FD_N	flight director signal, nozzle.
FD_s	flight director signal, stick.
g	gravitational constant, m/sec^2.
$\underline{G}$	control-rate cost functional weighting matrix.
h	altitude-deviation from glide-path, m.
h_N	height of glide slope, m.
$\|H\|$	magnitude of internal describing function, dB.
$<H$	phase of internal describing function, deg.
J	cost functional.
$K_{(\cdot)}$	flight director gain on (•).
$K(\sigma, a)$	describing function gain for threshold.
$\underline{K}$	solution to matrix Ricatti equation.
$\underline{L}^*$	optimal feedback gain matrix.
L_u	longitudinal turbulence scale length, m.
L_v	lateral turbulence scale length, m.
L_w	vertical turbulence scale length, m.
$p(\cdot)$	probability density.

P_c	maximum observation noise/signal ratio for achieving criterion level performance, dB.
P_i	observation noise/signal ratio for i^{th} display variable, dB.
P_m	motor noise/signal ratio, dB.
P_o	nominal observation noise/signal ratio for full attention, dB.
q	pitch rate, deg/sec.
$\underline{Q}$	output cost functional weighting matrix.
R	range, m.
$\underline{R}$	control cost functional weighting matrix.
t	time, sec.
$T_{(\cdot)}$	time constant, sec.
$\underline{T}_N$	"neuromotor-lag" matrix, sec.
u	ground speed perturbation, m/sec.
u_a	longitudinal component of perturbed airspeed, zero-wind, m/s.
u_g	longitudinal gust velocity, m/s.
u_i	airspeed error, m/s.
u_{mw}	longitudinal component of mean wind, m/s.
$\underline{u}$	general system control vector
$\underline{u}_c$	"commanded" control vector
U_o	nominal airspeed, m/s.
U_{mw}	a long-track component of mean-wind, m/s.
v_g	lateral gust velocity, m/s.
v_{mw}	mean crosswind, m/s.

$\underline{v}_m$	motor-noise vector.
$\underline{v}_y$	observation noise vector.
V	aircraft ground speed, m/s.
V_w	wind speed, m/s.
$\underline{V}$	observation noise covariance matrix.
w	vertical velocity perturbation, m/s.
w_a	vertical component of perturbed airspeed, zero wind, m/s.
w_g	vertical gust velocity, m/s.
w_{mw}	vertical component of mean wind, m/s.
$\underline{w}$	general system driving noise vector.
WI	workload index.
$\underline{W}$	driving noise covariance matrix.
$\underline{x}$	general system-state vector.
$\hat{\underline{x}}$	"estimate" of state vector.
y	lateral deviation from localizer, m.
$\underline{y}$	general system output vector.
$\underline{z}$	general system "disturbance-state" vector.
Γ_o	nominal glide slope angle, deg.
δ_e	elevator deflection, deg.
δ_N	nozzle deflection, deg.
δ_w	wheel deflection, deg.
θ	perturbed pitch angle, deg.
$\sigma_{(\cdot)}$	standard deviation of $(\cdot)$.

$\underline{\Sigma}$	error covariance matrix.
τ	human's time delay, sec.
ϕ	perturbed roll angle, deg.
ψ	perturbed heading angle, deg.
$(\bar{\cdot})$	mean of $(\cdot)$.
$\dot{(\cdot)}$	time-derivative of $(\cdot)$.

ABSTRACT

Pilot-vehicle-display systems theory is applied to the analysis of proposed vertical situation displays for manual control in approach-to-landing of a STOL aircraft. The effects of display variables on pilot workload and on total closed-loop system performance was calculated using an optimal-control model for the human operator.

The steep (7.5 deg) approach of an augmentor wing jet STOL aircraft was analyzed. Both random turbulence and mean-wind shears were considered. Linearized perturbation equations were used to describe longitudinal and lateral dynamics of the aircraft. The basic display configuration was one that abstracted the essential status information (including glide-slope and localizer errors) of an EADI display. Proposed flight director displays for both longitudinal and lateral control were also investigated.

It was found that with the basic EADI-status displays Category II window specifications would be exceeded more than 5% of the time unless unacceptable (or unachievable) levels of pilot workload were demanded. The proposed interim flight directors improved both performance and workload; they reduced the failure probability by about a factor of two or allowed a fixed success probability to be achieved with much less attentional demand. However, further improvements in performance via display design appeared unlikely, though greater reductions in workload may be possible.

A preliminary approach to designing display command information using the optimal-control model was also investigated. The procedure yielded a director law that resulted in substantially reduced workload.

INTRODUCTION

One of the design goals for an aircraft instrument panel is to minimize display workload. That is, acceptable system performance should be achieved with a minimum of the pilot's attention required by the flight displays so that the pilot may attend safely to the problems of vehicle management other than continuous control. Sophisticated displays such as flight directors and pictorial displays are sometimes included in the instrument panel to minimize workload, especially in approach and landing. Recent developments in pilot-vehicle-display systems theory [1-6] indicate the feasibility of determining analytically the relative workload associated with various displays for approach and landing. In particular, it is possible to assess the reduction in pilot workload that might be provided by flight-directors and other forms of display augmentation. These same techniques can also be used to predict closed-loop measures for evaluating overall system performance with the various displays.

The purpose of this program was to apply the pilot-vehicle-display systems theory developed in [1-6] to the analysis of proposed vertical situation displays for manual control and monitoring in approach-to-landing of a STOL aircraft. The effects of display variables on pilot workload and on total closed-loop system performance was to be calculated using the aforementioned techniques.

The steep (7.5 deg) approach of an Augmentor Wing Jet STOL Research Aircraft (AWJSRA) was analyzed. Both random turbulence and wind shears were considered. Linearized perturbation equations were used to describe longitudinal and lateral dynamics of the

aircraft. The basic display configuration was one that abstracted the essential status information (including glide-slope and localizer errors) of the STOLAND-EADI display [7] (hereafter, referred to as EADI-status or, simply, status display). Proposed flight director displays for both longitudinal and lateral control were also investigated. Allocation of pilot attention, performance at the approach-window and pilot-workload were all investigated.

In the course of this effort some modifications and extensions of the pilot-vehicle-display system model of [1-6] and of the corresponding computer programs were implemented. Multi-control problems were considered for the first time; the wind-shears that were analyzed were more general than those previously investigated [6]; and the programs were made more amenable to the investigation of time-varying situations and to workload analysis.

A concise summary of the main results of the analysis, with references to supporting data, is presented in the concluding chapter of this report. It is strongly recommended that the reader with insufficient time to go through the details of the analysis initially should refer to the conclusion directly. For convenience, the main conclusions are highlighted below.

1. The EADI-status displays are inadequate for the approach task in that the Category II window specifications are exceeded more than 5% of the time unless unacceptable (or unachievable) levels of pilot workload are demanded.

2. The proposed interim-flight directors improve both performance and workload. On the average, the flight-directors reduce the probability of a missed approach by a factor of two or, as a corollary, for a fixed probability of success the workload with the directors is less than half that without them.

3. Further improvements in performance via display design are likely to be small (using the measurements currently available), but greater reductions in workload may be possible.

4. Non-zero mean winds, with shear-variation, degrade performance by producing mean errors and by increasing response variability.

The organization of the report is as follows. The analysis procedures are reviewed in Section 2. The basic EADI-status configuration is analyzed in Section 3. In Section 4, proposed flight director laws are investigated. Section 5 contains a discussion and analysis of an approach to design of flight director laws that is based to the procedures used in this study. Only the longitudinal director is considered there. In Sections 3-5, the analysis is restricted to "steady-state" gust regulation at the decision-height; the response to wind shears is analyzed in Section 6. Concluding remarks are presented in Section 7 and pertinent mathematical details are included in three Appendices.

ANALYSIS METHODS

The procedures used in this study to analyze vertical situation displays for STOL approach have been developed, for the most part, over the past several years. The techniques and the basis for them (the optimal-control model for pilot-vehicle-display systems analysis) are described in detail in References 1-6. Here, we summarize the important features of the system model. Procedures for determining closed-loop system performance and indicators of pilot-workload are also outlined.

The pilot-vehicle-display system is illustrated in Figure 1. The model includes representations of vehicle dynamics, environmental disturbances, the display system and a model for the pilot. The model for the pilot is the so-called "optimal-control model" [1-6].

System Model

Dynamics

System dynamics are approximated by the following linear state equation:

$$\dot{\underline{x}}(t) = \underline{A}\,\underline{x}(t) + \underline{B}\,\underline{u}(t) + \underline{E}\cdot\underline{w}(t) \qquad (1)$$

with initial condition

$$E\{\underline{x}(t_o)\} = \bar{\underline{x}}_o \quad ; \quad E\{(\underline{x}(t_o) - \bar{\underline{x}}_o)(\underline{x}(t_o) - \bar{\underline{x}}_o)'\} = \underline{X}_o \qquad (2)$$

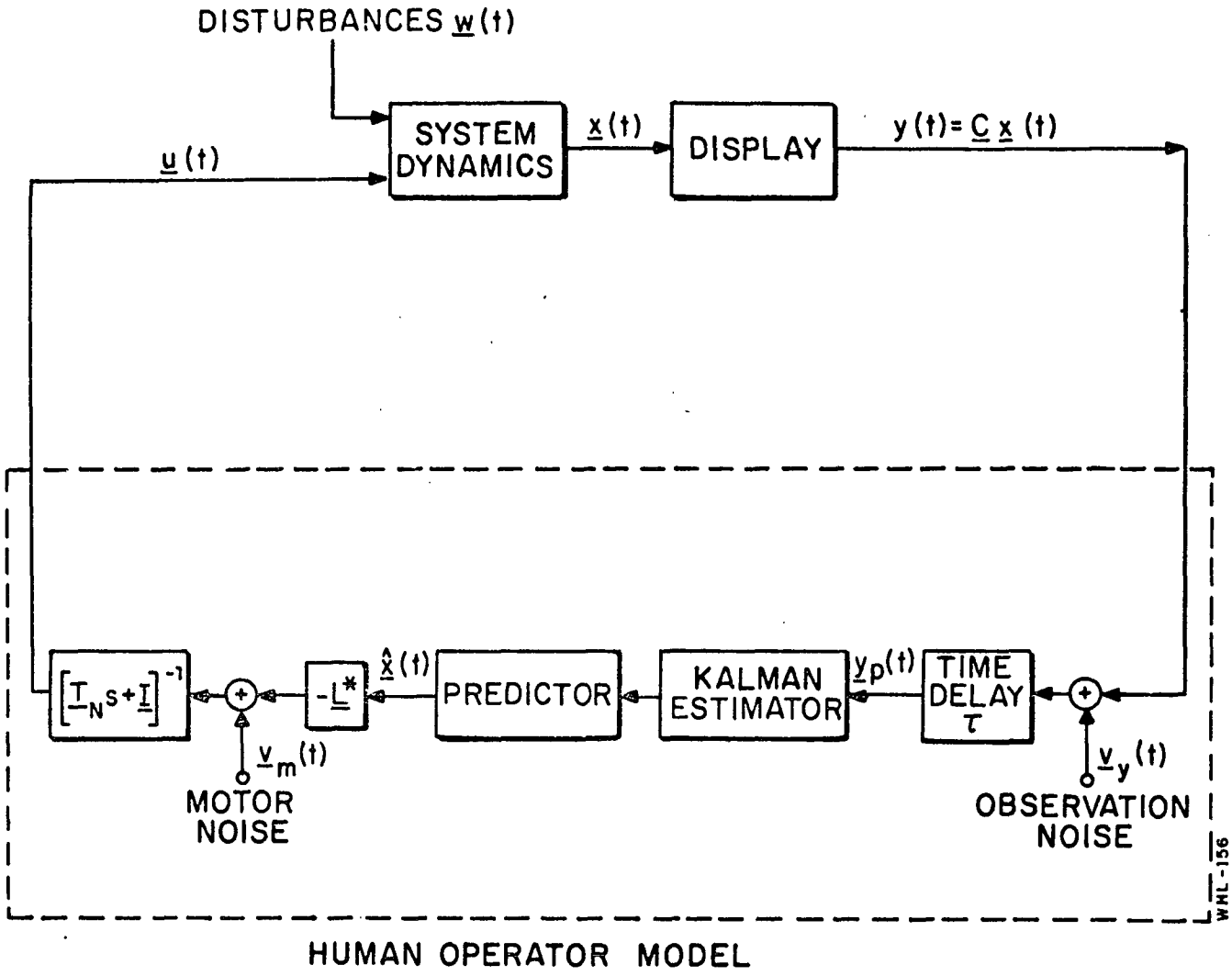

FIGURE 1. Structure of Pilot-Vehicle-Display System Model

where $\underline{x}(t)$ is the vector of system states, $\underline{u}(t)$ is the vector of the pilot's control inputs, and $\underline{w}(t)$ is a vector of linearly independent white noise disturbances. The system dynamics include vehicle dynamics, any "dynamic" filtering associated with the generation of input disturbances (see below) and, if necessary, sensor, actuator or display dynamics. In this study, the matrices A, B and E are constant, and correspond to a steep-approach flight condition. The constancy of $\underline{A}$, $\underline{B}$ and $\underline{E}$ is not a necessary requirement of the procedure. Piece-wise-constant matrices are allowed and may be used to explore some time-varying situations; however, this increases computational costs significantly and makes the interpretation of results more difficult.

Environmental Disturbances

If external forcing functions are rational noise spectra of first order or higher, as is the case for most turbulence models, they are represented by white noise ($\underline{w}$) passed through a linear filter. Then, "input states" are augmented to the system state and the filter dynamics form part of the $\underline{A}$ matrix.

Disturbances such as constant winds or wind-shears are modeled, essentially, by adding non-zero mean components to $\underline{w}$; any dynamics associated with these disturbances are accounted for in the manner described above. For this situation, the model for the human operator must be modified so as to account for time-varying adaptation to such disturbances. These modifications are discussed in Appendix A. The equations needed for the computation of the response of the overall system to a particular "sample" mean-disturbance are developed in Appendix B.

Display Variables

The display-variables are assumed to be linear combinations of the state and control variables and are given by the "display vector":

$$\underline{y}(t) = \underline{C}\ \underline{x}(t) + \underline{D}\ \underline{u}(t) \qquad (3)$$

The matrices C and D may be time-varying (piece-wise constant) to account for changes in the quantities being displayed or "observed". For example, in the STOLAND-EADI display [7] angular glide path deviations are presented in the early part of the approach, whereas linear glidepath deviations are presented as the runway threshold is neared.

As noted above, display dynamics are included in the $\underline{A}$ matrix. For the present study the only "display dynamics" considered were those associated with generating the "flight director" laws investigated in Chapters 4-6.

Task Requirements

Task requirements are stated in terms of "cost weightings" associated with various system variables in a quadratic cost functional of the form

$$J(\underline{u}) = E\ \{\underline{y}'\ \underline{Q}\ \underline{y} + \underline{u}'\ \underline{R}\ \underline{u} + \dot{\underline{u}}'\ \underline{G}\ \dot{\underline{u}}\} \qquad (4)$$

It is assumed that the pilot selects his control response to minimize the appropriate J.

The selection of cost functional weightings may, in general, be based on objective or subjective factors. For relatively simple, single-variable control situations, good approximations to experimental measurements have been obtained with a cost functional consisting simply of a weighted sum of system error variance plus control-rate variance [2]. The cost on control-rate represents, in part, a subjective penalty imposed by the controller on making rapid control motions. In addition, this term may account indirectly for physiological limitations on the pilot's bandwidth.

For complex multi-input, multi-output tasks, the cost weightings can not be chosen in so simple a fashion. There are several ways one can proceed. Values for the weightings can be selected to keep mean-squared output levels within prescribed tolerances; they can be assigned via pilot questionnaire; they can be chosen by trade-off analysis; finally, they may be assigned such that the resulting optimal closed-loop system has certain "desirable" properties.

For the analysis performed in this study, weighting coefficients were selected on the basis of maximum allowable deviations (or limits) for the various problem variables [8]. A unit amount of cost was associated with a given variable when the magnitude of the "error" (i.e., deviation from trim) was equal to the nominal limit. Thus, the weighting coefficient for each variable was computed simply as the inverse of the square of the corresponding limit. Values for the limits were determined partly from Category II window specifications, partly from physical limitations and partly from a knowledge of human preference and capabilities. This method for choosing cost-weightings represents a departure

from our previous approach (e.g., see [6]). We believe that it has the advantage of being relatively straightforward to apply. A possible disadvantage is that it may involve selection of more weightings than are actually necessary to give a reliable prediction of performance. Finally, it is worth noting that it is possible to allow the weightings to vary with range to represent the pilot's tendency or desire to "tighten" his control as touchdown is approached (see Chapter 6).

Pilot Model

For purposes of this discussion it is convenient to consider the model for the pilot as being comprised of three parts:

(i) An "equivalent" perceptual model that translates displayed variables $\underline{y}$ into delayed, "noisy" perceived variables $\underline{y}_p$ via the relation

$$\underline{y}_p(t) = \underline{y}(t-\tau) + \underline{v}_y(t-\tau) \qquad (5)$$

where τ is an "equivalent" perceptual delay and $\underline{v}_y$ is an "equivalent" observation noise vector.*

(ii) An estimation and control-command generation process that consists essentially of a Kalman filter, a least mean-squared predictor and a set of "optimal gains". This models human information processing and compensation behavior.

*The use of the word equivalent in this context is to emphasize that the parameters may be lumped representations of a variety of limitations that can not be "identified" separately by existing measurement techniques.

(iii) An equivalent "motor" or output model that accounts for possible "bandwidth" limitations of the human and his inability to generate perfect control responses, by transforming "commanded" controls, $\underline{u}_c$, into control inputs via the transformation

$$\underline{T}_N \dot{\underline{u}} + \underline{u} = \underline{u}_c + \underline{v}_m \qquad (6)$$

where $\underline{T}_N$ is an "equivalent" "Neuro-motor" lag-matrix and $\underline{v}_m$ is an "equivalent" motor-noise vector.

The optimal predictor, optimal estimator, and optimal gain matrix represent the set of "adjustments" or "adaptations" by which the pilot tries to optimize his behavior. The general expressions for these model elements are determined by well-defined mathematical rules that are described in Reference 2.

The time-delay, observation-noise, motor-noise, and, in some cases, the elements of the T_N matrix represent inherent human limitations, and those of the human/system interface, that tend to constrain the range of the pilot's behavior. These limitations are discussed below in more detail.

(a) *Time Delay.* The various internal time delays associated with visual, central processing and neuro-motor pathways are combined and conveniently represented by a lumped equivalent perceptual time delay τ. Typical values for this delay are 0.2 $\pm$ .05 sec. [5].

(b) *Neuro-Motor Dynamics.* We do not include "neuro-motor" dynamics directly among the inherent limitations of the human. The $\underline{T}_N$ matrix of Equation (6) limits the "bandwith" of the pilot's control inputs. This matrix is a direct consequence of the weightings on control-rate terms in Equation (4); if $\underline{G} \equiv 0$, $\underline{T}_N \equiv 0$. For single-control problems, simple, wide-band control dynamics and highly-responsive force-manipulators we have found that selecting g to yield a τ_N of approximately .1 sec. results in excellent agreement with measured data [2].

In more complex situations involving higher-order dynamics (with lower bandwidths) and less responsive manipulators, one might expect higher values of τ_N; in a sense, the system bandwidth limitations are dominating those of the pilot. In such cases, it seems reasonable to select control-rate weightings on the same basis as the other weightings, i.e., by considering allowable limits for control-rates. This was the approach we took here. As a matter of some interest, we checked the resulting control time constants in each case* and the values obtained are presented with the results; they lie in the range of .14 - .25 seconds, which is well within the range of values reported in the literature for neuro-motor time constants [9, 10].

*In a multi-control case, where the variables being controlled are coupled (as in the longitudinal control problem in Section 3), the interpretation of control time constants is more complicated. The τ_N for a given control axis could be the corresponding diagonal element of the $\underline{T}_N$-matrix, or it could be an eigenvalue of $\underline{T}_N$.

In the cases examined thus far, the eigenvalues did not differ significantly from the diagonal elements of $\underline{T}_N$. In the sequel, the value given for τ_N is the diagonal element of $\underline{T}_N$ corresponding to the specified control.

(c) *Pilot Randomness (Remnant).* We assume that the various sources of inherent human randomness are manifested as errors in observing displayed outputs and in executing intended control movements. Thus, observation noise, $\underline{v}_y$, and motor noise, $\underline{v}_m$, are our lumped representation of "remnant". These noises represent the combined effects of random perturbations in human response characteristics, time variations in response parameters, and random errors in observing displayed outputs and in generating control inputs.

When the displays and controls have been optimally designed as is the case in many laboratory situations, we would expect central-processing sources of pilot randomness to dominate. In other situations, involving more realistic displays and controls, display- or motor-related sources might be of greatest importance. All sources of remnant, however, affect the mathematical descriptions of the pilot-vehicle system in substantially the same way; thus, our measurements do not allow us to distinguish among these various noise processes. We find it convenient to reflect remnant largely to an equivalent observation process. Even in cases where the motor-noise process is needed to provide a good match to pilot behavior (at low frequencies), most of the measured remnant is accounted for by the equivalent observation noise.

For manual control situations in which the displayed signal is large enough to negate the effects of visual resolution ("threshold") limitations, the autocovariance of each observation noise component appears to vary proportionally with mean-

squared signal level. In this situation, the autocovariance may be represented as

$$V_{y_i}(t) = \pi P_i \cdot E\{y_i^2(t)\}$$

$$= \pi P_i \sigma_{y_i}^2(t) \qquad (7)$$

where P is the "noise/signal ratio" and has units of normalized power per rad/sec. Numerical values for P_i of 0.01 (i.e., -20 dB) have been found to be typical of single-variable control situations [3, 5].

As noted earlier, a motor noise term is added to the pilot's commanded control signal to represent random errors in executing the intended control movements and, in addition, to account for the fact that the pilot may not have perfect knowledge of his own control activity. The motor noise is assumed to be a white noise, with autocovariance that scales with the control variance, i.e.,

$$V_{m_i}(t) = \pi P_{m_i} \sigma_{u_i}^2(t) \qquad (8)$$

We have found, typically, that a value for P_m of .003 (i.e., a "motor noise ratio" of -25 dB) yields good agreement with experimental results [2]. Throughout this study the motor-noise ratio was set to approximately -25 dB.

(d) *Attention Sharing.* Because the numerical value associated with the pilot's noise/signal ratio [P] has been found to be relatively invariant with respect to system dynamics and display characteristics, we associate this parameter with limitations in the pilot's information-processing capability. This forms the basis for a model for pilot attention in which the amount of attention paid to a particular display is reflected in the noise/signal ratio associated with information obtained from that display [4]. Specifically, the effects of attention-sharing are represented as

$$P_i = \frac{P_o}{f_i} \tag{9}$$

where P_i is the noise/signal ratio associated with the i^{th} display when attention is shared among two or more displays, f_i is the fraction of attention allocated to the i^{th} display, and P_o is the noise/signal ratio associated with full attention to the display. For example, if "full attention" is represented by a noise/signal ratio of -20 dB, and if attention is equally divided between altitude-related and pitch-related information, then the noise/signal ratios associated with altitude- and pitch-related variables would be -17 dB.

(e) *Display-Related Limitations.* The perceptual model for ideal display conditions is given by Equation (5), with the covariance of the observation noise defined by Equation (7). In more general situations where display characteristics are not ideal it is necessary to alter this model. In essence, our approach is to retain Equation (5), and modify the expression for the observation noise covariance associated with a particular display variable.

In this study, two display limitations were important under certain circumstances, namely threshold limitations and the lack of a null-point indication. We account for these phenomena by letting the autocovariance for each observation noise process be

$$V_i(t) = P_i \left(\frac{\sigma_i^2}{K_i^2 (\sigma_i, a_i)} \right) + V_{i_o} \qquad (10)$$

where the subscript i refers to the i^{th} display-variable. The quantity $K(\sigma_i, a_i)$ in Equation (10) is the describing function gain associated with a threshold device

$$K(\sigma, a) = \frac{2}{\sqrt{\pi}} \int_{-\infty}^{-\frac{a}{\sigma\sqrt{2}}} e^{-x^2} dx$$

where "a" is the threshold and σ is the standard deviation of the "input" to the threshold device.* This factor is used primarily to account for threshold-type phenomena associated with viewing the display, but "indifference" thresholds will have an indistinguishable effect. Essentially, its effect is to cause the observation noise covariance to become greater as the signal becomes smaller relative to the threshold. It is worthwhile to note that we could have introduced the threshold as a "gain" on the display variable y_i, i.e., in the control loop directly. (See [6]). This is so because the optimal estimator then compensates for the gain and, in the process, scales the observation noise. Thus, it is primarily a matter of convenience as to whether one chooses to model threshold-related effects by additional elements in the control loop or by simple readjustment of observation noise parameters.

*For non-zero mean signals this expression must be modified (see [6]).

The term V_{i_o} in (10) is a residual-noise covariance and may be written as

$$V_{i_o} = P_i \sigma^2_{i_o}$$

The residual noise term will, in many cases, be similar in effect to a threshold. However, it can be viewed as a separate parameter and used to account for observed degradation in tracking performance that results from lack of reference indicators [4, 7].

Consider the situation in which the pilot is to maintain the display indicator at some desired distance from a given reference point. The basic model for perceptual variability assumes that such variability is proportional to the quantity being estimated. Representing the mean-square as the variance plus the square of the mean, we obtain*

$$V_y = (\sigma^2_y + \bar{y}^2) P_y$$

where the mean signal value $\bar{y}$ is simply the desired distance of the signal from the displayed reference point. If we treat the quantity $\bar{y}$ as an equivalent rms "residual noise" (i.e., let $\sigma_o = \bar{y}$), this expression reduces to the model for observation noise given earlier (with zero threshold).

*In most tracking studies $\bar{y} = 0$ and we have the observation noise proportional to the variance of the signal.

Theoretical prediction of the effective residual noise level is somewhat more complex for the situation in which an indicator is to be positioned between two reference marks. A reasonably good approximation, however, is to let σ_o be equal to the distance from the target point to the nearest reference.

Model Outputs

Once the system dynamics, displays, task requirements, and pilot limitations are specified it is possible to obtain a variety of measures of performance of both the pilot and the closed-loop system. These measures are obtained by solving the relevant optimization problems (to obtain the pilot model [2, 4, 5]) and by applying appropriate system analysis procedures to the results.

The following measures of performance are obtained directly from the model or may be derived from model results:

(a) *Mean System Response.* The mean time history of any system variable can be predicted. This is the average waveform that would be computed if the results of a large number of successive runs were averaged together at each point in space (time). This ensemble average is predicted during a *single run,* however; it is not necessary to exercise the model repetitively.

(b) *RMS System Response.* The rms variability about the mean response can be predicted for any system variable at each point in space. Variability arises from random inputs to the system such as wind turbulence and from the variability inherent in the pilot's response behavior (i.e., "pilot remnant").

(c) *Frequency-Domain Measures.* Representative steady-state control situations can be analyzed to yield predictions of pilot describing functions, "open-loop" describing functions, and power spectral density curves for the various system variables. In addition, spectra for pilot remnant can be obtained.

(d) *Estimation Performance.* The mean and variance of the estimate of the state of the system and of the error in that estimate (see Figure 1). These quantities are useful in analyzing the decision-making role of the pilot [12]. They are also useful for assessing monitoring performance with given display configurations.

(e) *Allocation of Attention and Workload.* The model for attention sharing may be used to predict the effects of task interference and to analyze workload requirements [4].* To predict what happens on a specific task when only partial attention may be paid to it, Equation (9) is used to establish the appropriate observation noise-signal ratio and the model equations are solved for this value. If the pilot's allocation of attention is unknown beforehand, model solutions may be used to determine the optimum allocation of attention, which, in line with the fundamental optimality hypothesis, may be taken as a prediction of the pilot's allocation.

The model of task interference lends itself straightforwardly to the prediction of the amount of "workload" associated with a given task. We define the "workload index" (WI)

*This approach may also be used as an approximate indication of the effects of visual scanning (see, e.g., [13]).

as the fraction of the controller's capacity that is required to perform a given task to some specified, or criterion, level of performance.

$$\text{Workload Index} = WI = P_o/P_c \qquad (11)$$

where P_c is the maximum noise/signal ratio that can be tolerated while performance is maintained within the criterion level. This metric can be predicted quantitatively with the existing implementation of the optimal-control model. The procedure is identical to that for predicting task interference: once the model is "calibrated" for single-axis behavior (either by doing a simple experiment or by using nominal values of parameters that have been found to match previous data), a curve of performance score versus observation noise ratio is obtained. By relating the observation noise ratio to fraction of capacity, a quantitative value of workload may be determined.

(f) *"Window" Performance.* Because the system is assumed to be linear and the disturbances Gaussian, all system variables are Gaussian. Consequently, the computation of the mean and covariance of all system variables provide sufficient information for determining the joint probability density functions of these variables. It is therefore possible to predict the probability that a variable will exceed a given value at a given time. In particular, the probability of a "missed approach" can be computed by establishing appropriate "approach windows" [14]. A single "run" of the optimal control model provides the probability of a missed approach for a given disturbance. It is also possible to obtain the probability of a missed approach "averaged" over all possible wind conditions. The procedure is described in Chapter 3.

STEADY-STATE ANALYSIS OF STOL APPROACH

In this chapter we analyze approach performance of a STOL aircraft using a display similar to the STOLAND EADI [7]. Steady-state analysis of performance at the decision height (approximately 230m from touchdown) is the basic tool employed. Both longitudinal and lateral control are examined. Attentional allocation, window performance and pilot workload are all analyzed. Potential improvements of the display configuration are also explored.

Vehicle Dynamics

The vehicle considered is the Augmentor Wing Jet STOL Research Aircraft (AWJSRA). The aircraft is assumed to be on the (7.5 deg) glide-slope at the decision height (30m), with a nominal airspeed of approximately 31m/s (60 knots).

Linearized perturbation equations for longitudinal and lateral-directional dynamics were used throughout. For longitudinal control unaugmented aircraft dynamics were considered. The pilot was assumed to control the elevator and "nozzle" (thrust vector) in a continuous manner, whereas the throttle was assumed to remain fixed at its trim setting. In the lateral case we considered augmented (SAS-on) dynamics. For this condition, we assumed that all turns were coordinated (i.e., zero sideslip). Longitudinal and lateral dynamics are presented in appropriate state-variable form in Appendix C.

Display-Related Parameters

An abstraction of the relevant EADI display of status information is shown in Figure 2. This display provides the pilot with glide path and localizer errors as well as attitude information. From such a display the pilot can also obtain the rates of change of these variables. Although we have not shown an airspeed error indicator in Figure 2, the pilot is displayed this quantity and we will assume that airspeed error is available in our analysis.

Effective visual thresholds were computed for the aircraft at the 30-meter decision height. On the basis of previous analysis of approach performance [6], an "indifference threshold" of 0.1 degrees visual arc was associated with perception of height error. Previous analysis of pilot remnant data [5] suggested thresholds of 0.05 degrees visual arc for other indicator displacements and 0.18 arc-degrees/second for indicator-rate quantities. Display gains given in [7] were used to convert thresholds into units related to system quantities.

Non-zero rms residual noise terms were associated with height and sink-rate information. Since the status display shows the height window of +3.7 meters, a residual noise on height perception was needed to account for the lack of an explicit zero reference. To approximate the effects of the non-zero reference, we simply set the value of the residual noise equal to the amount of the reference offset (i.e., 3.7 meters). The residual noise on sink-rate information was included to account, in a rough way, for the resolution limitations of the SBILS (Scanning Beam Instrument Landing System). As we show later, the latter noise term had no appreciable effect on predicted performance.

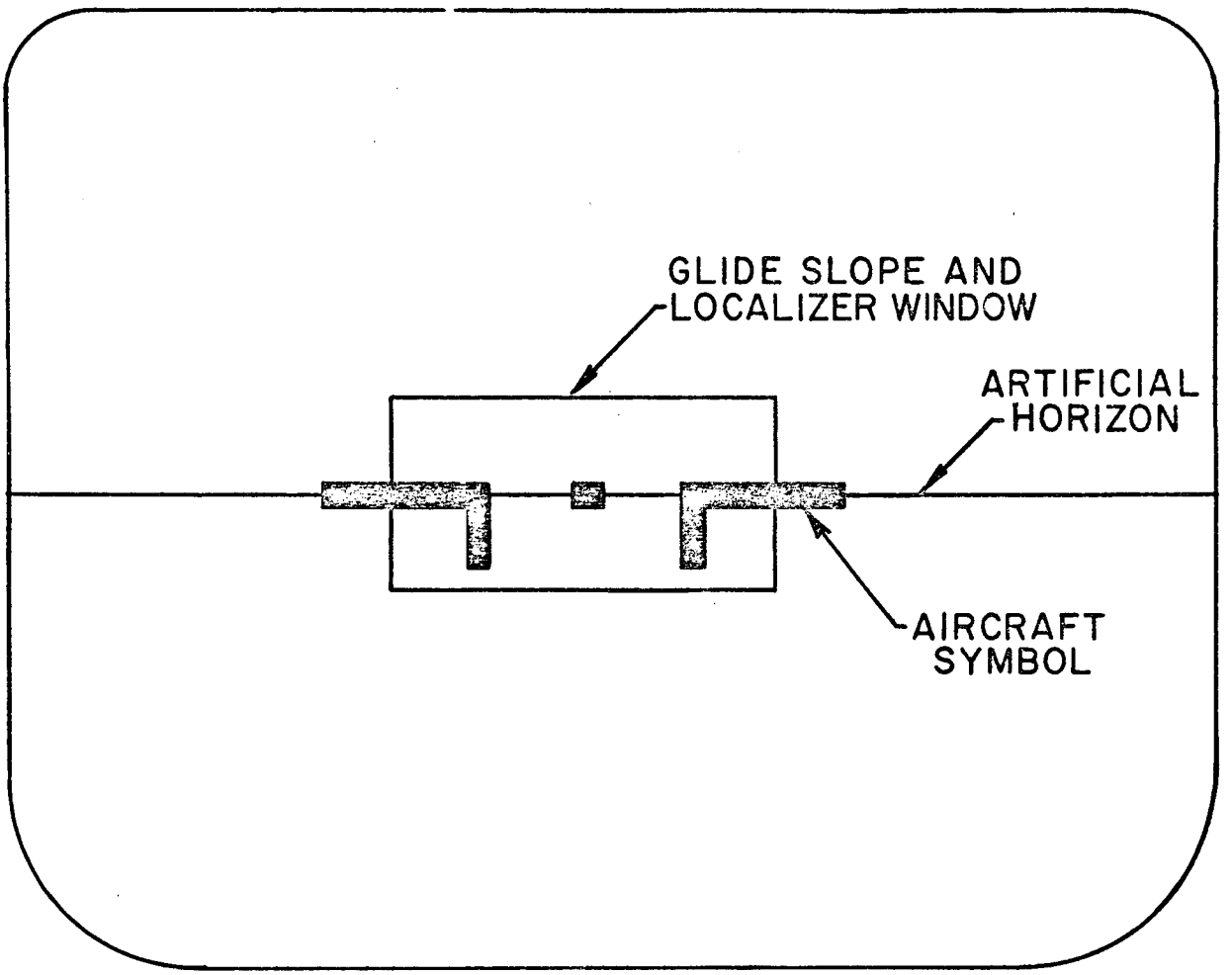

FIGURE 2. Display of Status Information

A non-zero rms residual noise term was also associated with lateral offset error. This was set to a value of 5.4 meters, corresponding to the lateral dimensions of the "window".

Thresholds and residual noises for all displayed variables are summarized in Table 1.

Disturbances

Zero-mean, random gusts provided the disturbances for this analysis. These were generated by passing white-noise through first-order filters, such that the gust spectra approximated those of Reference 16, for the 30m altitude. Specifically, the three components of turbulence (u_g, v_g, w_g) were generated by*

$$\dot{u}_g + \frac{V}{L_u} u_g = \sigma_u \sqrt{\frac{2}{\pi} \frac{V}{L_u}} \tag{12a}$$

$$\dot{v}_g + \frac{V}{L_v} v_g = \sigma_v \sqrt{\frac{2}{\pi} \frac{V}{L_v}} \tag{12b}$$

$$\dot{w}_g + \frac{V}{L_w} w_g = \sigma_w \sqrt{\frac{2}{\pi} \frac{V}{L_w}} \tag{12c}$$

where

$$L_u = L_v = 205\text{m} \; ; \; L_w = 30.5\text{m} \tag{12d}$$

$$\sigma_u = \sigma_v = \sqrt{\frac{L_u}{L_w}} \sigma_w \tag{12e}$$

*Effective angular rates due to gusts (p_g, q_g, r_g) were neglected.

Table 1

DISPLAY-RELATED PARAMETERS

Variable	Threshold	RMS Residual Noise
h (m)	0.48	3.7
$\dot{h}$ (m/s)	0.85	1.1
θ (deg)	0.22	0.0
q (deg/s)	0.78	0.0
u_i (m/s)	0.14	0.0
y (m)	.28	5.4
$\dot{y}$ (m/s)	.52	0
ϕ^* (deg)	0	0
$\dot{\phi}^*$ (deg/s)	0	0

*Studies of longitudinal control showed that the thresholds on attitude could be ignored, so in the subsequent analysis of lateral performance the thresholds associated with viewing the bank angle indicator were set to zero.

and V ≈ 31 m/s is the aircraft velocity. The longitudinal gust spectrum corresponding to (12a) is identical to that in [16], whereas the vertical and lateral gusts spectra are approximations to those of [16].

Gust intensities were assumed to be distributed according to a Rayleigh distribution [16]. For most of the analyses, gust intensities were either

$$\sigma_{u_g} = 2.1 \text{ m/s}, \quad \sigma_{w_g} = .82 \text{ m/s}, \quad \sigma_{v_g} = 2.1 \text{ m/s} \tag{13a}$$

or

$$\sigma_{u_g} = .8 \text{ m/s}, \quad \sigma_{w_g} = .31 \text{ m/s}, \quad \sigma_{v_g} = .8 \text{ m/s} \tag{13b}$$

According to [16], the probability of encountering gust amplitudes of the magnitude of (13a), given that any turbulence is encountered, is about 1%, whereas the magnitudes of the level of (13b) have about a 50% probability of being encountered. Thus, (13a) corresponds to a "worst-case" disturbance and (13b) to a "median" disturbance.

Task Requirements

As noted in Chapter 2, task requirements are stated in terms of cost weightings corresponding to "allowable" limits of variables. The "limits" and weightings corresponding to the longitudinal and lateral control tasks are given in Tables 2A and 2B, respectively. Height, airspeed and lateral deviation limits were based on Category II "window" specifications, control and control-rates were determined largely from physical considerations, and the remaining weightings were based on human preferences. Also

Table 2

LIMITS AND COST FUNCTIONAL WEIGHTINGS

A. Longitudinal

Variable	"Limit"	Weighting	τ_N
h	3.7 (m)	0.073	
$\dot{h}$	1.1 (m/s)	0.83	
θ	6.0 (deg)	0.028	
q	---	0.0	
u_i	2.6 (m/s)	0.15	
δ_e	9.0 (deg)	0.012	
δ_N	29. (deg)	0.0012	
$\dot{\delta}_e$	50. (deg/s)	0.0004	.14
$\dot{\delta}_N$	100. (deg/s)	0.0001	.25

B. Lateral

Variable	"Limit"	Weighting	τ_N
y	5.4 (m)	.034	
$\dot{y}$	---	0	
ϕ	20. (deg)	---	
$\dot{\phi}$	---	0	
δ_w	30. (deg)	.0025	
$\dot{\delta}_w$	60. (deg/s)	.0003	.25

shown in Tables 2A and 2B are the τ_N's (i.e., the corresponding diagonal elements in the $\underline{T}_N$ matrix) that result from the selected weightings.

Pilot Noise/Signal Ratios

In all the analyses performed here the motor noise/signal ratio for each control variable was approximately -25 dB. This value was based on previous results [2]. The "base" observation noise/signal ratio (P_o) was treated as a measure of overall attention to the task being considered and was made the same for all display quantities in the task. The noise/signal ratio associated with a given display variable was obtained by dividing this base level by the corresponding fraction of attention.* The value for P_o will be a parameter in our studies of workload. On the basis of previous analysis of remnant data [2, 3], an observation noise/signal ratio of -20 dB was considered as the "nominal" value. We will discuss this choice further in connection with workload analysis.

Analysis of Longitudinal Performance

The optimal-control model was used to analyze performance in longitudinal control with the dynamics of Appendix C, the display parameters of Table 1 and a cost functional corresponding to the "weightings" in Table 2A.

*The "total" noise associated with a display variable is then obtained by modifying this level to account for threshold and residual-noise effects as in Equation 10.

Allocation of Attention. – A "sensitivity" study was performed to determine the "optimal" allocation of attention among the three longitudinal display variables, height error (h), pitch (θ), and airspeed (u).

Table 3 shows the fractional allocation of attention to these display variables.* This distribution of attention was found to yield the lowest total predicted cost, subject to the constraint that the fractional attentions sum to unity. It is important to note that performance was relatively insensitive to attentional allocation, and one could vary the allocation over a fairly wide range without affecting the predicted results appreciably. The values for attention given in Table 3 were used for the remainder of the longitudinal analysis.

Table 3

ALLOCATION OF ATTENTION AMONG LONGITUDINAL DISPLAYS

Variable	h, $\dot{h}$	θ, q	u
Attention	.35	.1	.55

*The pilot is assumed to obtain derivative information from a given display indicator without additional attention being required. Thus, the fractional attentions to height-related quantities as a group, pitch-related quantities as a group, and airspeed sum to unity.

Performance. — Table 4 shows the predicted rms performance scores for the various display and control variables for the "worst-case" wind condition, with attention allocated "optimally" and all other model parameters set at "nominal" values. Also shown are the "limits" associated with each variable (repeated here for convenience) and the probability that the magnitude of a given variable will exceed its limit. The latter was computed as twice the integral of the Gaussian probability density function from the "limit" to infinity. (The factor of 2 was included to account for both positive and negative overvalues.)

Four variables have a probability greater than 0.001 of exceeding their respective limits: height (11%), sinkrate (10%), airspeed (5%), and nozzle (2%). If we assume that the probability distributions for height and airspeed errors are essentially independent, we can use the marginal probabilities to compute a joint probability of 16% for simultaneously exceeding the height and airspeed windows.

Table 4

PERFORMANCE SCORES FOR THE "NOMINAL" CONTROL SITUATION

(σ_{u_g} = 2.1 m/s, σ_{w_g} = .82 m/s, τ = .2 sec., P_o = -20 dB)

Variable	"Limit"	RMS Error	P(|Error| > Limit)
h (m)	3.7	2.3	0.11
$\dot{h}$ (m/s)	1.1	.68	0.10
θ (deg)	6.0	1.8	0.001
q (deg/s)	---	1.2	0.0
u_i (m/s)	2.6	1.3	0.05
δ_e (deg)	9.0	2.1	<0.001
δ_N (deg)	29.	7.4	<0.001
$\dot{\delta}_e$ (deg/s)	50.	12.	0.02
$\dot{\delta}_N$ (deg/s)	100.	21.	<0.001

The "nominal" control situation described above corresponds to the worst-case (1%) wind condition and one can generally expect better performance than indicated in Table 4. A more reliable indication of system performance would consider the "range" of possible wind conditions. In order to obtain such a measure of pilot/vehicle performance, it is necessary to specify how performance degrades as a function of gust intensity. If pilot-related noise processes were not considered, rms errors would simply vary linearly with rms gust amplitudes in the absence of other external inputs to the system. However, because thresholds and resolution limitations are included in the model, a more complex relationship can be generally expected.

The model was used to predict rms performance measures for five sets of gust intensities, ranging from the 80%-wind to the 0.25%-wind. The effects of gust intensity on rms height, sink rate, and airspeed errors are shown in Figure 3.* All three of the performance-versus-intensity curves are very nearly linear and straight-line approximations are obtained by connecting the rms levels corresponding to the 50%-and 1%-winds. Because of the consideration of threshold effects, the linear approximations for height and sink rate errors have positive zero intercepts.

We have shown thus far how to predict system performance as a function of rms gust intensity. Since all system variables are assumed to be Gaussian, we can use the predicted rms performance scores to obtain the probability density function for any variable, conditioned on the rms gust level. It is worth noting that although rms performance scores vary linearly with gust intensity, the probabilities of exceeding approach window limits do not (Figure 4).

*Note that specifying σ_{u_g} also specifies σ_{w_g} via Equation (12e).

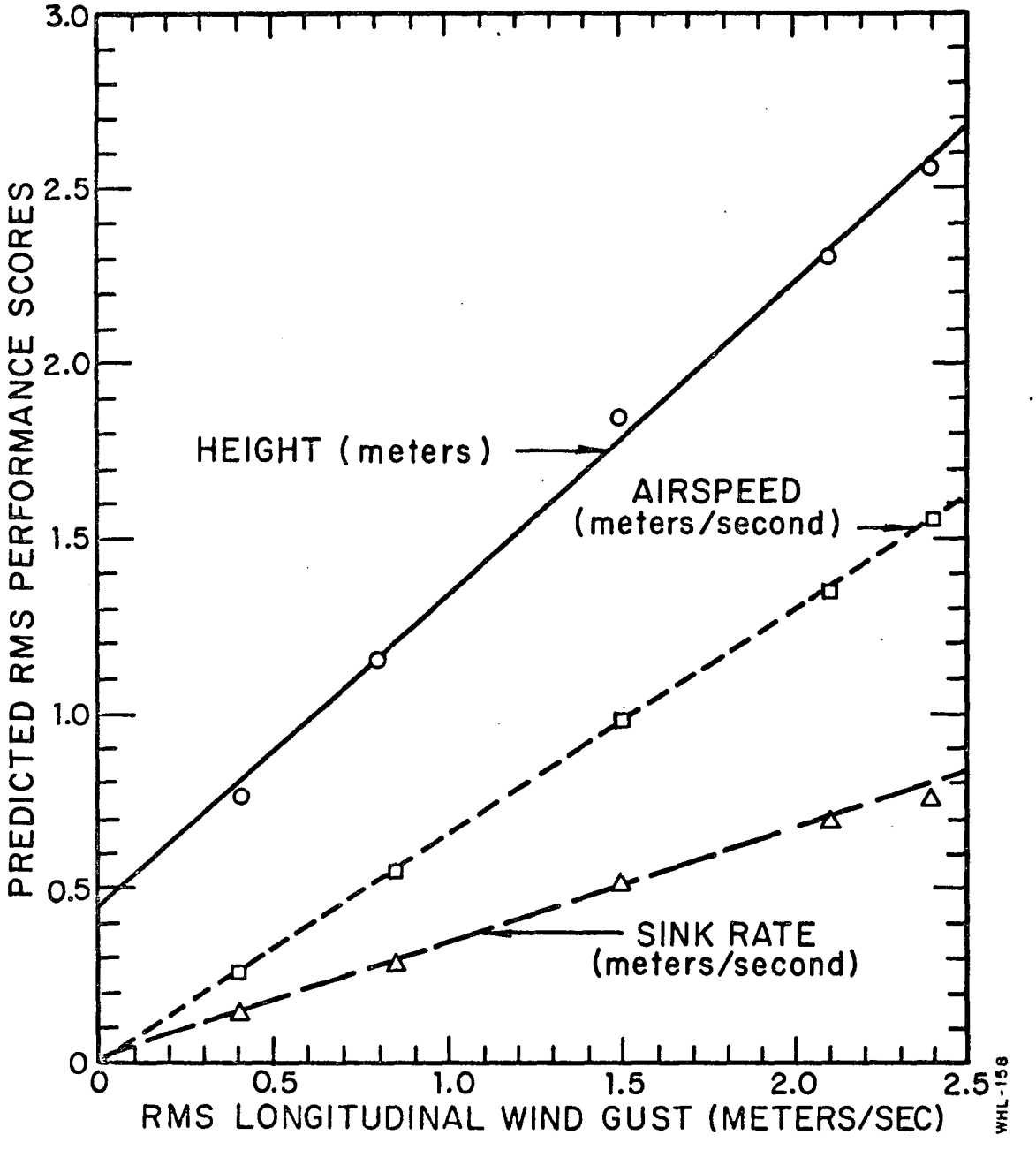

FIGURE 3. Effect of Gust Intensity on Performance Scores

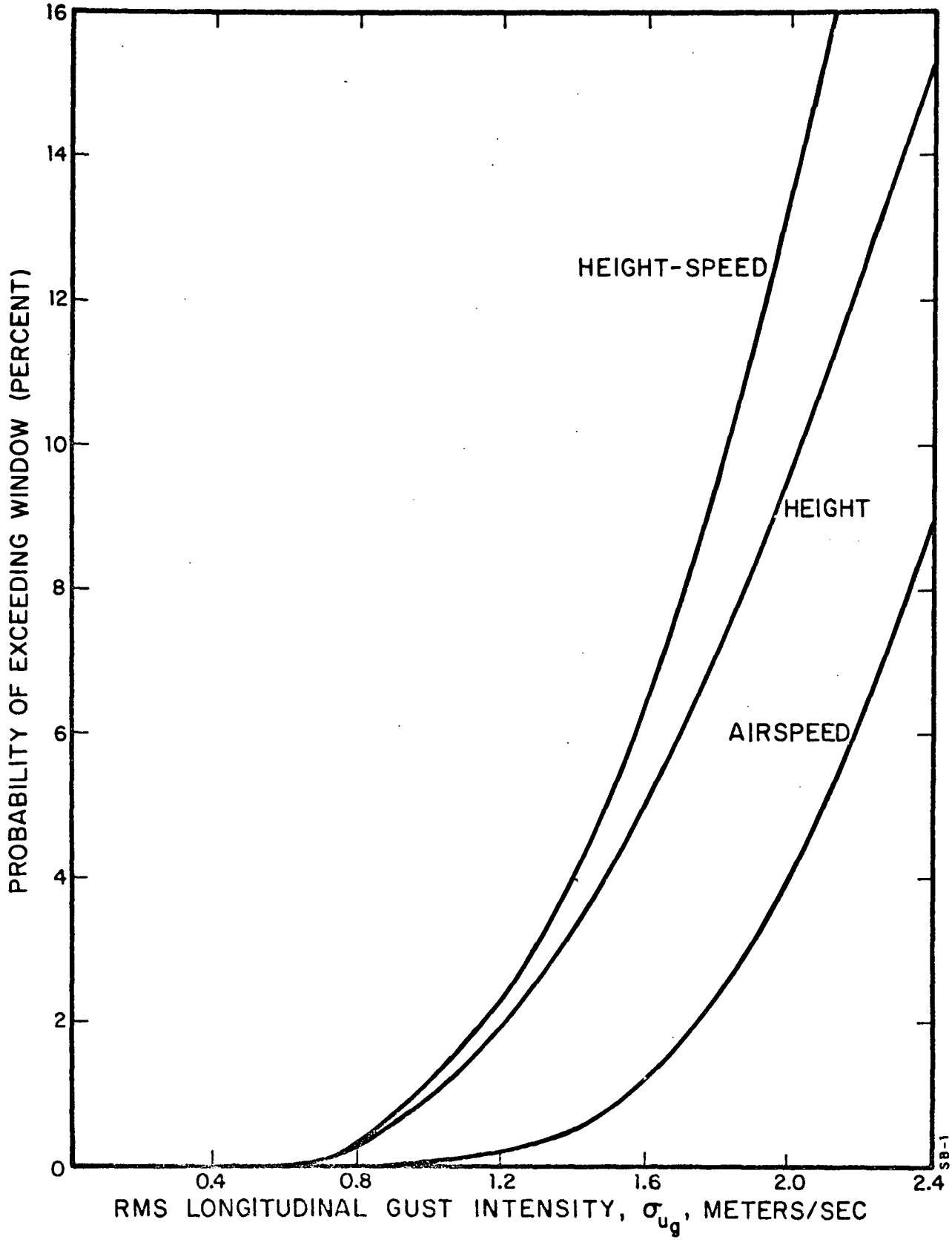

FIGURE 4. Effect of Gust Intensity on "Window" Probabilities

In order to predict a measure of system performance that is averaged over all possible wind conditions, the joint probability distributions of system variables and rms wind intensities has to be integrated. Thus, if one wishes to predict the overall probability of a height error greater than the maximum allowable value, the following expression must be evaluated:

$$P(|h| - h_L) = 2 \cdot P_g \cdot \int_0^\infty \left[\int_{h_L}^\infty p(h, \sigma_{u_g}) dh \right] d\sigma_{u_g}$$

$$= 2 \cdot P_g \int_0^\infty p(\sigma_{u_g}) \left[\int_{h_L}^\infty p(h|\sigma_{u_g}) dh \right] d\sigma_{u_g} \qquad (14)$$

where $p(\sigma_{u_g})$ is the probability density function of the rms longitudinal gust, $p(h|\sigma_{u_g})$ is the conditional Gaussian probability density function for height error, and P_g is the probability of encountering clear-air turbulence.* The factor of 2 is included so that negative as well as positive overvalues will be accounted for.

The density function $p(\sigma_{u_g})$ may be taken as that of a Rayleigh distribution [16].

$$p(\sigma_{u_g}) = \frac{\sigma_{u_g}}{c} \; e^{-1/2 \; \sigma_{u_g}^2 / c^2} \qquad (15)$$

*According to [16], there is a probability of about 0.2 that no turbulence will be encountered at an altitude of 30 meters.

where c = .703 m/s. If rms-height (or any other variable of interest) was directly proportional to σ_{u_g}, i.e., if

$$\sigma_h/\sigma_{u_g} = K = \text{constant} \qquad (16)$$

then Equation (14) could be evaluated analytically.* But, because of thresholds, Equation (16) does not hold. Consequently, a numerical integration technique was employed to evaluate Equation (14) and a similar expression for airspeed. Linear approximations to the curves of rms performance vs. rms gust intensity were used. For the case considered above (i.e., P_o =-20dB), the overall probability of being out the height-airspeed window turned out to be about 1.2%.

Workload Requirements. — Pilot workload requirements under the various gust conditions can be determined from the relationship between performance and noise/signal ratio. Recall the model for pilot attention, in which

$$f = P_o/P$$

where f is the fraction of attentional capacity devoted to the task, P is the noise/signal ratio achieved by the pilot when

*The easiest way is to integrate by parts. Let $s = \sigma_{u_g}/c$, $t = h/\sigma_h$ and $H = h_L/Rc$. Then Equation (14) may be written as $\int_0^\infty \left[\int_{H/s}^\infty \frac{1}{\sqrt{2\pi}} e^{-t^2/2}\, dt \right] se^{-s^2/2} ds = \int_0^\infty [u]dv$, which can be evaluated to yield $\frac{1}{2}e^{-H}$.

performing the task, and P_o is a reference ratio. Building on this model for attention, we have defined a "workload index" as the amount of attention required to achieve a specified criterion level of performance on the control task. Thus,

$$\text{Workload Index} = P_o/P_c$$

where P_c is the maximum noise/signal ratio that can be tolerated while performance is maintained within the criterion level.

In order to predict the workload index, we have to specify some relevant performance measure, the required level of performance, and the "reference" noise/signal ratio P_o. Ideally, we would like P_o to correspond to full attention. Unfortunately, we cannot conduct an experiment in which the pilot is guaranteed to use his total information-processing capability. Therefore, we let P_o correspond to the noise/signal ratio (namely, .01 or -20dB) obtained in a standardized laboratory situation in which the pilot is motivated to minimize his tracking errors. We know that this value does not correspond to "full capacity", because significantly lower noise-ratios have been found experimentally [4]. However, based on our laboratory experience, P_o = -20dB does appear to correspond to a high workload condition, and "operation" at this level for any prolonged time would undoubtedly be unacceptable. Of course, when we are interested primarily in the relative *change* in workload requirements from one situation to the next, the value for P_o is not too critical; this is the case in this study.

We consider the probability of a missed approach as the relevant measure of system performance for assessing workload. We define a "missed approach" as a situation in which either the height or the airspeed error exceeds the maximum allowable value as defined by the "limits" shown in Table 2A. The specification of a desired level of performance is somewhat arbitrary, but we suspect that a reasonable criterion lies between 1% and 5% (i.e., a probability of a successful approach between 95% and 99%).

The relation between noise/signal ratio and the probability of exceeding the height-airspeed window is shown in Figure 5 for the 1% and 50% wind conditions. Also shown are the curves for exceeding the height and airspeed limits individually for the 1% wind condition. The allocation of attention among the height, pitch and airspeed display variables was held at the levels shown in Table 3 as the overall noise/signal ratio was changed. Because of the low sensitivity of performance to attentional allocation, we do not expect that significantly different performance scores would have been predicted had we re-optimized the allocation at each stage in the analysis.

For the 1% wind condition, the predicted probability of a missed approach is about 10% for a noise/signal ratio of -26dB ($f \approx 4.0$) -- the lowest ratio explored. Thus, the workload index will be well above 4.0 for a criterion level in the range of 1% to 5%. Since noise/signal ratios as low as -26dB have been found experimentally only in extremely demanding control situations (unstable dynamics) [4], we would conclude that the workload requirements for the approach task in a 1% wind environment are excessive.

If the wind intensity is reduced to the 50% level, however, the task workload is reduced considerably. For a 1% criterion, the workload index is slightly less than 0.5, which represents an achievable (if not comfortable) level of attention. If we relax the criterion to 5%, the workload index is reduced to about 0.23. Thus, for a 5% criterion probability, the workload requirements for the task range from low-to-moderate for the 50% wind condition to excessive (if not impossible) for the 1% wind condition.

The contributions of height and airspeed to the overall probability of a missed approach can be seen from the corresponding curves shown in Figure 5. If the pilot were to operate at a noise/signal ratio of -26dB, height and airspeed errors would contribute about equally to the 10% probability of a missed approach in the 1% gust environment. Since height regulation is considerably more sensitive to pilot-induced noise than is airspeed regulation, however, the relative contribution of height errors increases markedly as attention is relaxed. For the 50% wind condition, a missed approach is caused by height errors only. For the range of noise/signal ratio explored, the probability of excessive airspeed errors is less than 0.1 percent.

Figure 6 shows the predicted probability of a missed approach as a function of observation noise/signal ratio, averaged over all possible gust intensities. If the pilot operates consistently at a noise/signal ratio of -20dB, he will achieve an overall probability of a missed approach of about 1.2 percent. Thus, the average workload index is about 1 if we specify a criterion performance level of 1%. If a probable missed approach

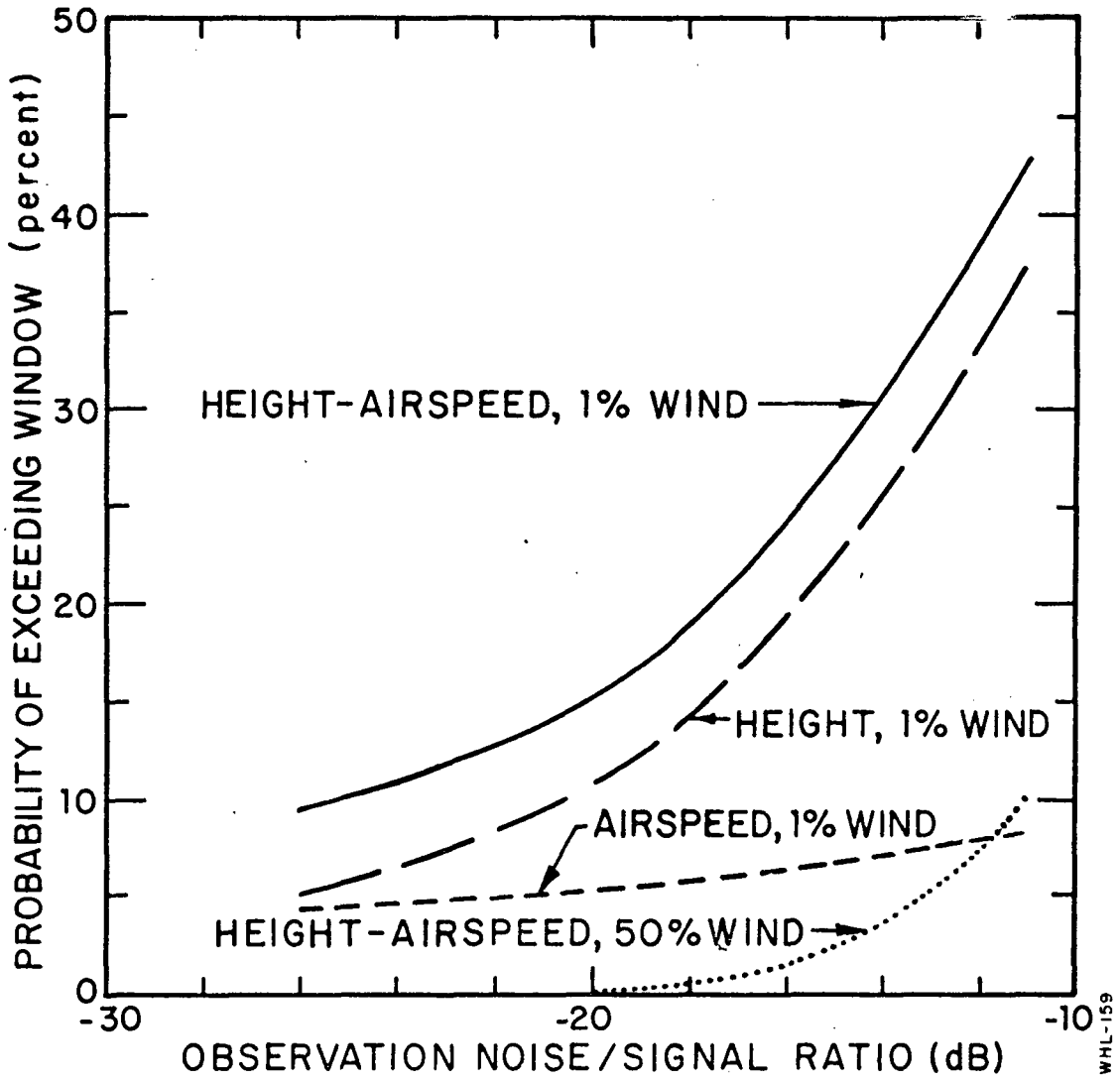

FIGURE 5. Sensitivity of "Window" Probabilities to Observation Noise/Signal Ratio

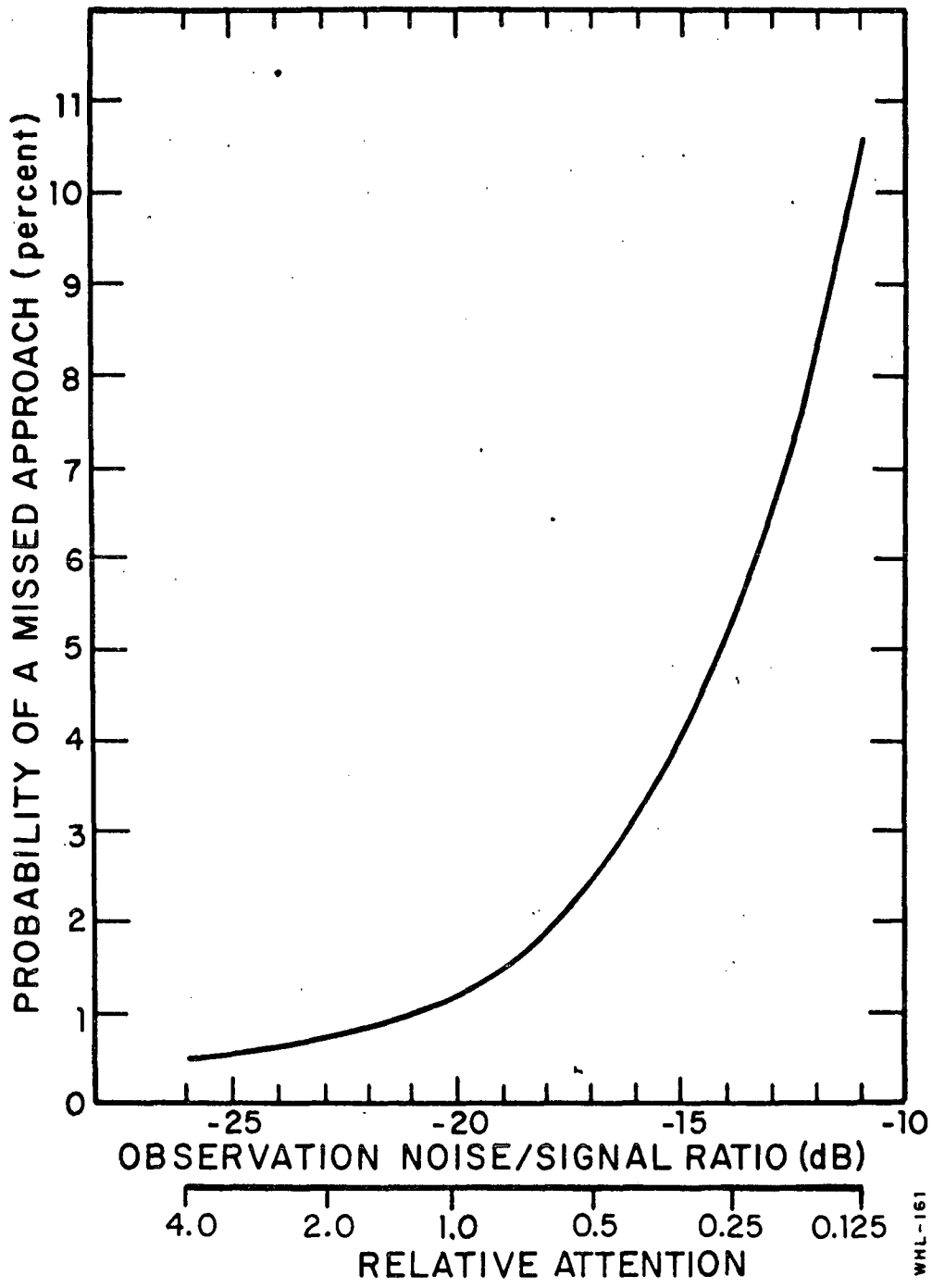

FIGURE 6. Effect of Attention on Missed Approach Probability

of 5% is adopted as the performance criterion, the average workload index is reduced to about 0.25. Figure 7 shows the trade-off between workload and performance (probability of a missed approach) for the longitudinal task and the given display.

Effects of Display Parameters. — The foregoing analysis was conducted for the nominal display condition (see Table 1) in which visual thresholds, other types of display-related noise, and attention-sharing requirements served to limit performance. In order to explore the benefits that could be obtained by reducing various display-related limitations, model analysis was performed in which these limitations were removed in stages. The display configuration was adjusted as follows:

Condition A: nominal display condition.

Condition B: removal of the residual noise term associated with height perception. This condition corresponds to providing the pilot with an explicit zero reference for glide-slope error.

Condition C: removal of the residual noise term on sinkrate to correspond to a noise-free SBILS presentation.

Condition D: zero threshold for sinkrate perception.

Condition E: zero thresholds on all remaining display variables.

Condition F: No modification of noise/signal ratios to account for attention-sharing. This condition corresponds to an idealized integrated display.

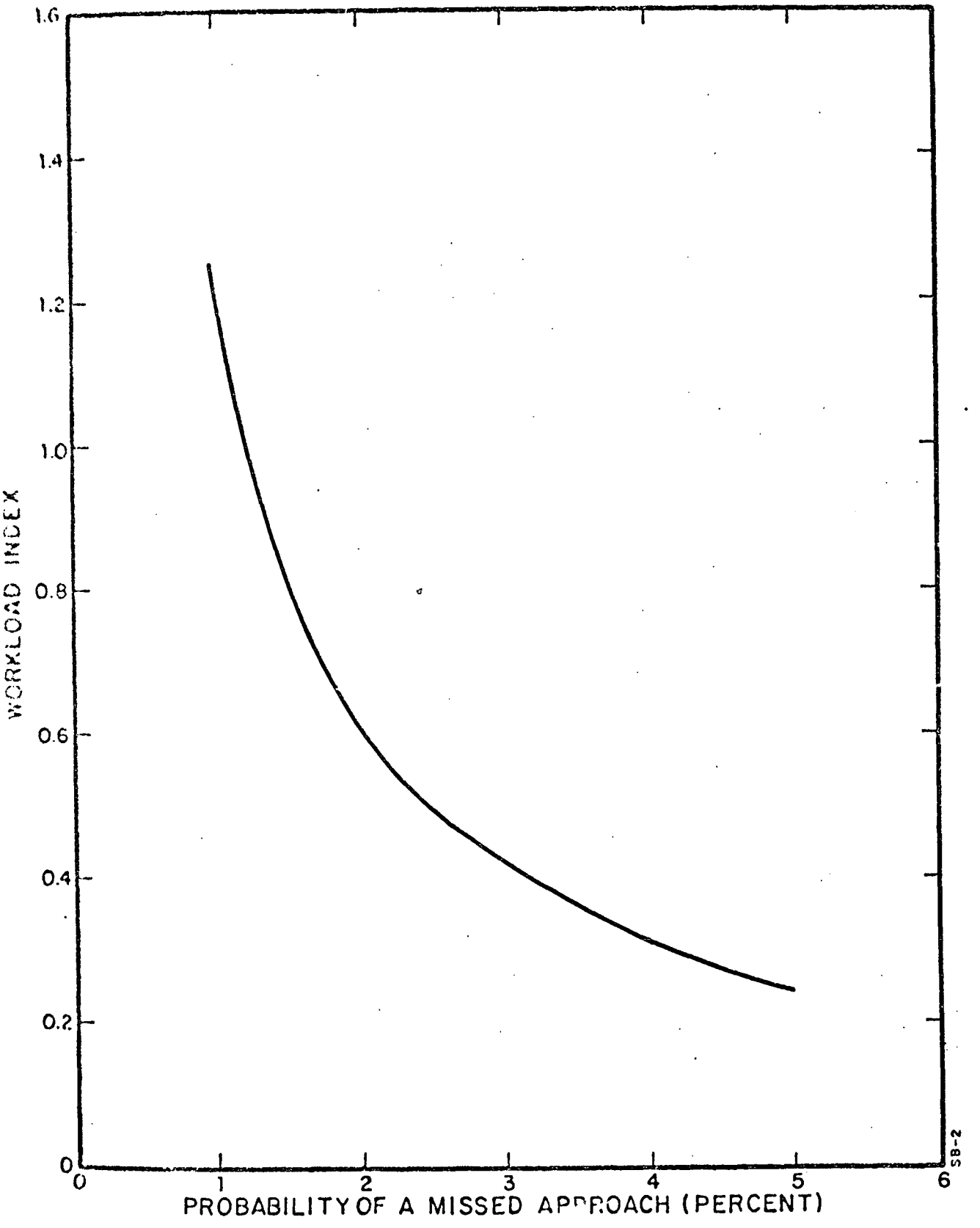

FIGURE 7. Tradeoff Between Workload and Missed-Approach Probability

The model conditions described above were cumulative. Once a deviation from the nominal condition was made, it remained in effect for the remaining parameter adjustments.

Not all of the above conditions are intended to be physically realizable. For example, a zero visual threshold corresponds to infinite display gain. Thus, this analysis serves to indicate the upper bounds on performance improvement that can be expected from modifying various display-related variables.

Except for changes in display-related parameters, the model parameters were selected for the nominal condition. Only the 1% wind condition was considered. The results of this analysis are presented in Figure 8. For each display condition defined above, probabilities of excess excursions were predicted for height, sinkrate, and airspeed. In addition, the probability of a missed approach (the combined probability of exceeding either the height or airspeed limits) was computed.

Performance along all dimensions except airspeed regulation improves considerably as the display-related limitations are removed. The greatest improvement is predicted when the effective visual threshold on sinkrate information is set to zero. Small-to-moderate benefits accrue from simulating a zero reference for glide slope error and from neglecting the effects of attention-sharing. Negligible improvements result when remaining threshold terms are set to zero.

Overall, the predicted probability of a missed approach decreases from about 15% for the nominal condition to about 6% for the idealized display condition. Thus, predicted work-

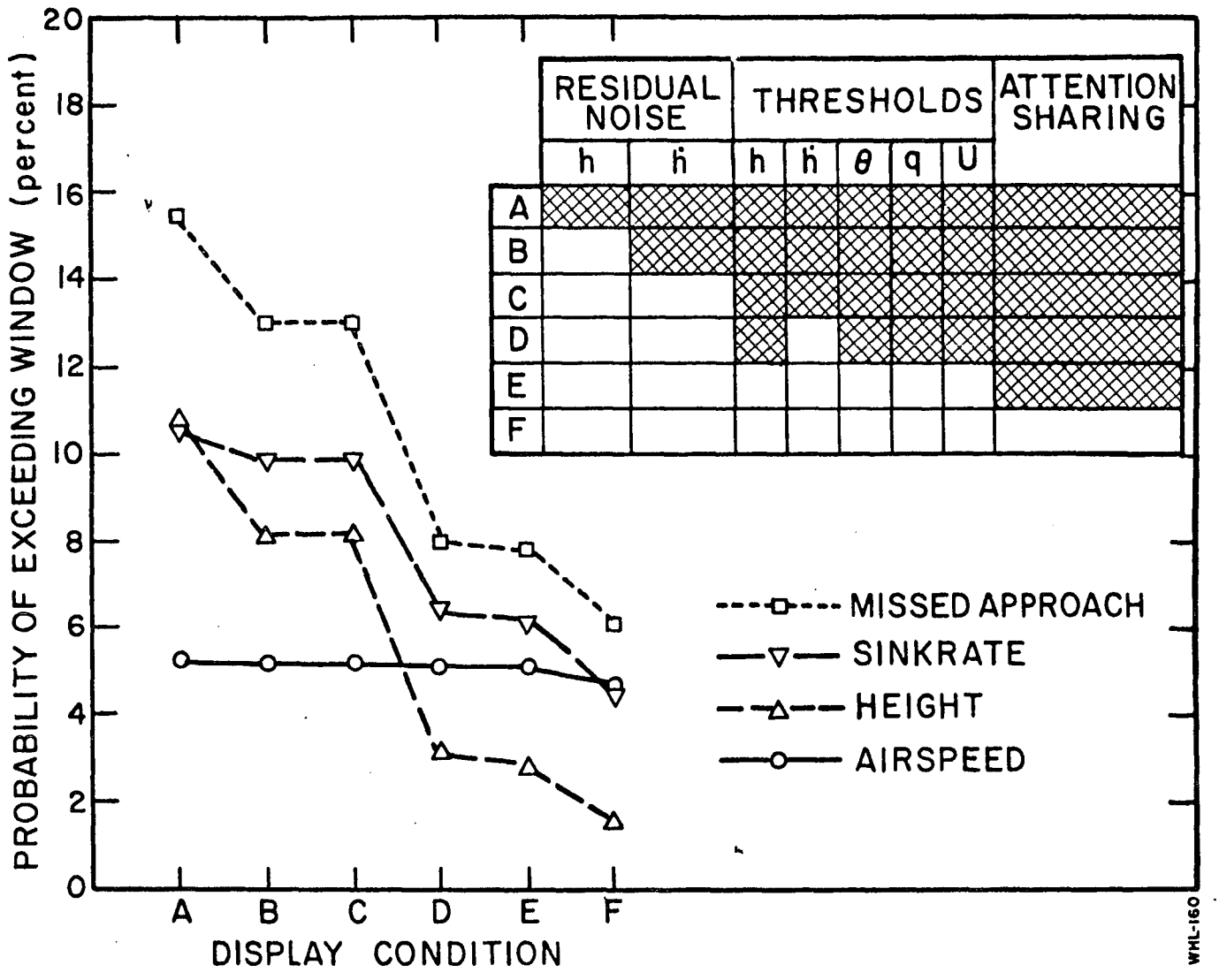

FIGURE 8. Effect of Display Condition on Probability of Exceeding Performance Window

load remains relatively high even for the idealized display condition. (Results were obtained for a noise/signal ratio of -20dB.) It must be remembered, however, that these predictions correspond to the 1% wind condition only, and that meaningful improvement might be observed if we consider performance averaged over all wind conditions.

It is not surprising that performance should improve considerably when the threshold on sinkrate is removed. Comparing Tables 1 and 4 we observe that the predicted rms sinkrate error is less than the assumed threshold. Thus, the pilot can be expected to obtain no useful sinkrate information from the velocity of the glide-slope error indicator for the nominal display configuration. Since sinkrate information is useful in predicting future flight-path errors, performance should be improved if the effective threshold on sinkrate can be sufficiently decreased. (Note that if we attempt to accomplish this by increasing the gain of the glide-slope indicator, we run the risk of unacceptably large excursions in the high-gust situation.) Experimental results recently obtained at Ames also support the prediction that a decreased threshold on sinkrate will lead to better height regulation. In a study of approach performance with a pictorial display, performance was found to improve considerably when the pilot was shown a predicted touchdown point [6]. In effect, a presentation of the aim point error provided the pilot with a high-gain display of sinkrate error.

The source of the improvement in performance with the idealized display is, more generally, an improvement in monitoring performance. The standard deviation of the estimation error predicted by the model normalized with respect to the

predicted standard deviation of the signal gives an indication of how well a pilot may be expected to monitor a given variable. The results for the status and the idealized display are presented in Table 5. It can be seen that monitoring of all variables is improved. The improvement is greatest for height errors and least for speed errors. The relatively small improvement in monitoring airspeed is reflected in the lack of substantial improvement in airspeed regulation.

Table 5

MONITORING PERFORMANCE FOR STATUS AND IDEALIZED DISPLAYS

(1% wind, P_o = -20 dB)

Variable	Status			Idealized		
	σ	σ_e	$\sigma_{e/\sigma}$	σ	σ_e	$\sigma_{e/\sigma}$
h(m)	2.31	.96	.415	1.53	.17	.111
$\dot{h}$(m/s)	.68	.41	.603	.55	.18	.327
θ(deg)	1.81	.47	.261	1.77	.22	.124
q(deg/s)	1.22	.20	.164	1.91	.17	.089
u(m/s)	1.34	.78	.586	1.30	.70	.537

$\sigma \equiv$ Standard Deviation of Signal

$\sigma_e \equiv$ Standard Deviation of Estimation Error

In summary, the results of the analysis of display-related parameters shows that significant improvement in system performance can be expected if the pilot is presented with a zero reference for glide-slope error, if the ability to obtain sink-rate information is considerably enhanced, and if the effects of attention-sharing can be avoided. One way to approach this ideal situation is by providing the pilot with a flight director. With this display the pilot need look at only one or two display indicators, zero references are provided, and the gains on the various display quantities are optimized so that the pilot is shown the appropriate "mix" of inputs on a display that is suitably scaled. Thus, the model predictions obtained under Condition F (described above) give a good indication of the maximum benefits than can be obtained from a flight director. Accordingly, the results of this analysis will be used later in Chapter 4 to evaluate proposed flight director laws.

Analysis of Lateral Performance

Lateral performance using the status display described earlier was also analyzed. Vehicle dynamics for the analysis are tabulated in Appendix C and correspond to a simplified situation in which all turns are assumed to be coordinated; lateral gusts are as described above; display parameters and cost weightings are given in Tables 1 and 2B above.

Stability Augmentation. — A brief preliminary investigation of SAS-off lateral dynamics (also tabulated in Appendix C) was conducted for the basic display configuration. Figure 9 compares lateral performance vs. observation noise/signal ratio (attention) for the SAS-on and SAS-off cases. It may be seen

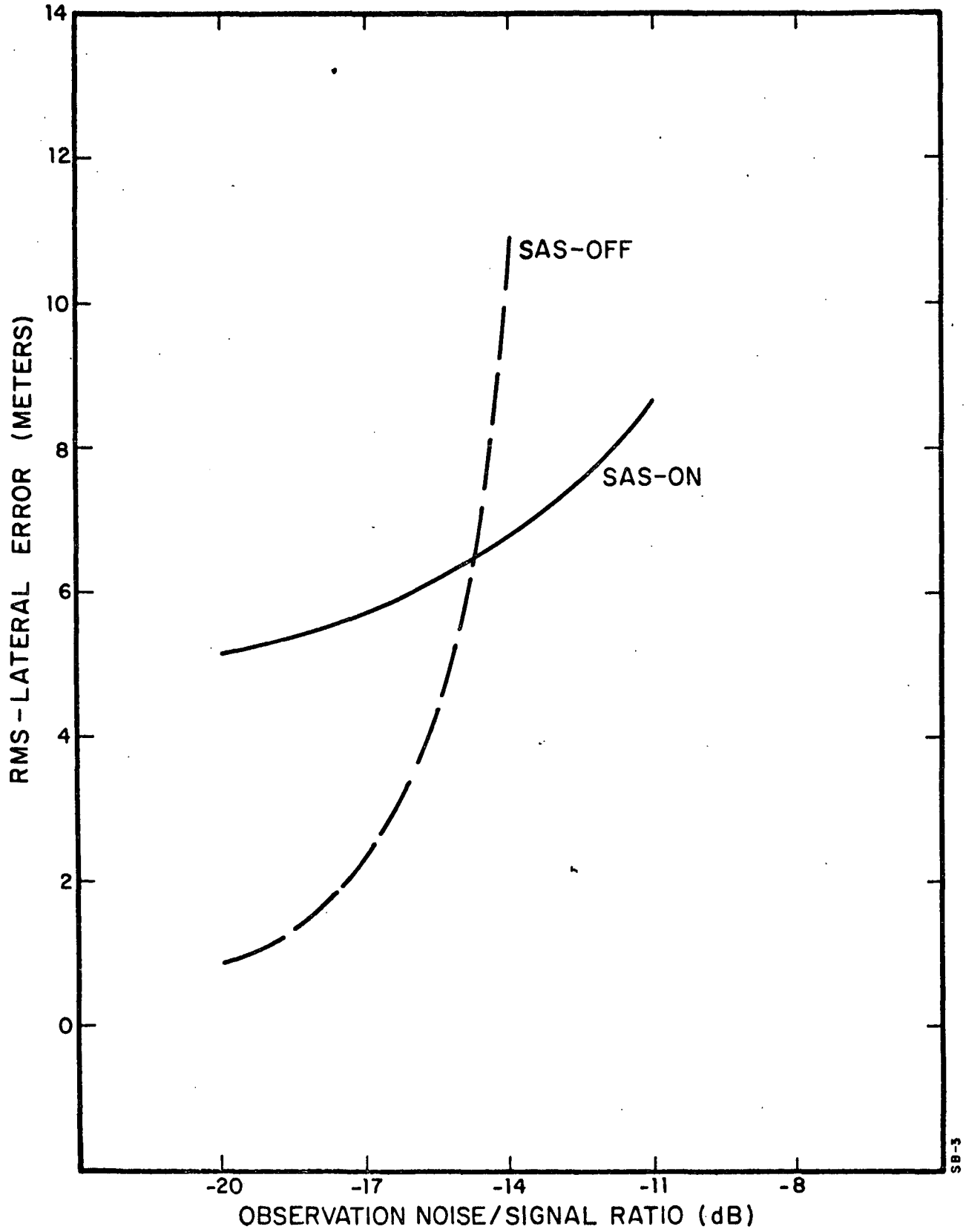

FIGURE 9. Effect of Stability Augmentation and Attention on Lateral Control Performance

that at low noise/signal ratios it is actually possible to achieve smaller lateral errors with the SAS-off. However, the SAS-off condition is extremely sensitive to observation noise/signal ratio* and is, consequently, quite demanding. It is quite likely that this sensitivity is what makes the SAS-off configuration unacceptable. In the remainder of our analysis we consider only SAS-on dynamics.

Allocation of Attention. — A sensitivity study was performed to determine the optimal allocation of attention between localizer and bank angle displays. The results, for two values of P_o, are presented in Table 6. At the lower noise/signal ratio the "optimal" allocation is about 70-75% attention to the localizer whereas at the higher noise/signal ratio it appears that full attention should be devoted to the localizer. However, in both cases the results are quite insensitive to allocation of attention. In the remainder of the analysis we assumed that 75% of the pilot's attention would be devoted to the localizer display.

Performance. — Lateral tracking performance was computed for the worst-case (1%) and median (50%) winds. Scores for the 1%-wind and the nominal observation noise/signal ratio of -20dB are shown in Table 7, along with the "limits" used in selecting the cost weightings and the probability of exceeding these limits.

The (assumed) linear relation between scores and gust intensity was determined by passing a straight line through the results for the worst-case and median winds. This line was then used in Equation (14) to compute the probability of exceeding the

*In conducting the computer analysis it was also found to be highly sensitive to motor noise.

Table 6

EFFECTS ON LATERAL PERFORMANCE OF SHARING ATTENTION BETWEEN LOCALIZER AND BANK ANGLE INDICATOR

Attention to Localizer	P_o = -20dB		P_o = -14dB	
	Cost(J)	σ_y(m)	Cost(J)	σ_y(m)
.25	1.57	5.70	-	-
.5	1.37	5.22	2.43	7.17
.6	1.35	5.15	-	-
.65	1.34	5.11	-	-
.7	1.33	5.08	2.21	6.75
.75	1.34	5.09	2.18	6.68
.8	1.34	5.09	2.16	6.62
.85	-	-	2.14	6.58
.9	-	-	2.14	6.56
.95	-	-	2.13	6.54
1.0	1.41	5.17	-	-

Table 7

LATERAL PERFORMANCE SCORES

(σ_{v_g} = 2.1 m/s)

Variable	Score	"Limit"	Prob. of Exceedance
σ_y(m)	5.08	5.4	.288
$\sigma_{\dot{y}}$(m/s)	1.99	-	-
σ_ϕ(deg)	5.06	20	.000
$\sigma_{\dot{\phi}}$(deg/s)	3.28	-	-
σ_{δ_w}(deg)	10.5	30	.004
$\sigma_{\dot{\delta}_w}$(deg/s)	19.9	60	.003

lateral window (5.4m) averaged over "all" winds. This was done for several levels of total attention devoted to the lateral task. The results for the "overall" average performance, as well as those for the 1% and 50% winds are presented in Figure 10.

Comparison with longitudinal results (Figures 5 and 6) reveals that the lateral control task, even with the SAS-on, is more difficult. The probability of missing the lateral window when averaged across all winds is 1.5 - 3 times as great as that for missing the longitudinal window at all levels of attention investigated. In other terms, if we establish a 95% probability of a successful lateral approach as a criterion level, the Workload Index for the lateral task, for the 50% wind is about .4, and it is about .7 when the average of all winds are considered. For the 1% wind, it does not appear that a success probability of 95% is achievable within the limits of behavior that we have observed heretofore.

Display Related Parameters. — An analysis of the sensitivity of performance to changes in display parameters, completely analogous to that for longitudinal control, was conducted. The display configuration was adjusted as follows:

Condition A: nominal configuration.

Condition B: removal of residual noise associated with lateral error (providing a zero-reference).

Condition C: zero threshold for lateral error-rate.

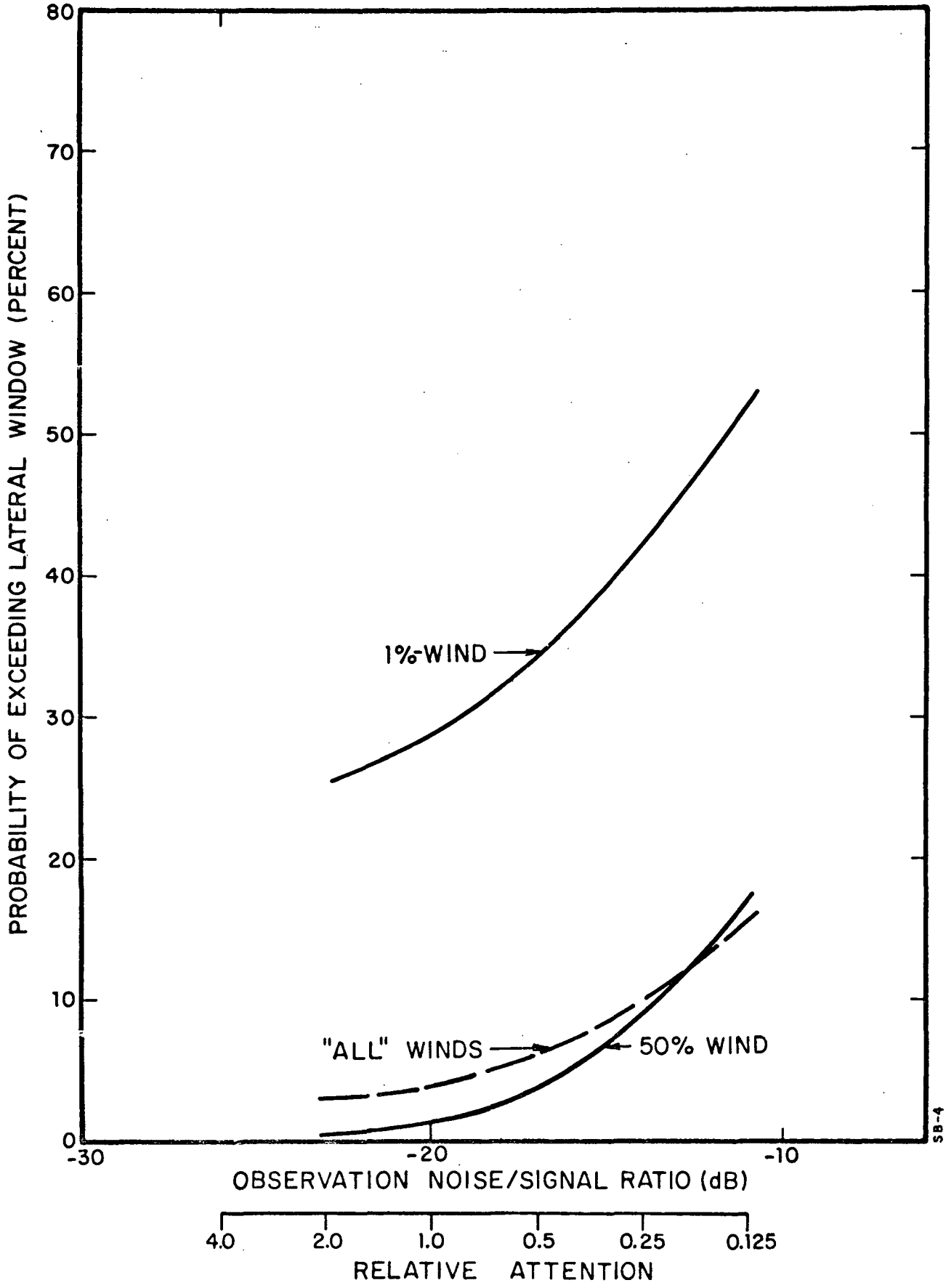

FIGURE 10. Effect of Attention on Lateral Window Performance

Condition D: zero threshold for lateral error.

Condition E: no modification of noise/signal ratios for attention-sharing (display integration).

The "worst-case" wind condition was used and the parameters relating to the pilot were "nominal". Relevant scores and monitoring performance (as defined earlier) are given in Table 8.

Table 8

EFFECT OF DISPLAY PARAMETERS ON LATERAL PERFORMANCE
(v_g = 2.1 m/s, P_o = -20dB)

Condition	A	B	C	D	E
σ_y(m)	5.09	5.05	4.89	4.87	4.59
$\sigma_{\dot{y}}$(m/s)	2.0	1.99	1.96	1.95	1.88
σ_ϕ(deg)	5.04	5.03	4.97	4.96	4.71
σ_{δ_w}(deg)	10.6	10.6	10.4	10.4	9.8
σ_{y_e}/σ_y	.19	.16	.14	.14	.12
$\sigma_{\dot{y}_e}/\sigma_{\dot{y}}$	.45	.45	.42	.42	.41
$\sigma_{\phi_e}/\sigma_\phi$	.12	.12	.12	.12	.10

Performance improvements with display changes are not too dramatic with the cumulative improvement in tracking performance being about 10%. Of the changes made, only two had any significant effect; namely, removing the lateral error rate threshold and removing the necessity for attention sharing,

although zeroing the residual noise on error did result in a significant improvement (15%) in monitoring that variable. This suggests that *performance* improvements with a lateral flight director might not be substantial. It should be remembered, however, that this analysis was conducted for a high-wind, high-workload (P_o = -20dB) condition. The advantages of a flight director may prove to be most significant in situations where less "attention" is involved. Alternatively, it might allow achievement of similar performance at reduced workload, i.e., it might reduce the workload index.

Combined Longitudinal and Lateral Tasks

Thus far, we have considered longitudinal and lateral tasks separately. This is possible because of the decoupling inherent in the linearized perturbation equations. Of course, the pilot must share his capacity between the longitudinal and lateral tasks, which implies some interference and a degradation in performance on each task. This interference may be treated within the same framework of the model of attention presented earlier. Moreover, one can make direct use of the results obtained in the separate studies of longitudinal and lateral control.

To account for the interference, we define a combined cost functional

$$J_{TOT} = J_{LONG} + J_{LAT}$$

where J_{LONG} and J_{LAT} are the cost functionals for the longitudinal and lateral cases, respectively (see Table 2). The combined cost

functional is meaningful because of the manner in which the separate cost functionals were defined and normalized. Now, if f_{LONG} is the fraction of attention devoted to the longitudinal task, then the fraction devoted to the lateral task is

$$f_{LAT} = 1 - f_{LONG}$$

Using the results of the earlier "attention" studies, it is possible to determine how attention should be shared between the two control modes so as to minimize J_{TOTAL}. (We assume that the attention sharing among displays within a given mode is unaltered.)

Figure 11a shows how performance varies with attention to the longitudinal task for the 1%-wind and Figure 11b presents the same data for the 50% wind. These results assume that P_o = -20dB corresponds to full attention. It may be seen that attention should be divided nearly equally between the two tasks with a slight bias to the lateral task in the high-wind case.

Figure 12 shows the effects of attention-sharing on window performance, averaged over all winds. Using the probability of a missed approach as the measure of performance leads to the conclusion that approximately a 40/60 split of attention between longitudinal and lateral tasks is optimal, thus confirming the results obtained using J_{TOT}. The corresponding overall probability of a missed approach (i.e., a miss on height or airspeed or lateral position) is about 8%.

Finally, if we assume that the pilot shares his capacity equally between the two tasks (which is not far from the optimal strategy), we can use the earlier results to obtain missed approach

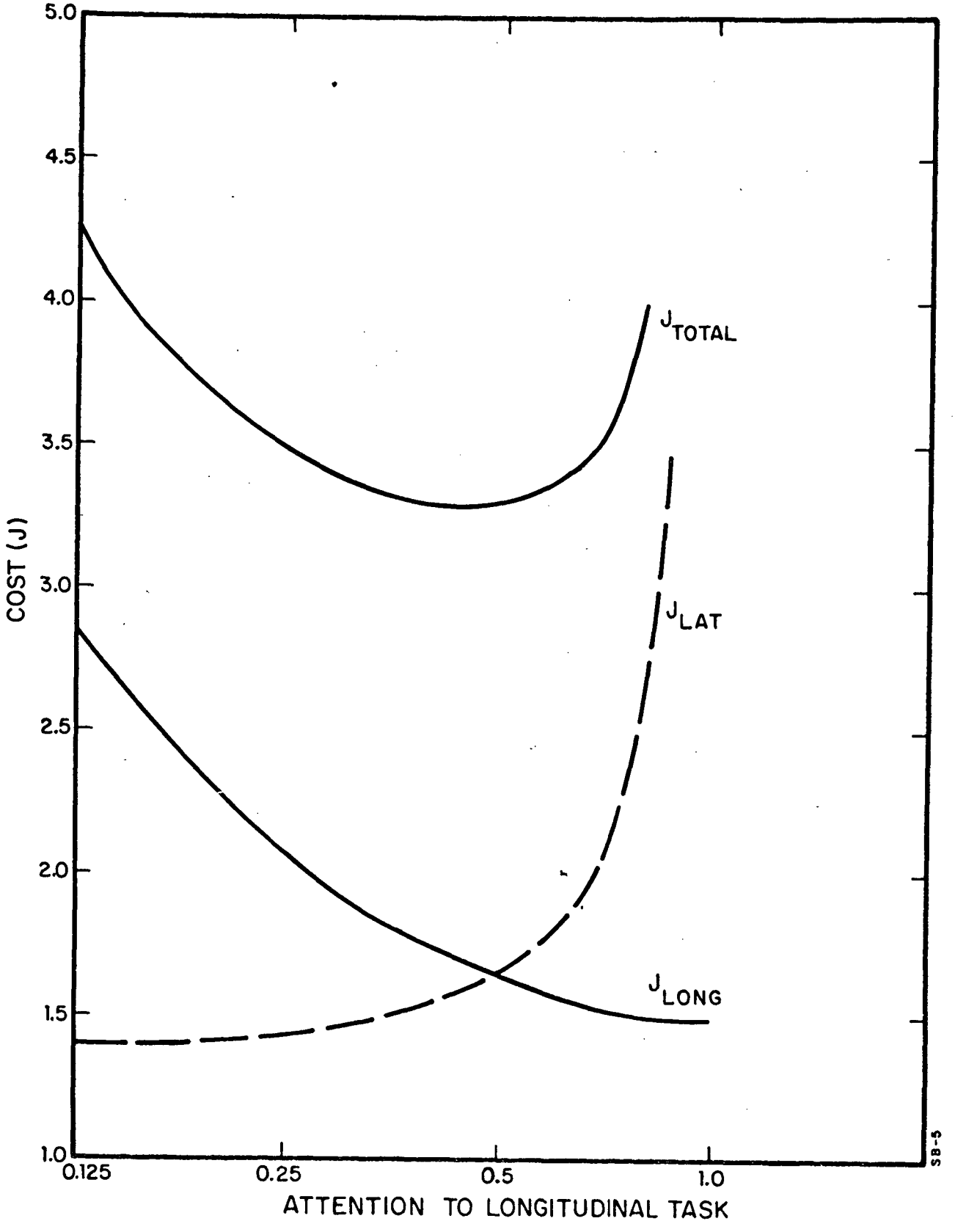

FIGURE 11a. Effect on Optimal "Costs" of Attention Sharing Between Longitudinal and Lateral Tasks (1%-Wind)

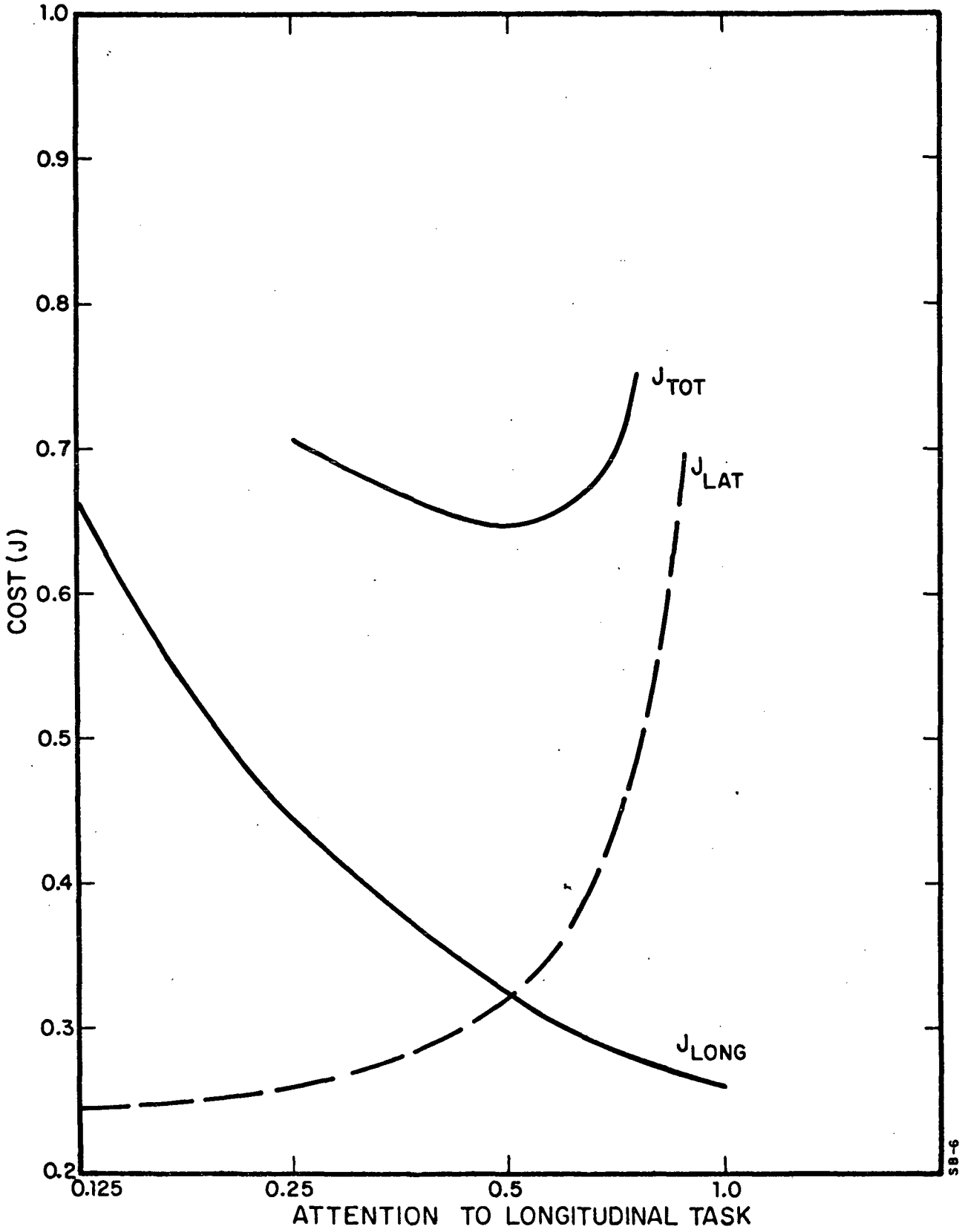

FIGURE 11b. Effect on Optimal "Costs" of Attention Sharing Between Longitudinal and Lateral Tasks (50%-Wind)

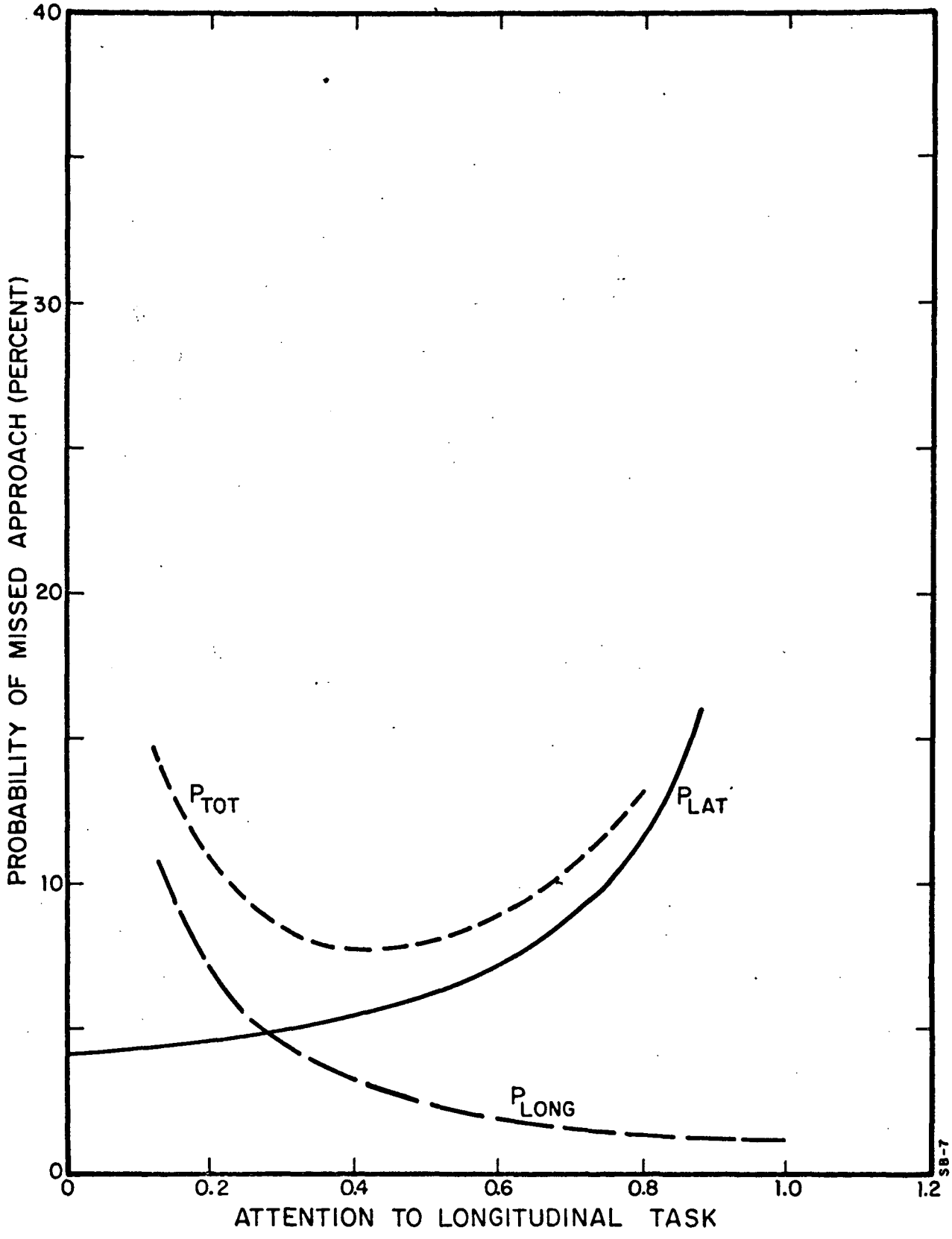

FIGURE 12. Effect on Approach Performance of Attention Sharing Between Longitudinal and Lateral Tasks

probabilities as functions of the relative attention devoted to the tracking task as a whole (assuming, for convenience, "full" attention ≃ -20dB, as before).* The result is plotted in Figure 13. This figure emphasizes the difficulty of the task. When all winds are considered, it does not appear possible to achieve a 95% approach success probability, at least within the range of pilot workload that is assumed acceptable. Even for the 50% wind condition, a success probability of 95% implies a Workload Index of about .9, hardly a desirable situation.

SUMMARY

The performance of the AWJSRA with an "unaugmented"EADI-display of status information was analyzed with the steady-state optimal control model for pilot-vehicle analysis. Both "window" performance and pilot workload were investigated for a range of turbulence conditions.

The results indicate that with the basic display the overall task is quite difficult. When the median wind level is considered, a 95% success probability for approach requires a high workload. If performance is averaged over all possible winds, such a success-probability does not appear to be attainable within a reasonable range of workload.

The lateral-directional task seems to be considerably more difficult than the longitudinal control task, even though

*Thus, in this analysis, the "base" observation noise/signal ratio for the longitudinal and lateral "subtasks" is -17dB. This, in turn, implies that we can't simply add the "relative" attentions for the longitudinal and lateral tasks, to obtain the relative attention for the combined task (that is, of course, the result of interference). It should also be mentioned that combined performance may be computed for any split of attention. The "equal-split" allows us to use earlier computations directly, i.e., without interpolation.

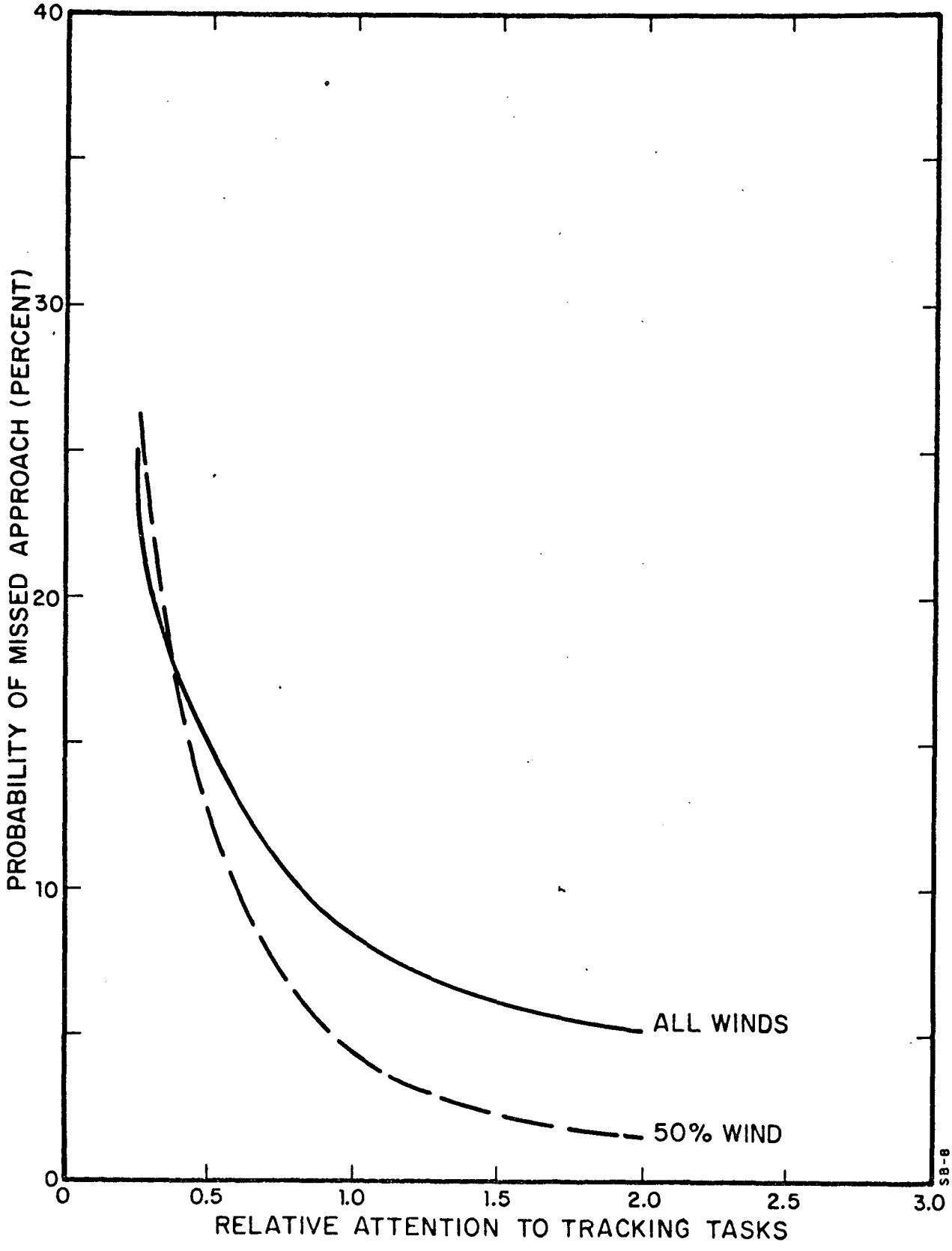

FIGURE 13. Effect of Attention on Missed Approach Probability

stability augmentation is provided for lateral control. For a 95% probability of being within the respective approach window, the lateral task has a workload index of about .63, as compared to a workload index of about .25 for longitudinal control.

Potential improvements to the basic status display were also explored. The greatest effects were observed when better error-rate (sink-rate, lateral error-rate) information was assumed, as might be provided, for example, by a display of longitudinal and lateral flight path angles. Significant effects were also observed when the requirements for attention-sharing were removed. These improvements, as well as a reduction in pilot workload, may be realizable with a flight-director display.

ANALYSIS OF PROPOSED FLIGHT DIRECTOR LAWS

In the preceding chapter it was shown that the unaugmented status display was probably unacceptable both from a closed-loop system performance and a pilot workload standpoint. Appropriately designed flight directors might serve to alleviate many of the problems. In this chapter we analyze potential improvements with a set of proposed "interim flight directors" [17] (or, more exactly, approximation thereto). Our analysis here is confined to steady-state gust regulation; it should be emphasized that the flight director laws we are examining were based on broader concerns, such as wind shear compensation.

Longitudinal Director System

The longitudinal director laws considered herein are simplifications of the interim director laws [17], but should retain the important features of those laws.* The simplifications serve to reduce the computational requirements. A block diagram of the approximate implementation is given in Figure 14. The corresponding gains are those of [17] and are listed in Table 9. A discussion of the basic design rationale for this director system may be found in [18].

*Private communication with R. Klein.

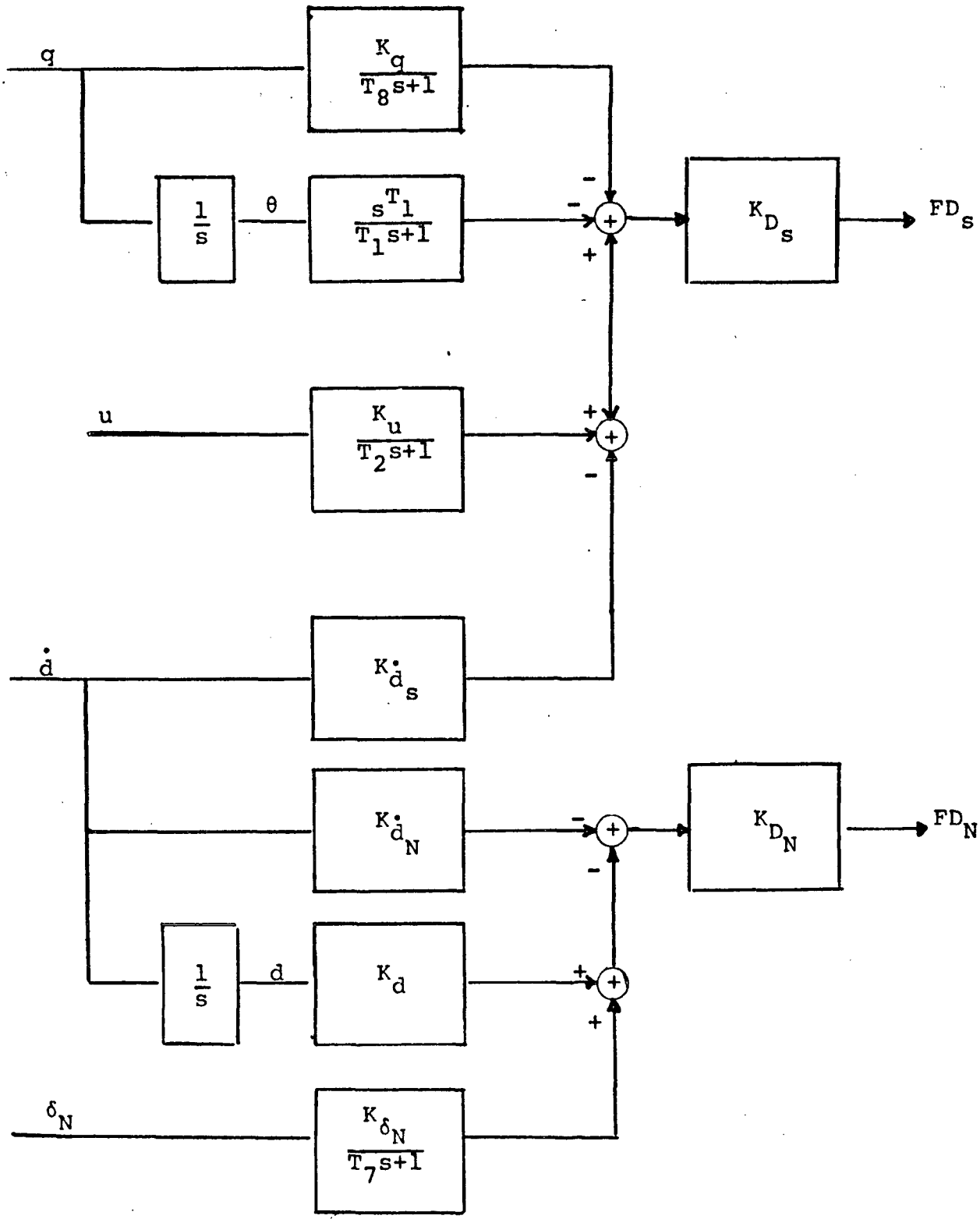

FIGURE 14. Approximate Interim-Directors for Longitudinal Control

Table 9

LONGITUDINAL FLIGHT-DIRECTOR GAINS

K_θ = 1.0 units FD/RAD; T_8 = 1.0 sec

K_q = 1.0 units FD/RAD/SEC; T_1 = 3.0 sec

K_u = .0328 units FD/METER/SEC; T_2 = 1.0 sec

$K_{\dot{d}_s}$ = .0328 units FD/METER/SEC

K_{D_s} = 1 degrees/unit

K_d = 1.62 units FD/METER

$K_{\dot{d}_n}$ = 3.28 units FD/METER/SEC

K_{δ_N} = 30.8 units FD/RAD-NOZZLE DEFLECTION; T_7 = 1.0 sec

Model Parameters

Thresholds for the stick director (FD_s) were set at the basic visual threshold values obtained from remnant studies [4]; given the scaling, the thresholds associated with the nozzle director were neglected. Inasmuch as both directors have zero-references, residual noises were set to zero. Pilot-centered parameters, of time-delay and motor-noise/signal ratio were set to the nominal values of .2 sec and -25dB, respectively; the "base" observation noise/signal ratio, P_o, was -20dB.

Task Requirements

The choice of a suitable cost-functional for analysis of the flight director displays is not so straightforward as in the no-director case. To choose this cost functional one must, in some measure, determine how the pilot interprets the task when a flight director is used. This will, of course, depend on his instructions, and his understanding and training. Four modes of operation suggest themselves as potential pilot strategies:

i) The task is viewed as a simple compensatory tracking task (2-axis, here) with the pilot attempting to minimize mean-squared flight director error.

ii) The task is viewed as being the same as for the no-director situation and the purpose of the director is, essentially, to provide better information.

iii) The director signal is interpreted in terms of its component inputs and its maximum allowable excursion is balanced against "limits" on control and control-rate.

iv) Maintain director errors small while keeping all other variables within bounds.

If the first strategy is assumed, the cost weightings are chosen on the same basis as for laboratory tracking tasks; i.e., only error and control-rate contribute to the score and the control-rate weighting is chosen to yield a desired τ_N. This assumption

has little to recommend it but simplicity* because it ignores flight experience. A few trial runs were made with such a cost functional; they resulted in extremely small tracking errors but unacceptably large control inputs.

If we assume the second strategy to be operative, then we use the same cost functional that was used before. This assumption has within it the implicit notion that the pilot will also use his status displays to assure that untoward vehicle motions are not induced by blind following of the director signal. Choosing this cost functional also has the advantage of providing for a direct, one-to-one, comparison between director and no-director cases. The principal objections to this approach would appear to be that it doesn't emphasize the zero-reader aspects of the use of the directors and it is less acceptable if one considers only director signals to be available.

To implement the third strategy we consider the inputs to the flight director. For example, the stick director signal is scaled so that one degree of pitch error is equivalent to one degree of FD error. Thus, a six degree pitch limit would correspond to a limit of six degrees of FD error. Similarly, the 2.6 m/s airspeed limit would result in about a 5 degree error on the FD. Thus, if the pilot wishes to maintain pitch or airspeed within tolerable limits, he should keep the FD error below 5-6 degrees. At the same time control and control-rate should be maintained within the previously stated limits (Table 2). If this logic is applied to both longitudinal director laws, the cost functional weightings are those given in Table 10.

*And the fact that it works so well in single-loop laboratory tasks.

Table 10

LONGITUDINAL FLIGHT DIRECTOR WEIGHTINGS

Variable	"Limit"	Weighting
FD_s	6(deg)	.028
δ_e	9(deg)	.012
$\dot{\delta}_e$	50(deg/s)	.0004
FD_N	1("DOT")	1
δ_N	29(deg)	.0012
$\dot{\delta}_N$	100(deg/s)	.0001

Analysis of the longitudinal flight director system was carried out using a cost functional corresponding to case (ii) ("standard weightings") and a cost functional corresponding to case (iii) (Director-Weightings). The results are compared below. The fourth strategy mentioned above was not investigated here, although it has substantial face-validity. The reason was that the corresponding cost-functional would be a combination (of sorts) of those for (ii) and (iii). Therefore, we would not expect substantially different results from those we obtained. (Indeed, one might expect the results for (iv) to be intermediate between (ii) and (iii).)

Analysis and Results

Comparison of Performance for Different Weightings. — Performance as a function of observation noise/signal ratio was computed for the 1% and 50% wind conditions and was averaged across winds, as before. It was assumed that only flight director signals were displayed and that attention was divided equally between stick and nozzle directors. The results for the two sets of weightings are presented in Figure 15. Also shown, is the result for the status display. It can be seen that in high workload situations (i.e., relative attention of 1/2 to 2), performance with the status display is nearly as good or better than performance with the flight director, depending on the choice of cost functional. In other words, if the pilot works hard enough, he can do about as well with the status display as with the flight directors. On the other hand, in the range of workload that is likely to be acceptable (1/2 to 1/8 relative attention), the flight director system yields improved performance for a given workload (for both sets of weightings). Moreover, the differences in overall performance obtained with the different weightings are relatively less significant.

It is of interest to examine the nature of the differences between the results for the two sets of weightings. This is illustrated in Figure 16 where height and airspeed performance are compared for the two weighting conditions (for the 50%-wind). It can be seen that the two cost-functionals lead to different performance tradeoffs. Height errors are regulated more tightly in the case where the director signals are weighted explicitly, but at the expense of relative degradation in airspeed regulation.

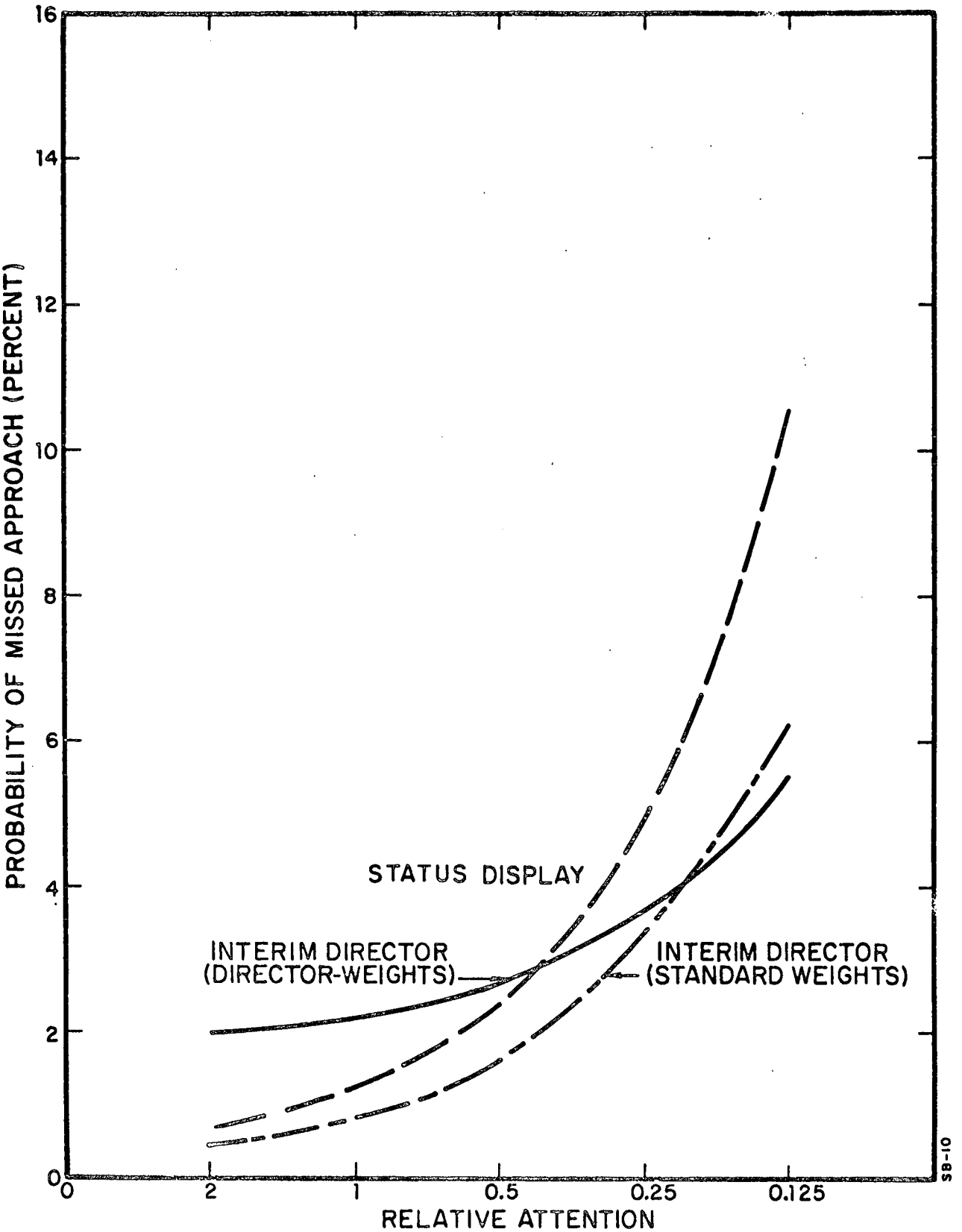

FIGURE 15. Effect of Cost Function on Missed-Approach Probability with Interim Director (Averaged for all-winds)

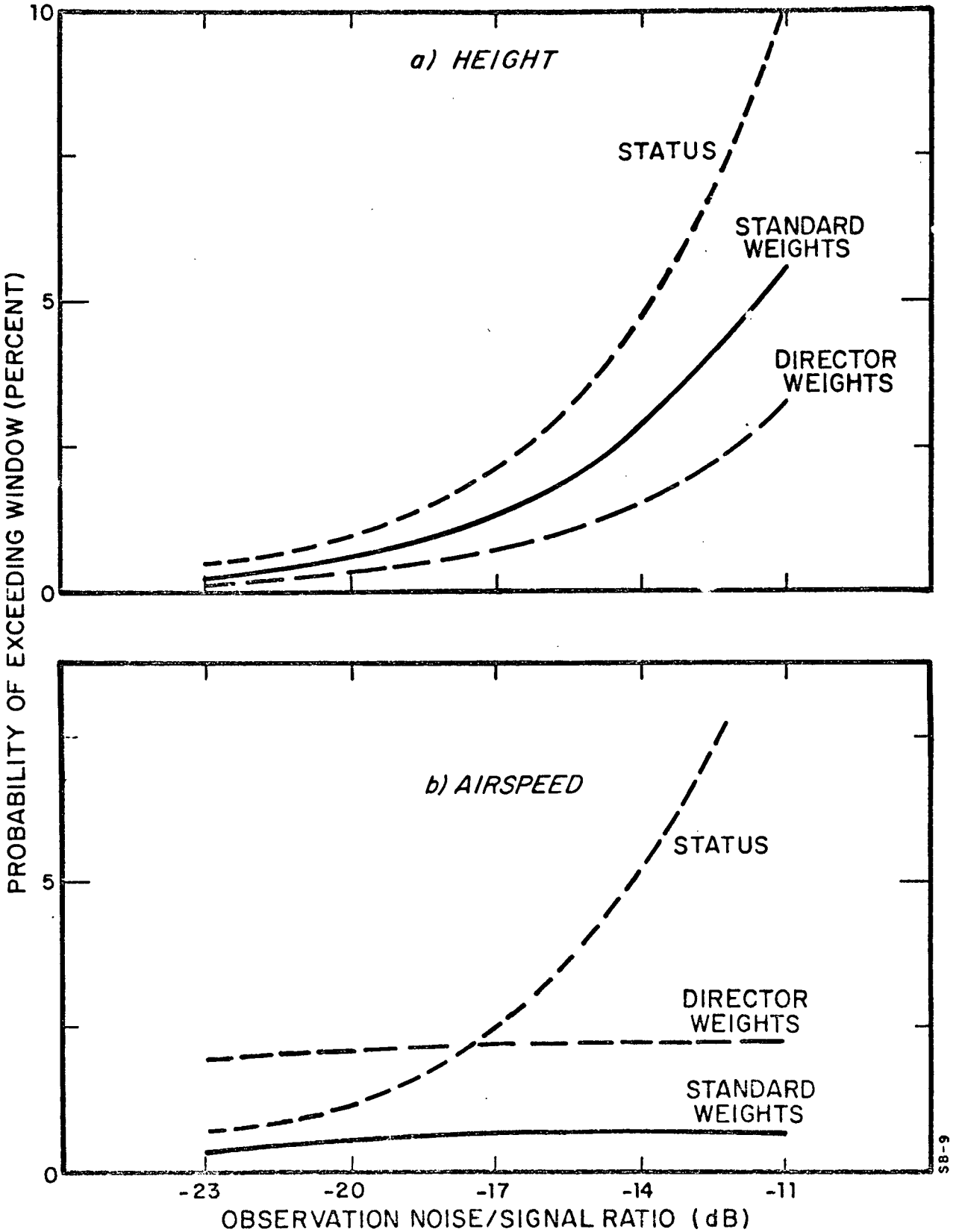

FIGURE 16. Effect of Cost Function on Height and Airspeed Performance with Interim Director (50%-Wind)

For the remainder of this investigation we shall use the standard weightings that correspond to (ii) above. As noted above, we cannot decide *a priori* how the pilot will use the directors and, therefore, what the appropriate cost functional will be. The cost functional corresponding to the standard weightings appears to be a reasonable choice and allows us to make direct comparisons with no-director results. Moreover, the situation in which the pilot uses only director signals is somewhat artificial; we suspect that when other instruments are available, the standard weightings are even more appropriate and, in addition, that the sensitivity to cost weightings is reduced.

Allocation of Attention. When the flight director is presented along with the basic status display, it may be profitable to share attention among the various display elements; in any case, it seems likely that the pilot will do so. To explore this possibility, we conducted a model analysis to determine the optimal allocation of attention between the flight directors and the "standard" instruments of the status display. To simplify the analysis, we considered the directors and the status display as two entities between which total attention was to be shared. Then, the fraction of attention devoted to the flight director as a whole was allocated equally between the stick- and nozzle-director whereas the fraction devoted to the status display was split up among the height, pitch and airspeed in the same proportion as was found to be optimal for the no-director case (namely, .35, .1 and .5, respectively).

Table 11 gives rms scores as a function of attention devoted to the flight director. Results are presented for a high-wind (1%), high-workload (P_o = -20dB) case; and for a median wind (50%), moderate workload (P_o = -14dB) condition. The scores indicate a good deal of insensitivity to allocation of attention, so that devoting anywhere from 25-75% attention to the flight directors is reasonable, with approximately 45% optimal. On the other hand, the results do confirm that it is undesirable to use only the flight directors. It is interesting to note that the penalty for paying full attention to either the flight director or the status is both poorer height regulation and increased stick activity. Airspeed errors and nozzle-control activity are less sensitive to attention but do increase somewhat as attention to the flight directors increases.

Table 11

EFFECTS OF ATTENTION SHARING BETWEEN LONGITUDINAL FLIGHT DIRECTOR AND STATUS DISPLAYS

		ATTENTION TO FLIGHT DIRECTOR						
	VARIABLE	0	.25	.375	.45	.5	.75	1.0
P_o=-20dB								
	σ_h(m)	2.2	1.9	1.85	1.82	1.81	1.84	2.2
1%-wind	σ_u(m/s)	1.33	1.34	1.34	1.35	1.35	1.38	1.46
	σ_θ(deg)	1.51	1.53	1.55	1.56	1.57	1.65	1.94
	$\sigma_{\delta e}$(deg)	1.85	1.74	1.77	1.79	1.81	1.93	2.42
	$\sigma_{\delta N}$(deg)	12	12.2	12.2	12.3	12.3	12.5	13.0
	J	1.31	1.17	1.16	1.15	1.16	1.22	1.57
P_o=-14dB								
	σ_h(m)	1.76	1.25	1.18	1.15	1.14	1.14	1.26
50%-wind	σ_u(m/s)	.57	.56	.56	.56	.56	.58	.60
	σ_θ(deg)	.78	.76	.71	.72	.72	.77	.87
	$\sigma_{\delta e}$(deg)	.95	.84	.86	.87	.88	.97	1.16
	$\sigma_{\delta N}$(deg)	4.33	4.67	4.71	4.72	4.73	4.77	4.78
	J	.44	.30	.29	.29	.29	.30	.37

In Chapter 3, we suggested that the results for the idealized display configuration might be indicative of the maximum performance improvement to be expected from the flight directors. Moreover, a reasonable portion of that improvement would be due to display integration in the sense of a reduction in attention sharing. In Table 12 the scores for the idealized display are compared with those obtained (above) with the flight directors and with the flight director-status combination (assuming optimal

Table 12

COMPARISON OF RMS PERFORMANCE OF IDEALIZED DISPLAY AND FLIGHT DIRECTOR CONFIGURATIONS (1%-wind, P_o = -20dB)

VARIABLE	IDEALIZED	FLIGHT DIRECTOR	FLIGHT DIRECTOR + STATUS (OPTIMAL ALLOCATION OF ATTENTION)
σ_h(m)	1.53	2.2	1.82
σ_u(m/s)	1.30	1.46	1.35
σ_θ(deg)	1.77	1.94	1.56
$\sigma_{\delta e}$(deg)	2.0	2.42	1.79
$\sigma_{\delta N}$(deg)	11.9	13.	12.3

allocation of attention). These results demonstrate that, at least for the worst-case wind condition, the regulation of height errors when the flight director information is available is not as good as might be hoped for. Moreover, the fact that it is optimal to devote about half the attention to the status display, suggests that the director laws are not "integrating" the available information as effectively as possible.

Monitoring performance, as predicted by the ratio of rms estimation error to rms value, for various longitudinal display configurations is shown in Table 13. These results bear out and shed light on those of Tables 11 and 12. It can be seen that monitoring performance for none of the actual display configurations

Table 13

EFFECTS OF DISPLAY CONFIGURATION ON LONGITUDINAL MONITORING PERFORMANCE
(1%-wind, P_o = -20dB)

	IDEALIZED	STATUS	FLIGHT DIRECTOR	FLIGHT DIRECTOR PLUS STATUS
σ_{h_e}/σ_h	.11	.42	.30	.36
$\sigma_{\dot{h}_e}/\sigma_{\dot{h}}$	.33	.60	.49	.53
$\sigma_{\theta e}/\sigma_\theta$	.12	.26	.47	.32
σ_{qe}/σ_q	.09	.16	.24	.19
σ_{ue}/σ_h	.54	.59	.78	.62

approaches that for the idealized display. The use of just the flight directors does lead to improved estimation of height errors but at the cost of a substantial penalty in pitch and airspeed estimation. When the status display is used in conjunction with the flight director a useful compromise among estimation errors for all variables is apparently achieved. Another interesting point is that estimation errors for height and sink-rate are less than for the status display. Apparently, the reduced thresholds and the zero-reference (lower residual noise) of the flight director offset the requirement for the processing of director signals to

obtain estimates of height and sink-rate. On the other hand, pitch, pitch-rate and airspeed are estimated better from the STOLAND status indicators (which are properly scaled and have references) than is possible via processing of the director signals.

Performance and Workload. – It was just shown that improved performance may be obtained when the "interim" longitudinal director is added to the status display. Figure 17 illustrates the average (over all winds) improvement in performance and the reduction in workload that may be expected for this display configuration. We assume that approximately 45% of the pilot's attention is devoted to the flight directors. The combination of status and flight director yields better window performance and a substantially reduced workload when compared with that attainable with either display alone. For example, if the criterion performance level is set at 1%, the workload index for the STATUS-FLIGHT DIRECTOR combination is approximately .45 whereas for either display alone it exceeds 1.0.

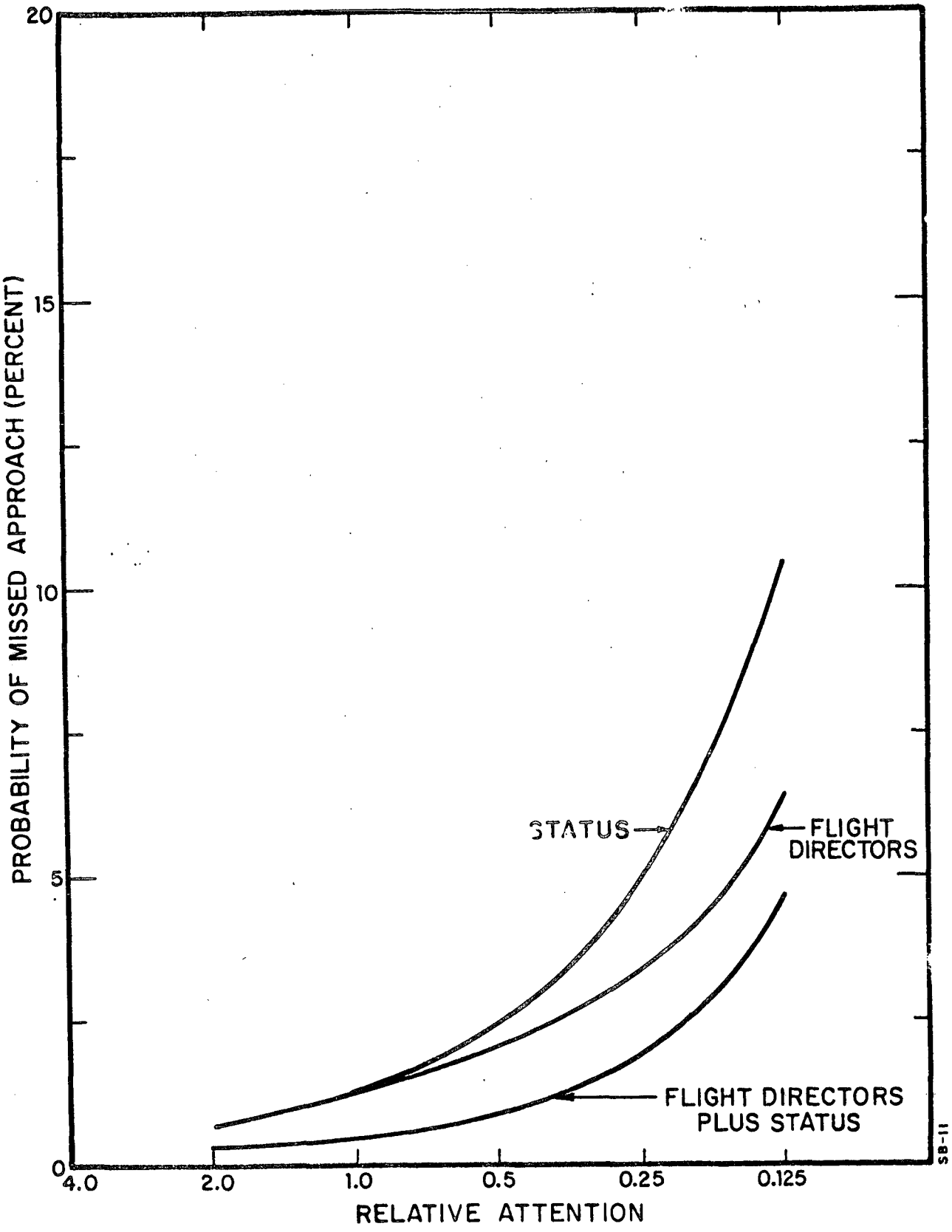

FIGURE 17. Effect of Longitudinal Displays on Missed Approach Probability

Lateral Director System

The proposed "interim" lateral flight director system is described and discussed in [17]. The approximation to that system used here is shown in Figure 18 (along with the representation of lateral dynamics). It should be noted that we assume here that lateral flight path angle may be obtained directly rather than by means of the complementary filtering techniques of [17]. Although this assumption is somewhat unrealistic, the idealization should provide a bound on the performance improvements that can be expected of the more practical system. The gains for the lateral director system are given in Table 14 (they correspond to case 2F of [17]).

Vehicle dynamics for this analysis were the SAS-on, coordinated turn dynamics used previously (Appendix C). Model parameters were all set at nominal values. Thresholds and residual noises were assumed to be negligible for the lateral flight director. Cost weightings were the same as those used in the basic analysis (Table 2B), so we assumed, effectively, the pilot's task is the same when the director is available as it is without it.

Table 14

GAINS FOR INTERIM LATERAL DIRECTOR

K_1	.00638 volts/meter
K_5	1.55 volts/RAD
K_6	1.61 volts/RAD
K_8	1.0 in display/volt
T_1	1.0 sec.

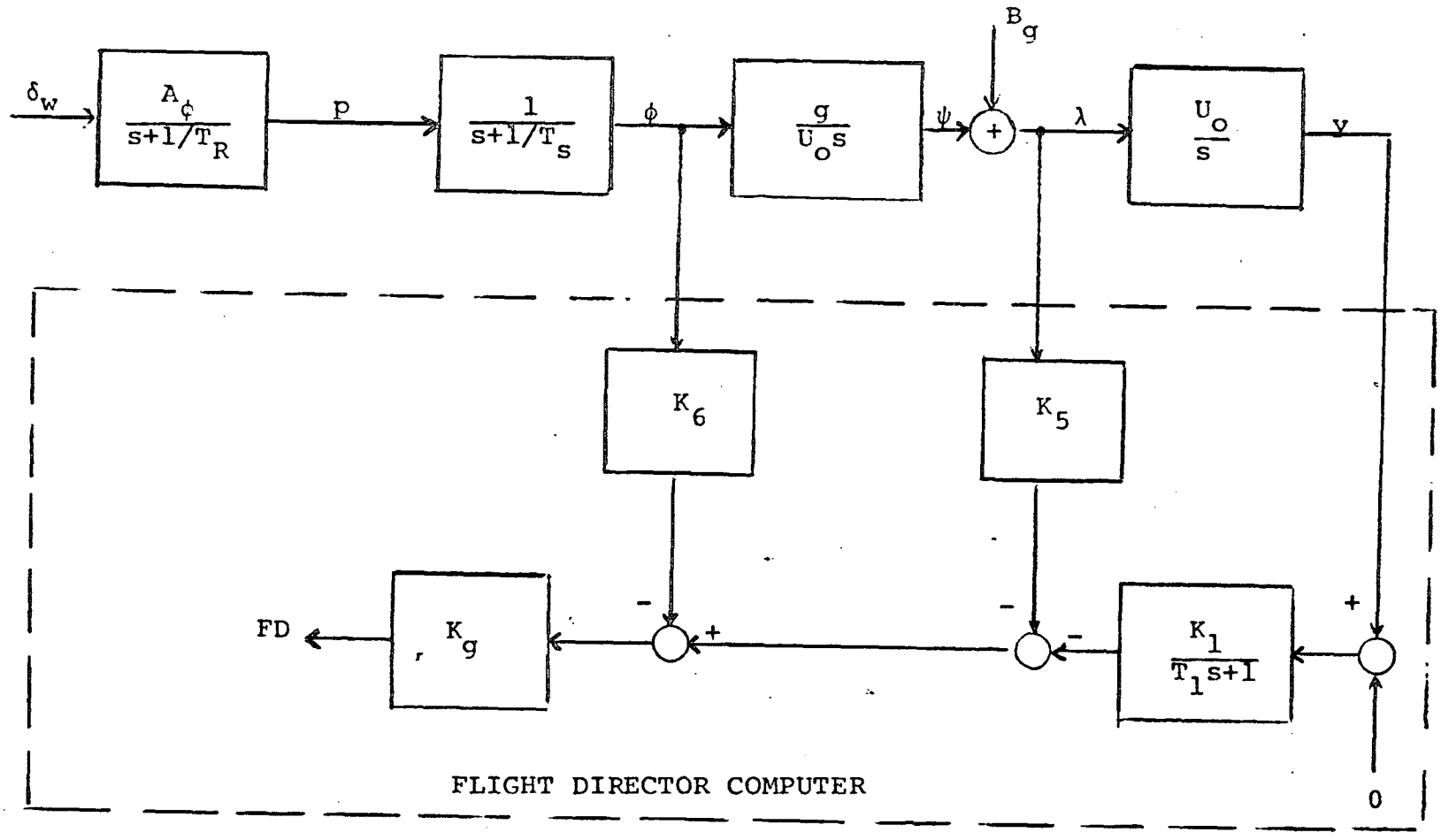

FIGURE 18. Approximation to "Interim" Lateral Director

Analysis and Results

The lateral director system was analyzed in the same manner as was the longitudinal director system. Results are presented below.

Allocation of Attention. — The effects on rms performance of sharing attention between the lateral flight director and the lateral status displays (considered as an entity) are shown in Table 15. It was assumed that the portion of attention devoted to the status displays was allocated between the localizer and bank angle indicators in the approximately optimal 3:1 ratio found in Chapter 3.

Table 15

EFFECTS ON LATERAL PERFORMANCE OF ATTENTION-SHARING BETWEEN FLIGHT DIRECTOR AND STATUS DISPLAY (1%-wind, P_o = -20dB)

	Attention to Flight Director						
Variable	0	.25	.5	.65	.8	.9	1.0
σ_y (m)	5.1	4.9	4.8	4.8	4.7	4.7	4.8
$\sigma_{\dot{y}}$ (m/s)	2.0	1.9	1.9	1.9	1.9	1.9	1.9
σ_ϕ (deg)	5.0	4.8	4.7	4.7	4.7	4.7	4.7
σ_{δ_w} (deg)	10.6	10.1	9.9	9.8	9.8	9.8	9.9
J	1.34	1.22	1.18	1.16	1.15	1.15	1.19

The results indicate that about 80-90% attention to the flight director is "optimal", but they are very insensitive to changes in attention. Referring to Table 8, column E (the idealized display condition), we see that results for the 80% division of attention are quite close to those for the idealized display; lateral error is about 3% greater for the flight director-status combination and other variables are virtually identical. Even when only the flight director is available, there is not a significant increase in lateral error. Monitoring performance, not shown here, exhibited the expected trends (given in the earlier results). In general, then, the attention-sharing results indicate that the "interim" lateral flight director comes closer to achieving the improvements implicit in an idealized display than does the longitudinal-director system. On the other hand, the improvements at this level of attention (-20dB) and wind-condition are far from dramatic indicating that at high workload the status displays perform nearly as well as the director.

Performance and Workload.- The improvement provided by adding the lateral flight director to the display at various "levels" of attention is shown in Figure 19. Averaged over all wind conditions, the probability of a missed approach without the flight director is 1.5 to 2 times greater than with it - at all levels of attention. Moreover, the improvement is greatest in the range of operation (attentions of .5 to .125) that are likely to be most important. The situation for the 50%-wind (also shown in Figure 19) is that the flight director provides even more substantial improvement.

In terms of workload, an approach success probability of 99% is unattainable, with reasonable workload, when all winds are considered; for the 50%-wind, the flight director reduces the

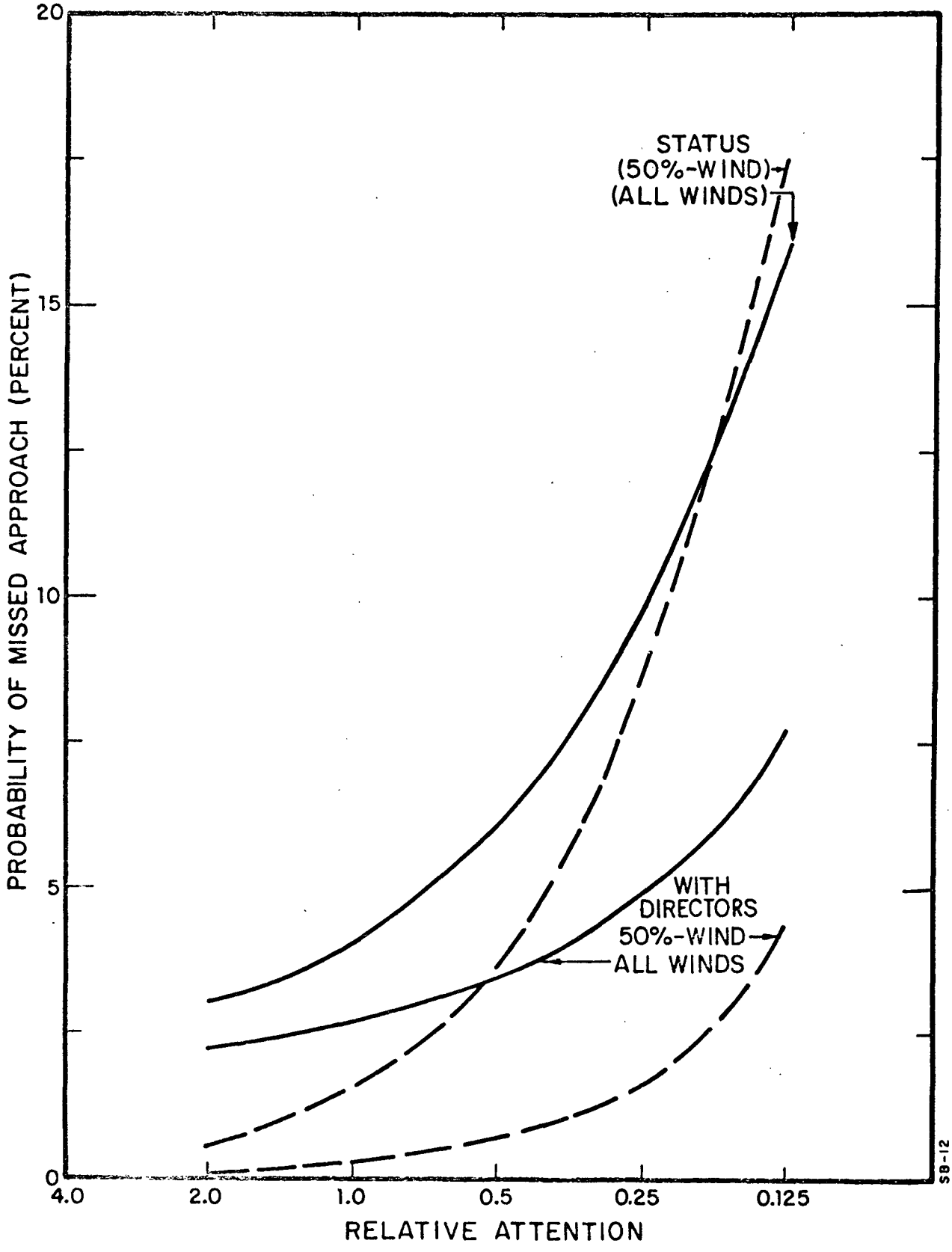

FIGURE 19. Effect of Lateral Director on Missed Approach Probability

Workload Index from about 1.4 to about .3. For the all-winds average, a 95% success probability requires a workload index of about .7 in the no-director case as opposed to about .25 when the director is available. In general, the curves of Figure 19 indicate that addition of the flight director will reduce the lateral workload by a factor of 2-4 for success probabilities that can be achieved, again with greatest improvement in the range of most interest.

Combined Longitudinal and Lateral Performance

The total longitudinal-lateral approach task with the flight directors was analyzed in exactly the same fashion as was the EADI-status display configuration. First, the "optimal" allocation of attention between longitudinal and lateral control was determined, assuming attention sharing within tasks is the "optimal" for that task being performed alone. It was found that attention should be shared equally (approximately) between the longitudinal and lateral control tasks. Given this attention-split the overall missed approach probabilities may be computed as functions of the relative attention devoted to the combined task. The results are presented in Figure 20.

When the average of all-winds is considered, the addition of the flight-directors reduces the miss probability by about a factor of two, with the most improvement in the lower attention levels. Even greater improvement (4-7 times better) is evidenced for the 50%-wind condition. It may be seen in Figure 20a that the missed approaches, for the all-winds average, are due largely to the lateral task; although not shown, this is even more true for the 50%-wind condition. Table 16 illustrates the effect of the flight directors on workload. It can be seen that for the 50%-wind

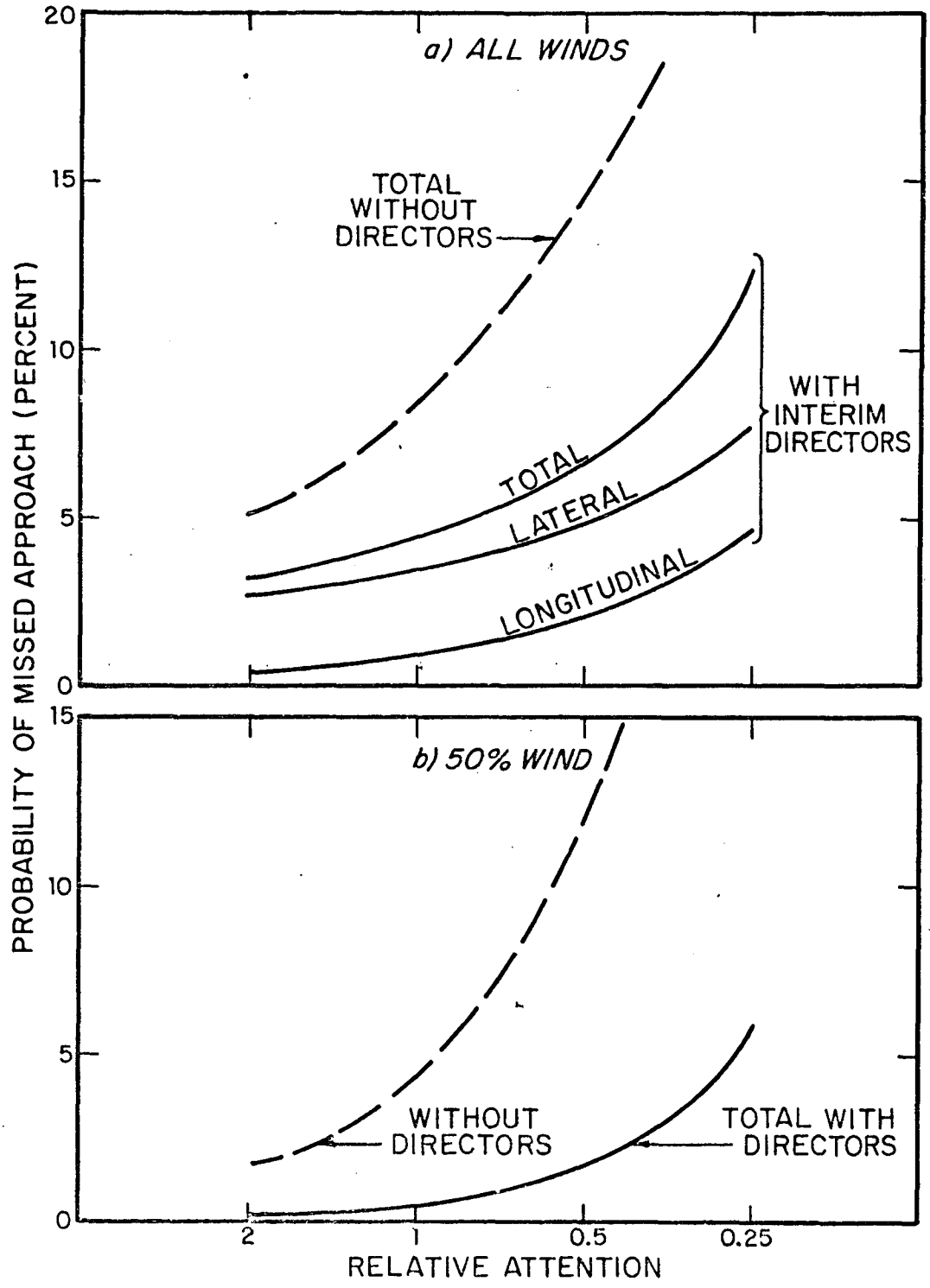

FIGURE 20. Effect of Director Systems on Combined Longitudinal/ Lateral Approach Performance

condition, the directors cut the workload by at least a third in the range of success probability of 95-99%. A similar reduction in workload is possible for the all-winds average, but the probability of success is much reduced. (The workload index for a 95% success probability is about .7 with the directors as opposed to 2 without them.)

Table 16

EFFECT OF INTERIM-DIRECTORS ON WORKLOAD
(50%-wind)

	Workload Index	
Probability of Missed Approach	Without Director	With Director
1%	-	.66
2%	1.6	.47
3%	1.25	.36
4%	1.04	.3
5%	.88	.28

SUMMARY

The addition of the "interim" longitudinal and lateral flight director systems improves performance considerably and reduces pilot workload by a significant amount. When the average of all-winds is considered, reducing the probability of a missed approach to 5% still requires a high workload. However, for the 50%-wind condition workload requirements seem well within capabilities.

C3

Lateral offset errors are largely responsible for the missed approaches. However, the lateral director comes very close to matching the performance that might be obtained with an idealized display whereas the longitudinal director is less successful in this respect. In addition, the attention-sharing studies suggest that the lateral director system is more effective in combining or "integrating" display information than is the longitudinal system. Thus, the poorer lateral performance would appear to be inherent in the dynamics, and further improvement in the lateral-directional axes via better display design may be quite difficult to achieve.

AN APPROACH TO FLIGHT DIRECTOR DESIGN

In the preceding chapter, proposed interim flight director laws were analyzed. These laws were derived on the basis of classical automatic and manual control theory in independent studies [17, 18]. We now describe and analyze a method for designing flight director laws that is based on, and is consistent with, the optimal control model that has been used throughout this investigation.

The approach and the director laws explored here represent only a preliminary attempt at flight director design. Other approaches based on the optimal control model are certainly possible. Moreover, a realistic flight director design procedure would involve consideration of factors (such as wind shears, beam capture) that were neglected in this analysis. Finally, we consider only longitudinal control. Nevertheless, we expect that the preliminary design developed here is sufficient to indicate the degree of performance improvement and workload reduction that is attainable in practice and to demonstrate the design approach.

Director Design Philosophy

Design Goals and Constraints

The basic purpose of a flight director is to reduce the pilot's workload and/or to reduce system errors. In terms of the optimal control model, this goal is accomplished by providing the pilot with information necessary for flight control in such a way that the effects of display-related sources of pilot remnant are minimized.

The director variables must be composed of signals that can be generated by available aircraft measurement devices. These signals are commonly combined in such a way as to make the combined director-vehicle dynamics approximate a K/s-like behavior so that the need for pilot lead is minimized. Considerations of pilot acceptance also suggest that required control inputs and resultant vehicle motions be similar to those that are appropriate to flight with conventional displays. In addition, the director signal should provide the pilot with a good indication of instantaneous flight-path and attitude errors so that frequent reference to status displays is not required.

If the director is a control director, a director signal must be generated for each control variable. It is likely that an ideal design should require little or no pilot coupling. That is, the output of a given director would command a control response along a single dimension.

Preliminary Design Procedure

The preliminary design procedure outlined below allows one to approach many of the above design goals in a relatively straightforward manner. The following design steps have been followed in deriving the control-director laws used in this study:

1. Define the control situation in terms of system dynamics, input characteristics, sensory information, performance cost functional, and pilot parameters.

2. Use the pilot/vehicle model to predict the pilot-generated feedbacks between each display variable and each control variable. These feedbacks are designated as the "internal transfer functions" in the current implementation of the model.

3. Approximate each of the internal transfers by a first- or second-order filter. (This approximation is done primarily to minimize the computational requirements for evaluating the proposed director design.)

4. The commanded control signal is generated by summing the outputs of the transfers between all sensor variables and the control variable appropriate to the director. The director signal is thus expressed as

$$D_i(s) = \sum_j y_j(s) \cdot T'_{ij}(s)$$

where D_i is the director signal appropriate to the i_{th} control variable, y_j is the j_{th} sensor variable, and T'_{ij} is the approximate describing function between the j_{th} sensor variable and the i_{th} control variable.

In essence, the flight director laws are designed to perform the equalization and cross-coupling that the pilot would otherwise have to do. With the director in the system then the pilot's task is basically that of generating a control response proportional to the deflection of the corresponding director indicator. Thus, cross-coupling should be at a minimum, and the pilot's response strategy should be approximately that of

a pure gain at low and mid frequencies. Since the transfers used in generating the director laws are only approximations to the predicted pilot transfers, the compensation provided by the flight director will be suboptimal with respect to the stated mission requirements. Consequently, a certain amount of cross-coupling is expected in the "pilot's" control strategy with the director. If the sensor variables and cost functional used in the design procedure are the same as would apply to the control task with a more conventional display panel, the characteristics of control and vehicle motions should not be appreciably changed by the use of the director. Improvement in performance and work-load reduction will accrue from the reduced effects of pilot-induced noise. If additional sensory information (such as linear and/or rotational accelerations) is used in generating the director signal, further improvement may be expected.

Definition of the Control Situation

The first step of the design procedure calls for a definition of the control situation. A description of the vehicle dynamics, input characteristics, and to a large extent sensory information, are known quantities and can be readily specified in a format appropriate to the pilot/vehicle model. The selection of appropriate cost functional and, in this case, of the model noise/signal ratios requires some careful thought. The choice of cost functional for analysis of flight director performance was discussed in Chapter 4. For the reasons given there (and with the same caveats), we use in this analysis the same cost functional that was employed in the no-director studies.

The selection of model noise/signal ratios for flight director design depends on whether one views the benefit of the director as primarily the reduction of system errors or the reduction of pilot workload. If the pilot is expected to maintain a high level of workload so that he can minimize errors, the noise/signal ratios used in the analysis should be those appropriate to maximal effort. (Observation noise/signal ratios of -20dB and motor noise/signal ratios of -25dB are nominal values.) On the other hand, if the director is intended mainly to allow the pilot to maintain performance with reduced workload, then the director should be optimized for substantially larger noise/signal ratios.

Although a director designed for a low-noise situation will allow better performance under conditions of maximal effort, the alternative design will be less sensitive to pilot noise and should thus be more "forgiving" of non-optimal pilot behavior. Accordingly, the director laws designed and evaluated in this section have been obtained by computing predicted pilot describing functions for a high-noise situation.

Derivation of Director Laws

Pilot describing functions were obtained from a steady-state analysis of pilot/vehicle performance under conditions of high noise/signal ratios. Vehicle dynamics and input characteristics were the same as those used in previous analysis and the same cost functional was used to describe mission requirements (Table 2A). Wind gust intensities corresponded to the "1-percent" wind condition. The sensory variables used in designing the director

laws were the same as those assumed to be obtained from the STOLAND display (glide path error and rate, pitch error and rate, and airspeed error). No additional acceleration inputs were considered.

A time delay of 0.2 seconds was assumed for the pilot, and both observation and motor noise/signal ratios were set at -10dB. Attention-sharing was assumed not to be a factor, and thresholds and residual noise sources were ignored.

The internal pilot describing functions (magnitudes only) are shown for the elevator and nozzle controls in Figures 21 and 22, respectively. In the process of deriving the flight-director laws, these curves were approximated by transfer functions of second-order, critically-damped, low-pass filters. In order to minimize the number of state variables needed to describe the director characteristics, the critical frequencies of all responses corresponding to a given control variable were made identical. Thus, each of the two director signals was represented as follows:

$$D_i(s) = \sum_j K_{ij} \cdot \left(\frac{1}{1+s/\omega_i}\right)^2 y_j(s)$$

where ω_i is the critical frequency of the filter associated with the i_{th} control variable and K_{ij} is asymptotic low-frequency behavior of the approximate transfer function relating the i_{th} control variable to the j_{th} sensory input.

Second-order approximations to the predicted internal describing functions were obtained by visual inspection. The resulting director parameters are shown in Table 17. The units of the low-frequency gains are in terms of relevant display and

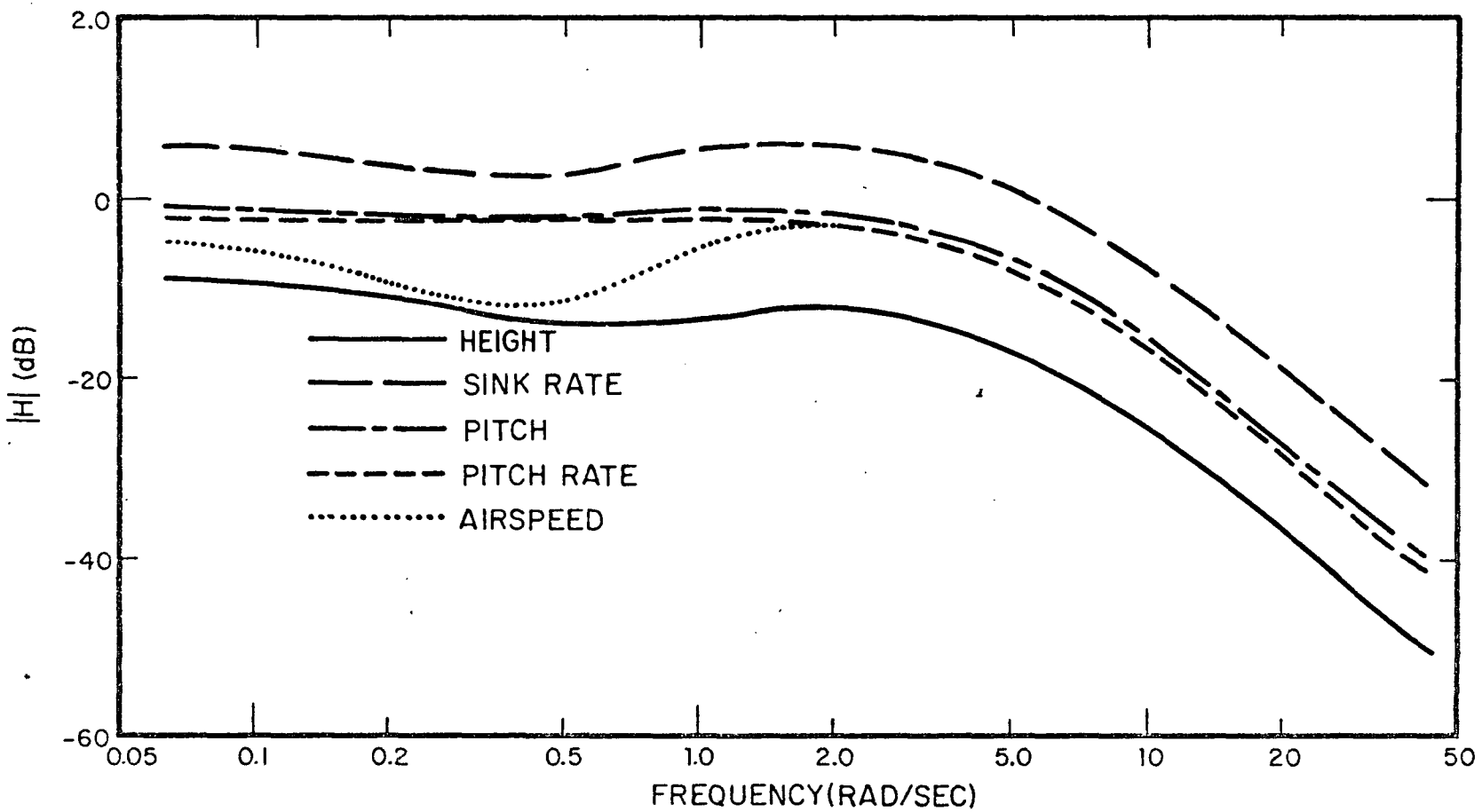

FIGURE 21. Magnitudes of Internal Describing Functions for Elevator Control

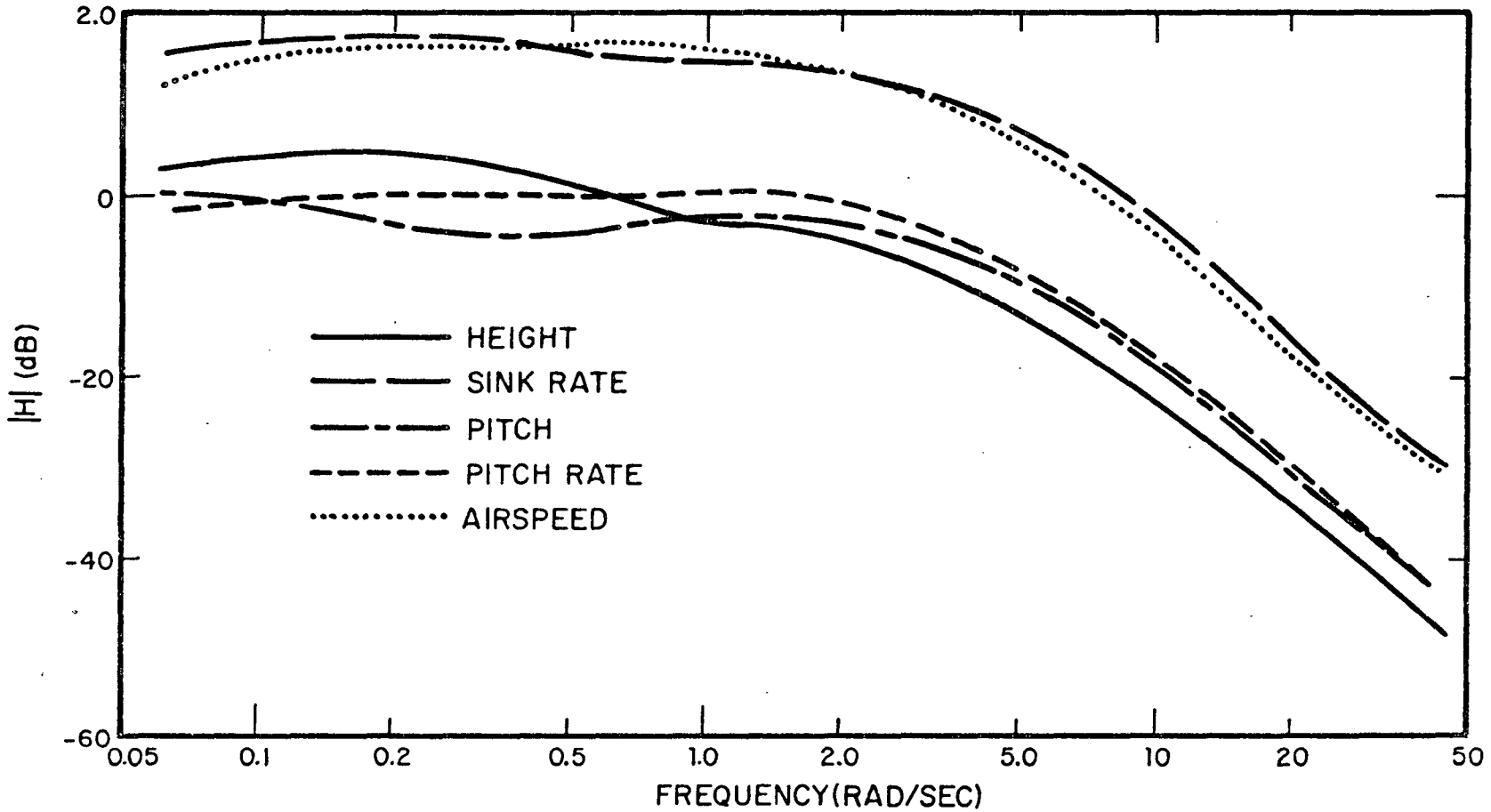

FIGURE 22. Magnitudes of Internal Describing Functions for Nozzle Control

control variables. For example, the gain associated with the contribution of height information to the elevator director has units of degrees (of control surface deflection) per meter (of height error). Critical frequencies are in radians/second. In the subsequent discussion, we shall refer to the directors using these parameters and laws as "model-based directors".

Table 17

PARAMETERS FOR MODEL-BASED LONGITUDINAL DIRECTOR LAWS

Director	Sensory Variable	Critical Frequency	Low-Frequency Gain
Elevator	Height	5.0	0.25
	Sink Rate		1.8
	Pitch		0.9
	Pitch Rate		0.8
	Airspeed		0.5
Nozzle	Height	3.5	1.1
	Sink Rate		6.3
	Pitch		0.8
	Pitch Rate		1.0
	Airspeed		6.3

Analysis and Results

As opposed to the design phase, motor noise/signal ratios were fixed at approximately -25dB, and observation noise/signal ratio was a parameter for the analysis. Attention was assumed to be shared equally between the elevator and nozzle director signals. (No attempt was made to find the optimal allocation of attention. On the basis of previous analysis, it was assumed that performance would be relatively insensitive to attentional allocation.) Thresholds for the stick and nozzle directors were set at the same values that were used for the analysis of the interim directors. Other model parameters were the same as those used in the design of the laws for the directors.

Performance. — Predicted rms performance scores for the 1%-wind condition and an observation noise/signal ratio of -20dB are shown in Table 18. Also shown for comparison are the scores predicted for the status display without a flight director (Condition A of Figure 8) the scores associated with the idealized display condition (Condition F of Figure 8), and the scores for the interim director. The interim director results are presented as a matter of interest and comparison of them with model-based director results is not wholly warranted. The interim director design and analysis were based on slightly different dynamics (See Appendix C). Furthermore, the interim director design did consider a number of factors other than gust regulation. On the other hand, comparison of model-based director results with those of the basic status- and idealized-display conditions is entirely appropriate.

The performance variable most effected by display parameters is the rms height error, as expected from previous results. The score predicted with the flight director is about 26% less than the score predicted for the status display. (The idealized display yields about a 35% reduction with respect to the status display.) A similar reduction is predicted for the sink rate error score. A reduction of about 10% is predicted for rms stick and stick rate. Other performance scores are virtually unchanged.

Table 18

COMPARISON OF RMS PERFORMANCE WITH VARIOUS DISPLAY CONFIGURATIONS

(1%-wind, P_o = -20dB)

Variable	Display Condition: Without Flight Director, Status	Without Flight Director, Idealized	With Flight Director, Interim	With Flight Director, Model-Based
σ_h (m)	2.3	1.5	2.2	1.7
$\sigma_{\dot{h}}$ (m/s)	.68	.55	.72	.55
σ_θ (deg)	1.8	1.8	1.9	1.8
σ_q (deg/s)	1.2	1.2	1.6	1.1
σ_u (m/s)	1.3	1.3	1.46	1.3
σ_{δ_e} (deg)	2.1	2.0	2.4	1.9
$\sigma_{\dot{\delta}_e}$ (deg/s)	7.4	7.0	8.9	6.6
σ_{δ_N} (deg)	12.	12.	13.	12.
$\sigma_{\dot{\delta}_N}$ (deg/s)	21.	21.	23.	21.

Except for improved flight-path performance, then, vehicle motions and control responses are essentially the same with and without the model-based flight director.

Estimation or monitoring performance for the above case is quite interesting and is shown in Table 19. It may be seen that height estimation-errors are greater percentage-wise than for any of the other configurations. Pitch, pitch-rate and airspeed estimation performance for the model-based director is about the same as for the status display and better than for the interim director; sink-rate errors are smaller than for obtained with STOLAND and the same as for the interim director. Thus, when compared with the status display, the improved height-regulation evidenced in Table 18 appears to be the result of better sink-rate estimation (even though height errors themselves are not so well estimated). On the other hand, the improvement in performance over the interim director seems to result from better estimation of pitch and airspeed.

Table 19

MONITORING PERFORMANCE FOR MODEL-BASED DIRECTOR SYSTEM

(1%-wind, P_o = -20dB)

	Display			
Variable	Idealized	Status	"Interim" Director	"Model-Based" Director
σ_{h_e}/σ_h	.11	.42	.30	.56
$\sigma_{\dot{h}_e}/\sigma_{\dot{h}}$	.33	.60	.49	.48
$\sigma_{\theta_e}/\sigma_{\dot{\theta}}$	.12	.26	.47	.28
σ_{q_e}/σ_q	.09	.16	.24	.18
σ_{u_e}/σ_u	.54	.59	.78	.59

Allocation of Attention. – To assess the extent to which the flight director is providing the required "mix" of system variables, the effects of sharing attention between the model-based director and the status display were investigated (Table 20).* The "optimal" allocation to the flight director is to devote 80-90% attention (recall, for the interim directors about 45% to the directors was optimal). Again, the results are highly insensitive to the exact allocation. However, unlike the case of the interim director, in this case devoting full attention to the flight directors imposes virtually no penalty. Thus, it appears that the model-based director laws provide signals that are an effective mix of the system variables.

Table 20

EFFECTS OF ATTENTION-SHARING ON PERFORMANCE WITH MODEL-BASED FLIGHT DIRECTOR

(1%-wind, P_o = -20dB)

	Attention to Flight Directors						
Variable	0	.4	.5	.75	.8	.9	1.0
σ_h(m)	2.2	1.77	1.75	1.72	1.72	1.72	1.75
σ_u(m/s)	1.33	1.32	1.32	1.32	1.32	1.32	1.32
σ_θ(deg)	1.51	1.76	1.76	1.76	1.76	1.76	1.76
σ_{δ_e}(deg)	1.85	1.99	1.98	1.96	1.96	1.95	1.94
σ_{δ_N}(deg)	12.0	12.0	12.0	12.1	12.1	12.2	12.3
J	1.31	1.14	1.13	1.12	1.11	1.10	1.12

*As in the earlier studies of Section 4, it was assumed that the flight directors and status displays could be considered as entities, with attention within these entities divided as before.

Workload. — In order to assess the degree to which workload can be reduced by the use of the flight director, we examine the relationship between the probability of a "missed approach" and "attention". A missed approach is defined, as before, as the situation where either height and airspeed errors exceed their respective "limits" of 3.7 meters and 2.6 meters/second. Attention is related inversely to the observation noise/signal ratio, with a relative attention of unity associated with a ratio of -20dB.

The relation between predicted performance and attention is shown for the 1%-wind condition in Figure 23a. In addition to results for the model-based director, curves for the status display and the interim director plus status display combination* are shown for comparison. For the 1%-wind condition performance is still poor for the model-based directors, but it is appreciably better than for either of the other display configurations. In particular, the model-based flight director reduces significantly the sensitivity of performance to observation noise (both display-related and human related) and, therefore, shows relatively greater improvement at lower levels of pilot attention. This is very evident in the 50%-wind case (not shown) where, with the model-based director, the probability of a missed approach is essentially zero throughout the range of attention-levels investigated. This insensitivity was, of course, a prime objective of the design approach.

*Recall that performance and workload for the combination was better than that for the interim director alone.

The effect of attention on performance averaged across gust conditions is shown in Figure 23b. The value of the flight director is now even more apparent. The predicted workload requirements are substantially lessened even for relatively stiff performance demands. For example, if we require a 99-percent probability of a successful approach, a relative pilot attention of slightly greater than unity is required when no director is provided. The interim director-status combination reduces this "attentional demand" by about a factor of 2 (i.e., to .4 - .5). With the model-based director, however, attention requirements are reduced by about a factor of 10. Conversely, performance is improved for a pilot operating at a constant level of attention. For a relative attention of 1/4 the predicted probability of a missed approach is reduced from about 5 percent for the status display and 2 percent for the interim-director-status combination to around .6 percent for the model-based director.

Predicted Pilot Describing Functions. — One of the design goals set forth earlier was that the flight director should allow the pilot to adopt a control strategy that resembles a simple gain at low and mid frequencies. We predicted that the design procedure adopted in this study would meet this requirement by allowing the director laws to perform the required equalization. It was also anticipated that cross-coupling in the pilot's response strategy would be unnecessary with a properly designed set of flight directors.

Inasmuch as the model for the pilot is relatively "free form", pilot transfers will in general be predicted between all display and all control variables. Thus, for the control situation investigated here, there are two sets of predicted

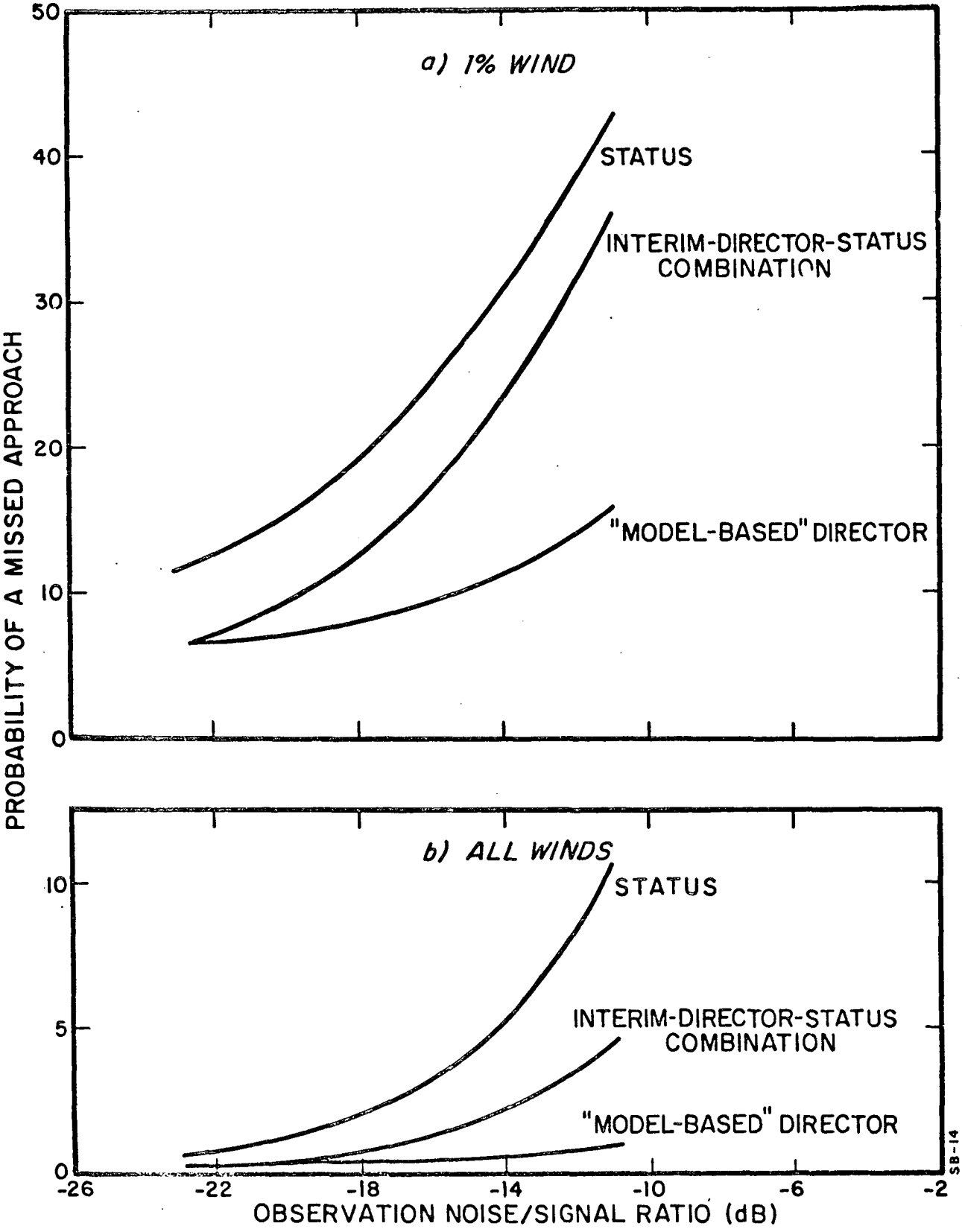

FIGURE 23. Effect of Attention on Missed Longitudinal Approach for "Model-Based" Directors

pilot describing functions to consider: the "direct" transfers which relate each control response to the corresponding director command, and the "cross" transfers which relate control responses to commands on non-associated directors. In cases where pilot cross-coupling is unimportant, the magnitudes of the predicted cross transfers should be numerically small.

The predicted direct transfers are shown in Figure 24. As expected, these transfers approximate a pure gain at frequencies up to about 4 rad/sec (which is beyond gain-crossover for flight-path and attitude control). The high-frequency peaks in the amplitude ratios are typical of actual pilot response behavior obtained in K/s tracking situations.

Predicted cross transfers are shown in Figure 25. The frequency-dependency of the phase-shift indicates that both describing functions are non-minimum-phase (i.e., there are zeros which have positive real parts).

In order to determine whether or not the magnitude of the cross transfers are small enough to be neglected, we must compare the open-loop describing functions for the direct and cross paths. (The open-loop transfer is defined as the cascade combination of a predicted pilot describing function and the associated vehicle transfer function.) Such a comparison (not shown graphically in this report) reveals that the magnitudes of the cross control paths are <u>not</u> substantially less than the magnitudes of the direct paths at all frequencies. Thus, we cannot claim that the predicted pilot cross couplings are numerically small.

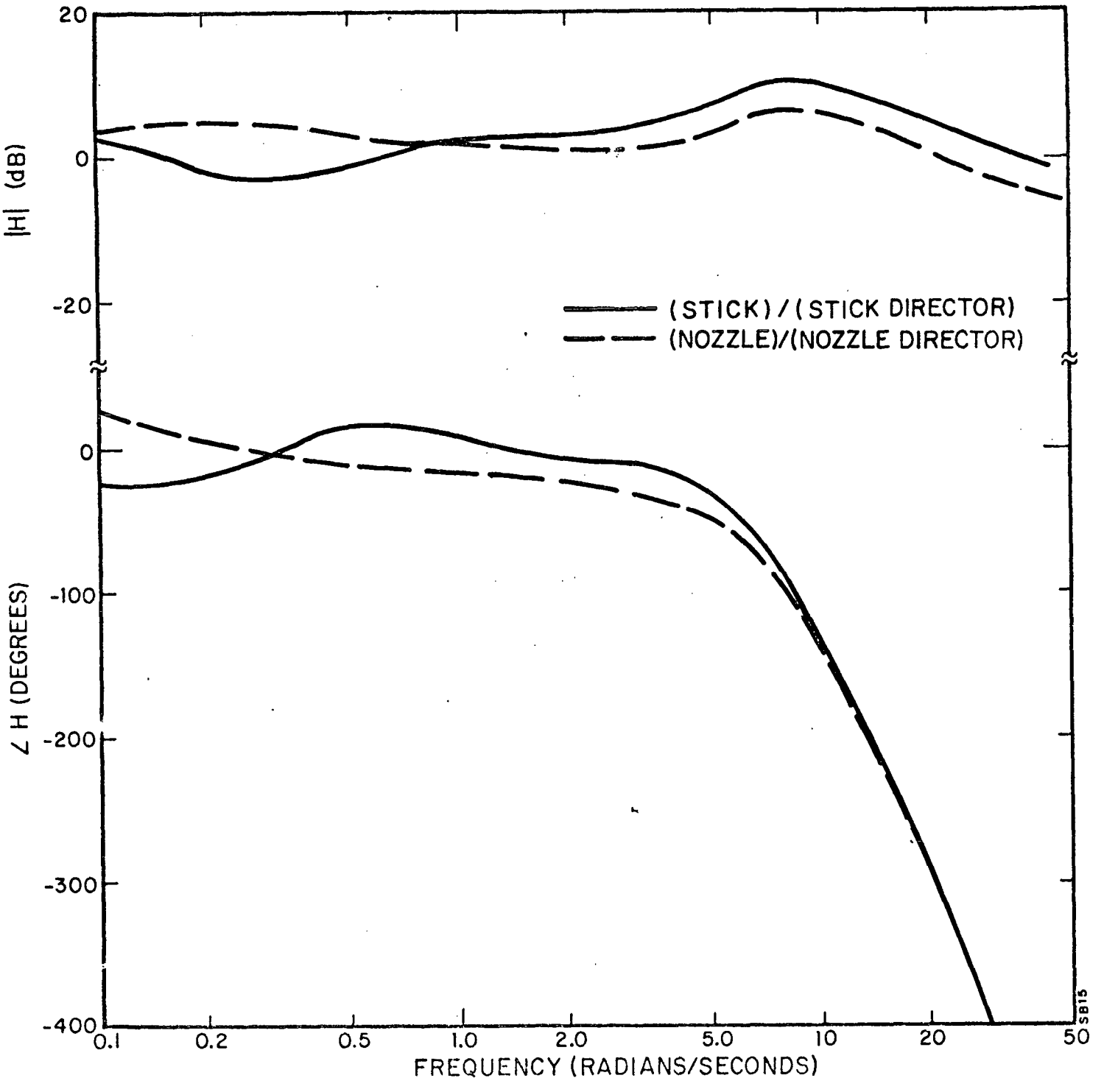

FIGURE 24. Predicted Director-Control Describing Functions: "Direct" Transfers

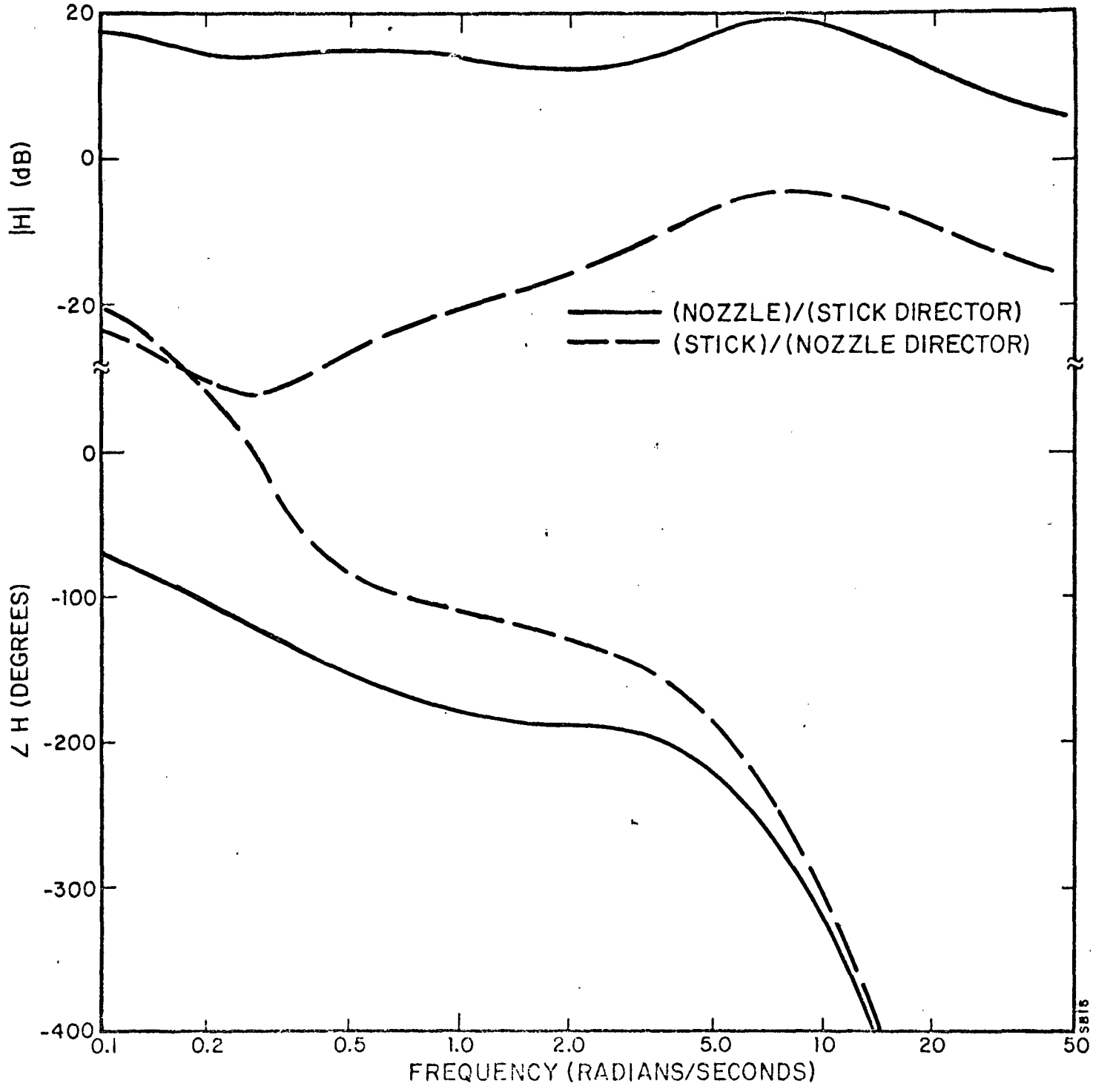

FIGURE 25. Predicted Director-Control Describing Functions: "Cross" Transfers

A true test of the importance of cross-coupling would be to determine the levels of performance and workload that would be obtained if cross coupling were prohibited. There is no simple way to make this test at present, however, because current implementation of the pilot/vehicle model does not allow for such a constraint on the predicted control strategy. Thus, it is presently not possible to determine conclusively whether or not the pilot must introduce cross-coupling in order to realize the benefits of the flight director.

SUMMARY

In this section, an approach to designing flight director laws based on the "optimal-control model" of the human operator was suggested. Director laws for longitudinal control were developed using this approach. These were evaluated in the same fashion as was the status display and interim-director analyzed previously. It was found that the model-based director provided improved performance at substantially reduced workloads and thus achieved its major design objectives. On the other hand, the results do not substantiate the belief that the need for control cross-coupling would be reduced by this design procedure. Further work is necessary to evaluate this aspect of the design.

It should be reemphasized that the design procedure presented here is only in a preliminary stage. Consideration was not given to aspects of the design, other than gust regulation, and design compromises that are perhaps inevitable in practice were unnecessary here. Nonetheless, we believe the results to be highly encouraging and worthy of further investigations.

RESPONSE TO WIND SHEARS

In previous chapters, we have examined the performance of proposed vertical situation displays in gust-regulation tasks. Steady-state analysis was used to evaluate performance and workload at the approach window. However, the pilot's control task involves more than gust-regulation. An important aspect of his task is compensation for errors introduced by winds with a non-zero mean component. These "mean-winds" will, in general, vary with altitude. The rate of variation of mean-wind speed with altitude is referred to as the shear variation. In the sequel, we shall often refer to these altitude-dependent winds as wind-shears.

The mean-wind may, itself, be described in statistical terms, i.e., the wind direction and speed is a random variable. However, in a given approach-to-landing, a specific "sample" mean-wind is encountered. It is the response to some particular samples that we shall be concerned with here, rather than to the distribution as a whole.

As noted in Chapter 2, the modification of the optimal control model for the human operator to account for pilot adaptation to disturbances with a "time-varying" mean is described in Appendix A and the equations needed to compute the response to a particular "sample" disturbance are given in Appendix B. It is noteworthy, that the computed model-response to a sample-disturbance is a random variable because of the inherent randomness of the human. In other words, the model predicts the distribution of responses that would be obtained if the approach were repeated by the pilot a number of times (theoretically, an infinite number) with the same

"sample" disturbance. For this analysis, we shall assume that the system disturbances will consist of "sample"-shears and turbulence that is described as in Equation (12), Chapter 3. Therefore, there will also be a random component of the response that is attributable to the statistical model for turbulence.

Longitudinal Analysis

Modelling the Wind-Shears. – In modelling the wind-shear effects there are both dynamic and kinematic effects to consider. In addition, from the standpoint of implementation of the optimal control model, it is desirable (though not necessary) to convert the altitude dependence of the shear to an "equivalent" time dependence. In this section we discuss the approach taken to these issues concerning modelling of the wind-shears. We consider only the horizontal wind-shears.

Figure 26 illustrates the pertinent geometry. The aircraft's altitude (h) is given by

$$h = h_n + \delta h = R \tan \Gamma_o + \delta h \qquad (16)$$

where h_n is the "nominal" altitude, i.e., the altitude of the glide-slope at the aircraft's range, R, and δh is the altitude error. The rate of change of the nominal altitude may be expressed in terms of the ground speed (or range-rate).

$$\dot{h}_n = \dot{R} \tan \Gamma_o \simeq (U_o + u) \tan \Gamma_o \qquad (17)$$

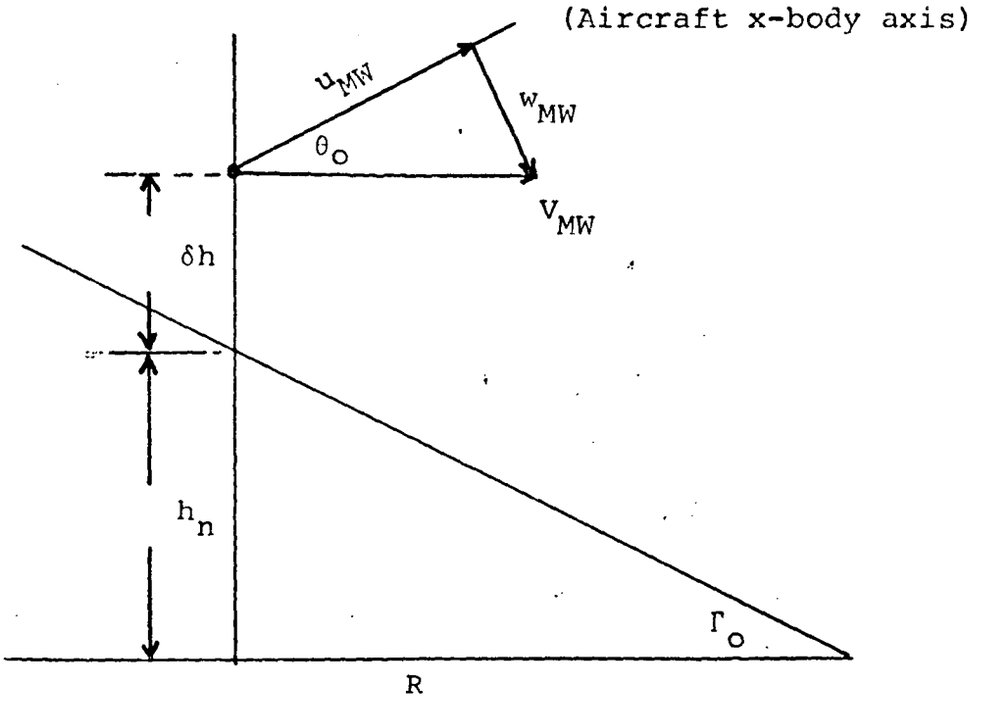

FIGURE 26. Geometry for horizontal wind-shear analysis (not to scale)

where

u = perturbation in ground speed

U_o = nominal airspeed

The aircraft's sink-rate is

$$\dot{h} = V \sin \gamma \approx (U_o + u) \sin (\Gamma_o + \Delta\gamma)$$

$$\approx (U_o + u) (\sin \Gamma_o + \cos \Gamma_o \cdot \Delta\gamma)$$

and

$$\dot{\delta h} = \dot{h} - \dot{h}_n$$

$$\approx (U_o + u) \cos \Gamma_o \cdot \Delta\gamma = (U_o + u) \cos \Gamma_o \cdot (\theta - \alpha)$$

or

$$\dot{\delta h} \approx (U_o + u) \cos \Gamma_o \cdot \theta - \left(\frac{U_o + u}{U_o}\right) \cos \Gamma_o \cdot w \qquad (18)$$

Let u_a and w_a be the zero-wind longitudinal and vertical airspeed perturbation components and

$$\left.\begin{aligned} u &= u_a + u_{MW} \\ w &= w_a + w_{MW} \end{aligned}\right\} \qquad (19)$$

Then, the dynamic effects of the shears are accounted for by modifying the equations of motion (Appendix C) to*

$$\left.\begin{aligned} \dot{u} &= X_u\,(u - u_{MW} + u_g) + X_w\,(w - w_{MW} + w_g) + \ldots \\ (1-Z_{\dot{w}})\dot{w} &= Z_u\,(u - u_{MW} + u_g) + Z_w\,(w - w_{MW} + w_g) + \ldots \\ \dot{q} &= M_u\,(u - u_{MW} + u_g) + M_w\,(w - w_{MW} + w_g) + \ldots \end{aligned}\right\} \quad (20)$$

Equation (18) is used to account for kinematic effects (in the sense that the equation for altitude errors in Appendix C is no longer valid). However, Equation (18) is nonlinear if u is substantial, as is the case for the winds to be considered here. Rather than neglect the nonlinear terms in (18) we shall use the "average" wind velocity during approach in computing glide-path errors. Thus, if $u_{MW}(0)$ is the initial wind velocity and Δu_{MW} is the change in wind velocity during the approach, we let

$$\left.\begin{aligned} \dot{\delta h} &= \bar{U}\cos\Gamma_o \cdot \theta - \frac{\bar{U}}{U_o}\cos\Gamma_o \cdot w \\ \bar{U} &= U_o + u_{MW}(0) + \Delta u_{MW}/2 \end{aligned}\right\} \quad (21)$$

This choice tends to minimize the maximum error associated with assuming constant ground speed for linearization purposes.

The wind-shears to be considered here are enumerated in Table 21. These winds are idealizations of more exact models for mean-winds. They were used in this analysis so as to be compatible with a concurrent simulation study at Ames Research Center. We now show how these winds may be represented as time-varying disturbances; it turns out that this can be done with considerable fidelity.

*X_u, X_w, Z_u, Z_w, $Z_{\dot{w}}$, M_u and M_w are dimensional stability derivatives.

Let U_{MW} be the longitudinal (along track) wind component of interest (crosswinds may be treated analogously). Given the profiles of Table 21, we may write

$$U_{MW} = U_{MWO} + a\ h \tag{22}$$

where a is the change in windspeed with altitude, i.e., the shear-variation. Thus, using (17)

$$\dot{U}_{MW} = a\ \dot{h} \approx a\ \dot{h}_n = a(U_o + u)\ \tan \Gamma_o \tag{23}$$

Differentrating (23) gives

$$\ddot{U}_{MW} = (a\ \tan \Gamma_o)\dot{u} \tag{24}$$

This equation along with the dynamical equation for $\dot{u}$ (Equation (20)) allows the wind shear to be expressed in terms of other, non-input related, state-variables. An even simpler representation is possible and seems warranted in terms of the objectives of this study. If we assume that the pilot attempts to maintain airspeed ($u_a \approx 0$), then Equation (19) implies that we may substitute u_{MW} for u in Equations (23) and (24). But

$$u_{MW} \simeq U_{MW} \cos \theta_o \tag{25}$$

and, the state-variable representation for the mean wind is

$$\left.\begin{aligned} \dot{x}_1 &= \dot{U}_{MW} = x_2 \ ;\ x_1(0) = U_{MW}(0) \\ \dot{x}_2 &= \ddot{U}_{MW} = (a\ \tan \Gamma_o \cos \theta_o)\dot{U}_{MW} \\ &= (a\ \tan \Gamma_o \cos \theta_o)x_2 \ ;\ x_{2_{so}} = a(U_o + u_{MWO})\tan \Gamma_o \end{aligned}\right\} \tag{26}$$

where $x_{2_{so}}$ is the mean-wind velocity at the onset of the shear.

In Equation (20), we set $w_{MW} = U_{MW} \sin \theta_o$, completing the model for horizontal wind-shears.

Table 21

WIND-SHEARS FOR LONGITUDINAL AND LATERAL ANALYSIS

Wind	Initial Altitude	Initial Speed	Final Speed	Final Altitude
Decreasing Tailwind	152m(500 ft)	$15.45\frac{m}{s}$(30KTS)	$5.15\frac{m}{s}$(10KTS)	0
Increasing Tailwind	152m	$-5.15\frac{m}{s}$(10KTS)	$+5.15\frac{m}{s}$	0
Increasing Crosswind	152m	$-2.575\frac{m}{s}$(5KTS)	$+7.725\frac{m}{s}$(15KTS)	0

+ Indicates tailwind or crosswind from left side.

Scenario. — An analysis of the wind-shear performance as extensive as that conducted for the steady-state conditions was not performed. Instead, some typical results for the status display configuration were obtained. A major purpose was to see how performance with wind shears compared to that for the steady-state analysis. A second important objective was to test the sensitivity of the model results to various alternative assumptions.

The basic scenario for the longitudinal analysis involved starting at an initial range of 1500m with a constant wind velocity corresponding to the value at h = 152m (R ≈ 1160m). In all cases, turbulence having the spectral form of Equation 12 was employed. The scale-lengths were not varied with altitude; they were set at the constant value appropriate to the decision height. Gust intensities were σ_{u_g} = 1.5m/s, σ_{w_g} = .58m/s, the 10% wind condition. In all cases where the STOLAND display was used the glide-path error shifted from an angular presentation to a height presentation at R ≈ 575m (h ≈ 75m ≈ 250 ft.), as indicated in [7]. Thresholds and residual noises were adjusted accordingly. Attention among display variables was assumed to be allocated in the manner that was found to be optimal for steady-state (Table 3). The above-mentioned conditions were fixed throughout the analysis. Several variations with respect to other factors were investigated. These variations are described below.

The aircraft was assumed to be on the glide slope, but two types of initial trim were investigated.

Trim Condition A. — The component of the wind along the aircrafts x-body axis is trimmed out but the z-body axis component is not, so $w(0) = 0$. From Equation (21) it can be seen that this implies $\dot{\delta}h(0) = 0$. However, there will be, for this condition, an initial acceleration along the z-body axis.

Trim Condition B. — Both x and z components of the initial wind are trimmed out. This implies an initial $w(0)$ and a corresponding initial glide path error-rate. For the decreasing tailwind, this rate is $\dot{\delta}h(0) = 1.28$m/s whereas for the increasing tailwind, $\dot{\delta}h(0) = -.31$ m/s.

It had been noted in [6] that the pilot might vary his gains so as to tighten control as the decision-height was approached. An analogous result can be obtained with the model by making cost functional weightings range-dependent. Indeed, if it is assumed that the pilot attaches a fixed penalty to angular deviations from the glide-path, rather than linear deviations, then the weighting on height-errors will be range-dependent. We investigated two conditions with respect to this "gain-scheduling".

Constant Gains: The cost functional was fixed and equal to that used in the steady-state analysis.

Varying Gains: It was assumed that the angular glide-path error corresponding to the "window" dimension was appropriate. Then, the gains were changed in three stages. This was accomplished by changing the weighting on linear-height errors according to the following schedule:

$$1500m \leq R \leq 1160m \quad : \quad q_h = .0029, \quad \dot{q}_h = .0326$$

$$1160m \leq R \leq 575m \quad : \quad q_h = .0117, \quad \dot{q}_h = .133$$

$$575m \leq R \leq 230m \quad : \quad q_h = .073, \quad \dot{q}_h = .83$$

Thus, the weighting over a range-interval corresponded to the weighting appropriate to the end-point of that interval, a conservative choice. The intervals were chosen, as a matter of convenience, so that the end-points corresponded to points where other changes were required.

It was expected that the human's time delay would increase scores but would not alter the basic character of the results. Because inclusion of the time delay increases significantly the costs of the time-varying computation, we decided to assume the time delay was zero. However, a comparison case in which a time delay of .2 sec. was used was run to illustrate the differences one might expect from including time delay.

Results. – Mean and standard deviation scores, at the decision-height, are compared in Table 22. Several points are worth mention. First, the constant gain-no shear, zero-delay results are virtually equal to those of the corresponding steady-state analysis. This is more than a check on the program; it shows that in the absence of shears, the approximately 1250-1300m approach distance is sufficient for the errors to reach steady-state. Second, the effect of the wind-shear is more than just a non-zero mean response. It may be seen that the standard deviation of the tracking errors and of the controls is increased.

Table 22

PERFORMANCE AT DECISION-HEIGHT FOR VARIOUS ANALYSIS CONDITIONS

(Status Display, σ_{u_g} = 1.5m/s, P_o = -20dB)

	Steady-State		Constant-Gains			Varying-Gains
Variable	τ = .0	τ = .2	τ = 0	τ = 0	τ = .2	τ = 0
			No-Shear	With Shear		
$\bar{h}$(m)	0	0	0	.16	.22	.31
σ_h(m)	1.73	1.83	1.72	2.02	2.2	2.03
$\bar{\dot{h}}$(m/s)	0	0	0	-.01	-.016	-.05
$\sigma_{\dot{h}}$(m/s)	.48	.50	.47	.63	.70	.63
$\bar{\theta}$(m)	0	0	0	-.6	-.6	-.62
σ_θ(m/s)	1.24	1.29	1.23	1.27	1.35	1.26
$\bar{u}$(m/s)	0	0	0	-.10	-.095	-.10
σ_u(m/s)	.94	.96	.96	.98	1.03	1.00
$\bar{\delta}_e$(deg)	0	0	0	-1.44	-1.43	-1.46
σ_{δ_e}(deg)	1.38	1.5	1.39	1.75	1.94	1.82
$\bar{\delta}_N$(deg)	0	0	0	16.3	16.2	16.5
σ_{δ_N}(deg)	8.6	8.5	8.6	11.5	11.8	11.7

This is a result of the coupling in the model of mean-and variance-responses that arises from the dependence of the observation noises on the rms signal values and that of the motor-noise on rms control. In terms of missed approach probabilities, the increase in variance is the more significant effect. Third, the effect of time delay is, as expected, to increase mean and standard deviation of the error. The magnitude of the effect is largest for height-error with approximately a 35% increase in mean and a 10% increase in standard deviation.

The final effect illustrated in Table 22 is that resulting from allowing the gains to vary. When compared with the constant gain case, it is seen that the principal effect at the window is on the mean-response. This effect, though large percentage-wise, is virtually negligible in terms of the missed-approach probability. The differences between constant and varying gains are more pronounced in the time-histories shown in Figure 27. These time-histories are curves passed through data points obtained every 50m. The jump-discontinuities for the varying-gain case arise from the instantaneous gain-change and the associated jump in control value. These "jumps" apparently decay very rapidly. Because height errors are weighted less, they are allowed to build up to a greater extent in the varying-gain case; however, as the threshold is approached the errors begin to be reduced rapidly (because of the higher weighting), so that window performance is not significantly different for the varying- and constant-gain cases (Table 22). Apart from differences in height control, the principal difference between the two-cases is in the initial transient in elevator and pitch. It seems clear that the early reduction in height errors for the constant-gain case is a result of a rapid pitch-down.

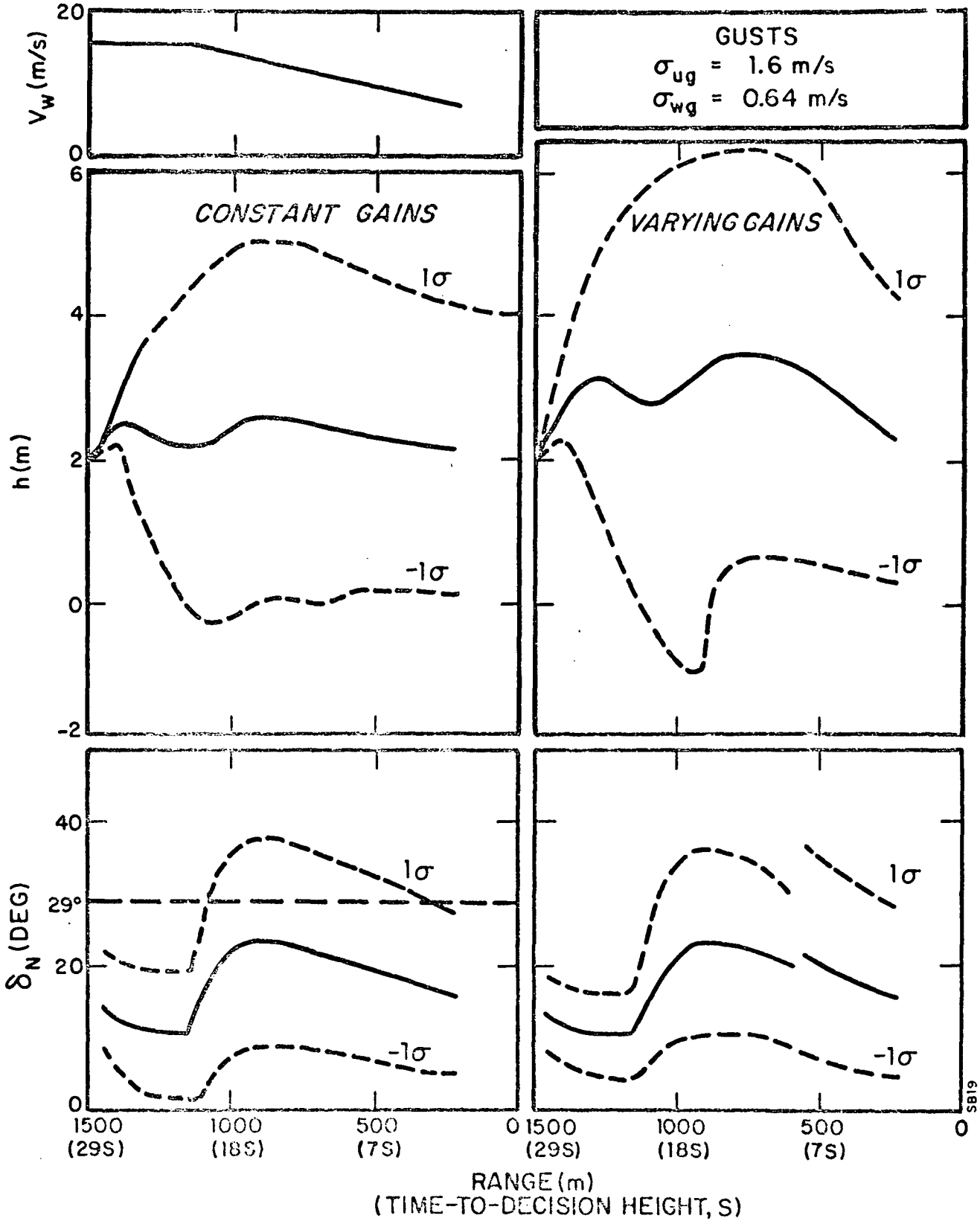

FIGURE 27. Effect of Varying Gains on Approach Trajectories
a) Height and Nozzle Response

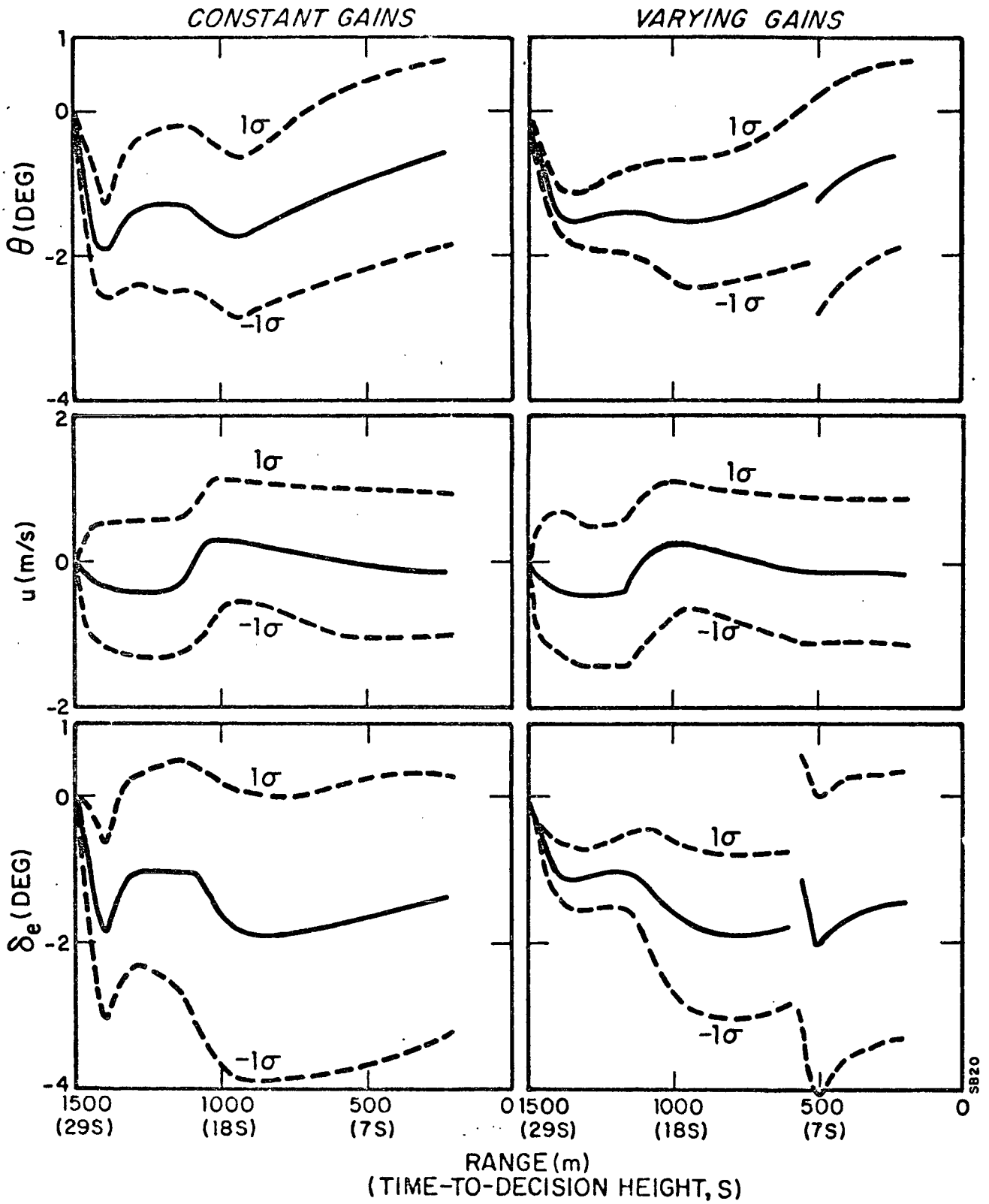

FIGURE 27. Effect of Varying Gains on Approach Trajectories
b) Pitch, Airspeed and Elevator Response

The above results were all obtained for trim-condition A (zero initial glide-path error-rate). The only significant effect of starting in trim-condition B was on mean height error, namely the mean-height error starting in condition B was about twice as large as that for starting in A throughout the approach. The problem is, simply, that with the more adverse initial condition, there is insufficient time (on the average) to compensate for the constant wind before the wind velocity starts to change. Thus, at the onset of the shear ($R \approx 1160m$) the height error for B is about twice that for A, and it remains so. In terms of "window" performance, the effect is to increase the probability of exceeding the window by about 1%.

The excellent "window" performance obtained in the above analyses is somewhat misleading. As can be seen from Figure 26, the nozzle limit of 29° is less than one standard deviation from the mean for much of the approach (after the window-velocity starts changing). Thus, in a high percentage of the time the nozzle exceeds its limit. What this means is that the rate of descent capability of the aircraft, with throttle fixed, is insufficient for this wind. Further, the wind is of sufficient severity to place the entire linearized analysis in question. On the other hand, the analysis suggests that suitably scaled-down winds may be adequately controlled by nozzle and elevator inputs alone.

In an attempt to get some estimate of the control-limited performance for the decreasing tailwind, a trajectory was obtained for a case in which nozzle control and control-rate were heavily penalized in the region where excessive nozzle-control had been observed, i.e., in the $1160m < R < 575m$ interval. (Weightings

on nozzle and nozzle-rate were multiplied by 50). To allow transient effects resulting from the initial constant wind to die out, the approach was started at 2000m. The result for height-error and nozzle-position is shown in Figure 28. It can be seen that nozzle responses to the shear variation in the heavily penalized region are virtually nil and the height errors increase accordingly. When the penalty is reduced, R < 575m, a relatively large mean-nozzle motion ensues in an attempt to reduce the mean-error. While some reduction occurs, the mean height error at the decision height is still three times the allowable error. Although these results are not intended to be definitive, they do illustrate the problem posed by this wind, when throttle is fixed.

A constant-gain trajectory for the increasing tailwind was also obtained and the results are shown in Figure 29.* For this case both longitudinal and normal components of the wind were initially trimmed out (analogous to condition B above). The window performance for this wind is compared with that for the decreasing tailwind in Table 23. Note that the turbulence intensity and spectrum is the same for the two cases. It may be seen that height errors are controlled more effectively for the increasing tailwind; airspeed is less-well controlled. The overall effect is a definite improvement. Two other points are worth noting. Referring to Table 23, we find that the standard deviation of the height and sink-rate errors for the increasing tailwind are very close to those obtained for the steady-state (no-delay) case. Thus, it appears that with the tailwind (which

*As can be seen the wind approximation is not as close to the idealized wind as for the previous case, but certainly good enough.

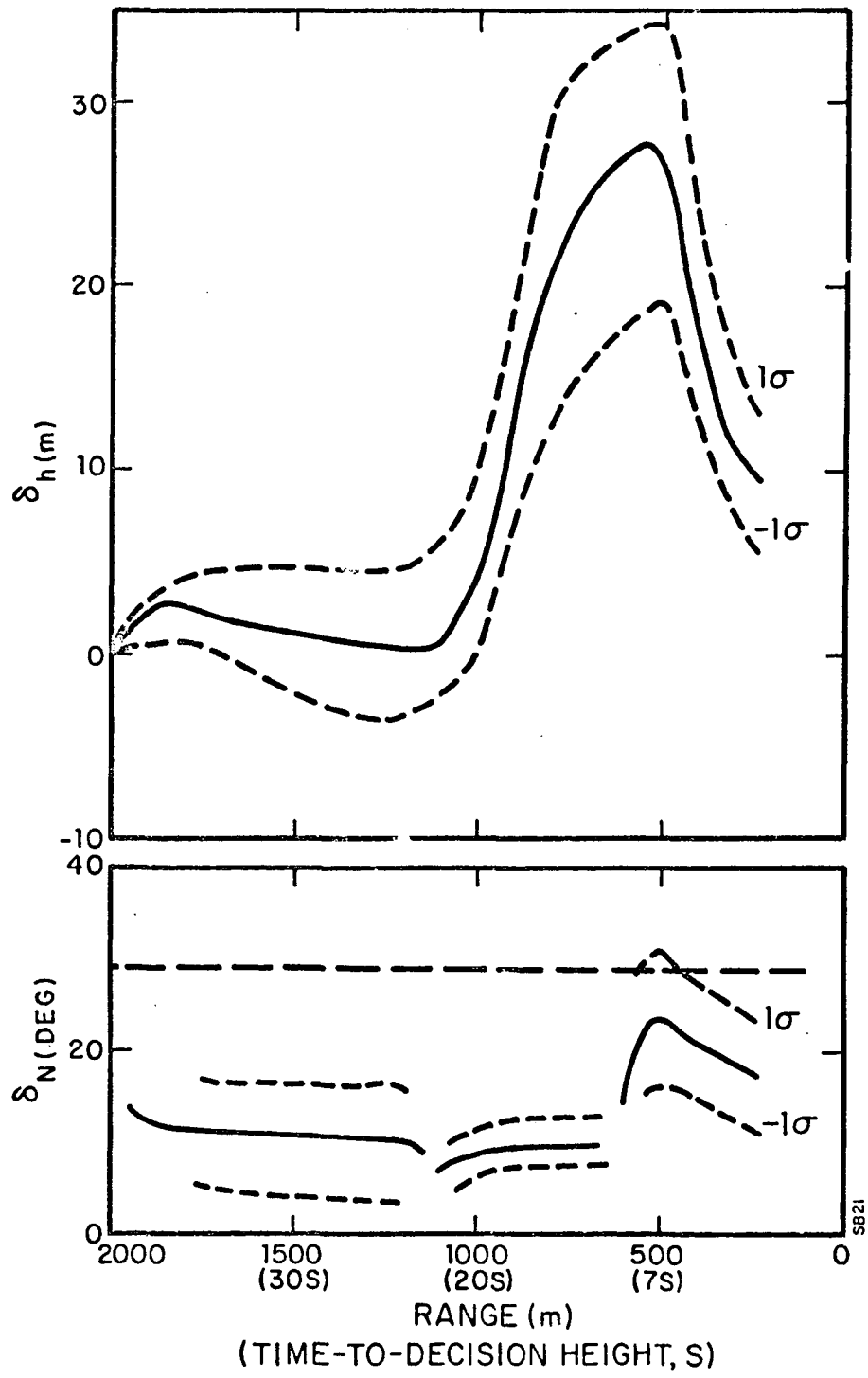

FIGURE 28. Nozzle-Limited Response For Decreasing Tailwind

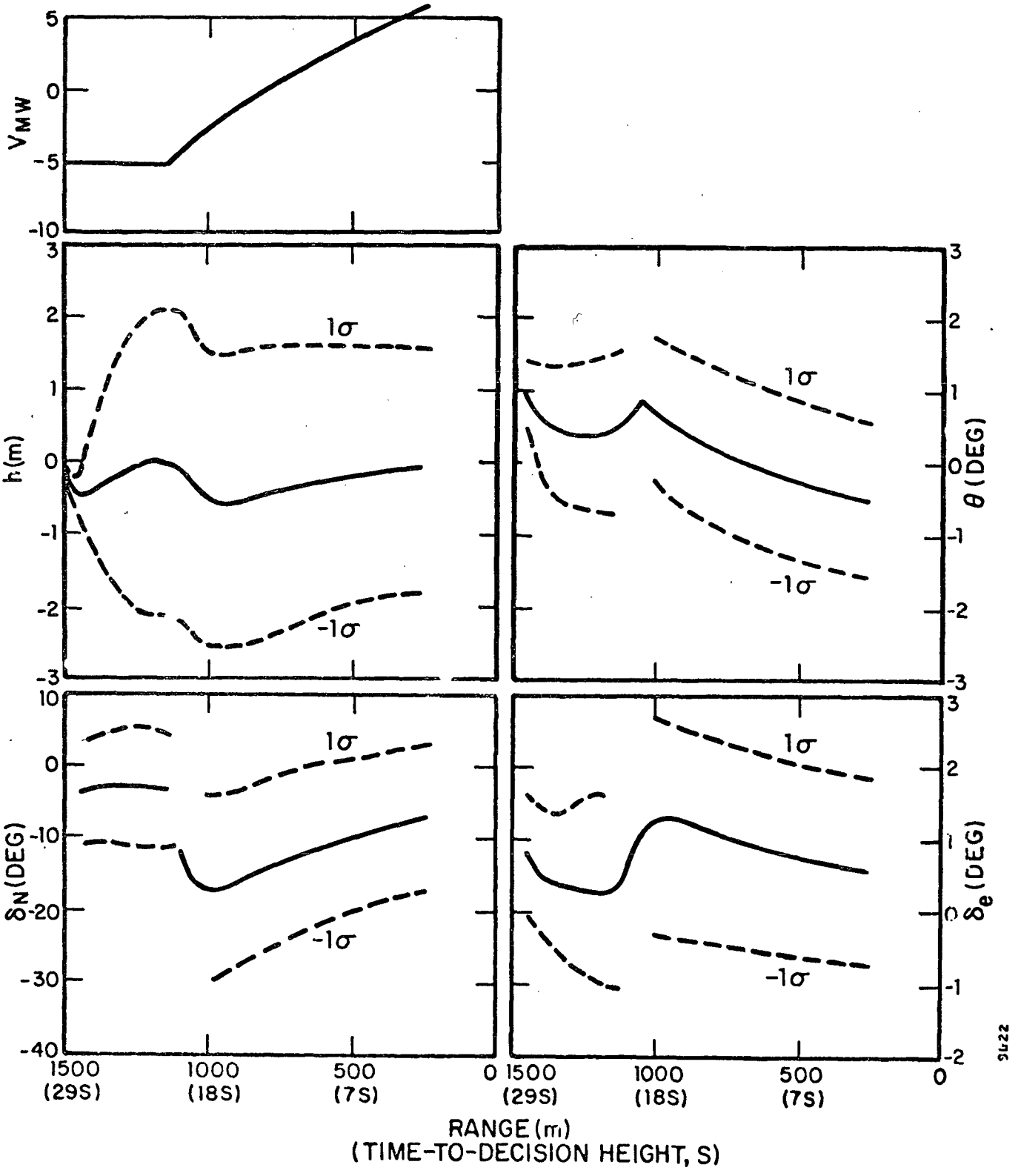

FIGURE 29. Response History for Increasing Tailwind Shear

Table 23

COMPARISON OF WINDOW PERFORMANCE FOR DIFFERENT TAILWINDS

Variable	Decreasing Tailwind	Increasing Tailwind
$\overline{h}$(m)	.16	-.12
σ_h(m)	2.02	1.69
$\overline{\dot{h}}$(m/s)	-.01	.006
$\sigma_{\dot{h}}$(m/s)	.63	.46
$\overline{\theta}$(deg)	-.6	-.49
σ_θ(deg)	1.27	1.13
$\overline{u}$(m/s)	-.10	-.19
σ_u(m/s)	.98	.99
$\overline{\delta}_e$(deg)	-1.44	.56
σ_{δ_e}(deg)	1.75	1.3
$\overline{\delta}_N$(deg)	16.3	-7.4
σ_{δ_N}(deg)	11.5	10.0
Time-for-Approach(s)	~ 29.	~ 43

starts out as a headwind), enough time is added to the approach to allow the "pilot" (model) to reduce the errors to values commensurate with an approach of infinite length. The second point is that the nozzle-control requirements are not so excessive (in relation to capability) as for the decreasing tailwind. Thus, one might expect these results to correspond more closely to a realistic situation.

Lateral Analysis

The analysis of lateral control in the approach was performed for the status display and for the status-Interim-Director combination. In each instance allocation of attention was distributed according to the "optimal" values found in Chapters 3 and 4. That is, when the status display was being attended to, 75% of that attention was devoted to the localizer; when both displays were available, 80% of the attention was devoted to the interim-director.

Thresholds and residual noises were determined from [7]. Localizer thresholds were in angular units, so that the effective observation noise on lateral error and error-rate increased with distance from the runway-threshold. Thus, when approach was initiated, the lateral-error threshold was about 1.25m as compared to .28m at the decision height.

For the lateral approach analysis we assumed that the forward ground speed (i.e., range-rate) was maintained at 31m/s This made the generation of the crosswind quite simple, i.e., we let

$$\dot{v}_{MW} = a\,\dot{h}_N = a\,U_o \tan \Gamma_o$$

D

Because of the simplified dynamic representation used for the lateral analysis, the crosswind affected only the cross-track velocity of the aircraft. As opposed to the longitudinal case, no aerodynamic effects of the wind-shear considered.

Results. — "Window" performance for the two display conditions is shown in Table 24 and compared with corresponding steady-state results. It should be noted that mean lateral errors were still decreasing but variances had very nearly converged when this "snap-shot" was taken. It can be seen that the mean-values for the shear cases are little affected by the display condition. Moreover, it turns out that the percentage change in variance from steady-state to wind-shear is also about the same for both display configurations. From an absolute standpoint, the director configuration shows considerably better performance in that smaller errors are achieved with less control.

The above results are further illustrated in the time-histories of Figure 30. It can be seen that in the initial portion of the trajectory, when the wind is constant, the director configuration does better. After the shear starts the director continues to do better for some time and its peak mean lateral error is less than for the status display. However, as the window is approached, the mean error becomes virtually equal for both displays.

One might expect the director-system to show to advantage with respect to workload requirements. To test this notion, trajectories were obtained with a reference observation noise/signal ratio of -11dB for both the status display status and the status-director configuration. Scores at the decision-height for the two cases

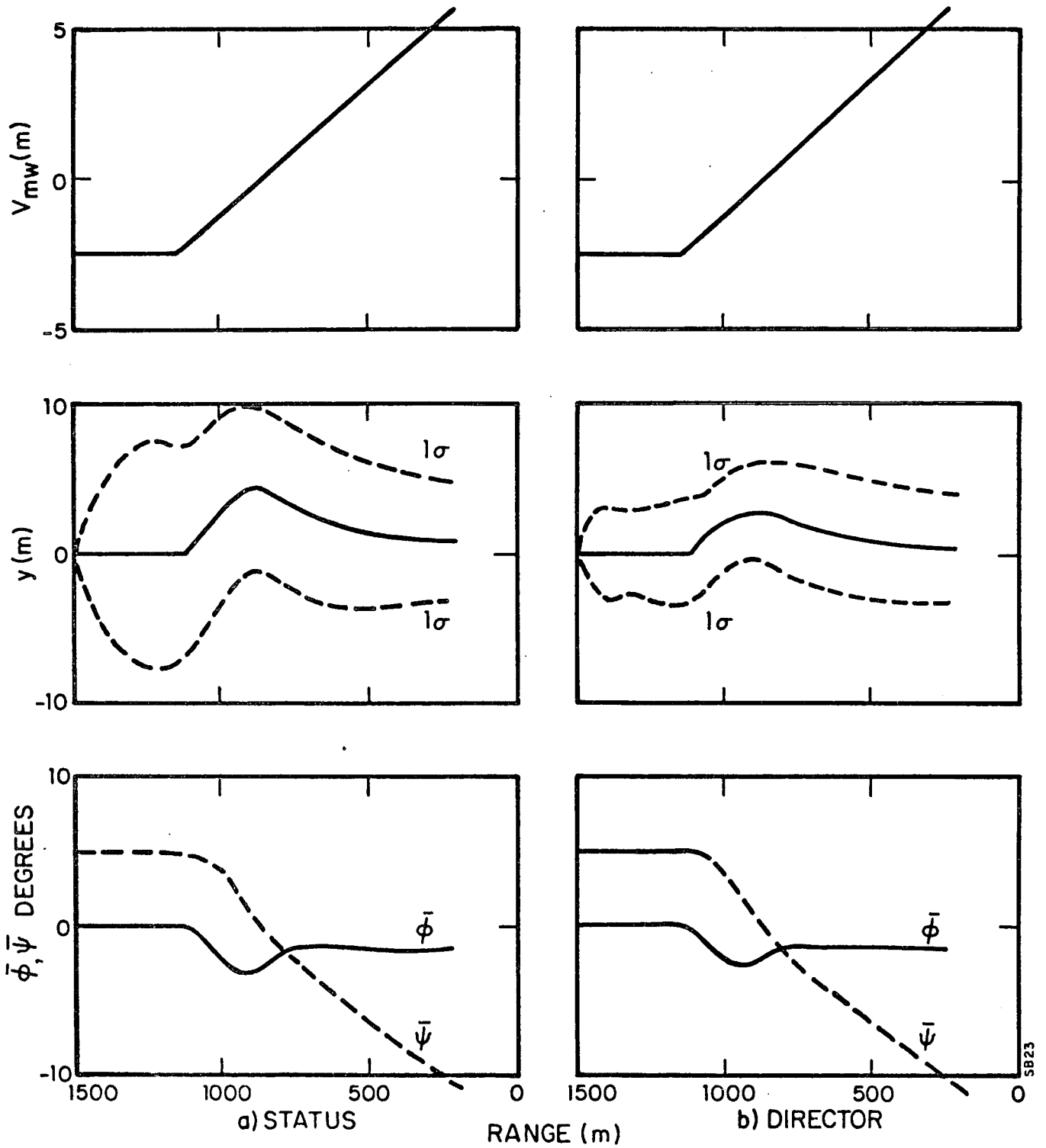

FIGURE 30. Lateral Time Histories for STOLAND and Director Displays

Table 24

LATERAL PERFORMANCE AT DECISION HEIGHT FOR CROSSWIND AND TURBULENCE (σ_{v_g} = 1.5m/s, P_o = .20dB)

	Status		Status + Interim Director	
Variable	Steady-State	Crosswind	Steady-State	Crosswind
$\bar{y}$(m)	0	.73	0	.73
σ_y(m)	3.49	4.13	3.17	3.77
$\bar{\dot{y}}$(m/s)	0	-.045	0	-.047
$\sigma_{\dot{y}}$(m/s)	1.38	1.61	1.30	1.47
$\bar{\phi}$(deg)	0	-1.58	0	-1.59
σ_ϕ(deg)	3.54	4.36	3.24	3.90
$\bar{\delta}_w$(deg)	0	-.40	0	-.4
σ_{δ_w}(deg)	7.4	9.2	6.75	8.27

(repeated for -20dB) are shown in Table 25. The STOLAND-Director combination is less sensitive to the change in noise/signal ratio. In terms of lateral error there is a smaller percentage increase in both the mean and standard deviation. Again, we see better performance for less control effort.

Another aspect of director design that can be analyzed is beam capture. It was decided to try a simple test of this aspect of the problem by introducing an initial (mean) displacement of 10m from the localizer center-line. The small displacement was chosen, in keeping with the linearizing assumptions that were made. The results for status and Director cases are shown in Figure 31. The mean response for the two cases is indistinguishable, so only one curve is drawn. However, the variability of the two cases is quite different as is seen by the plots of rms (not standard deviation) values. For localizer intercept the director also appears to improve performance.

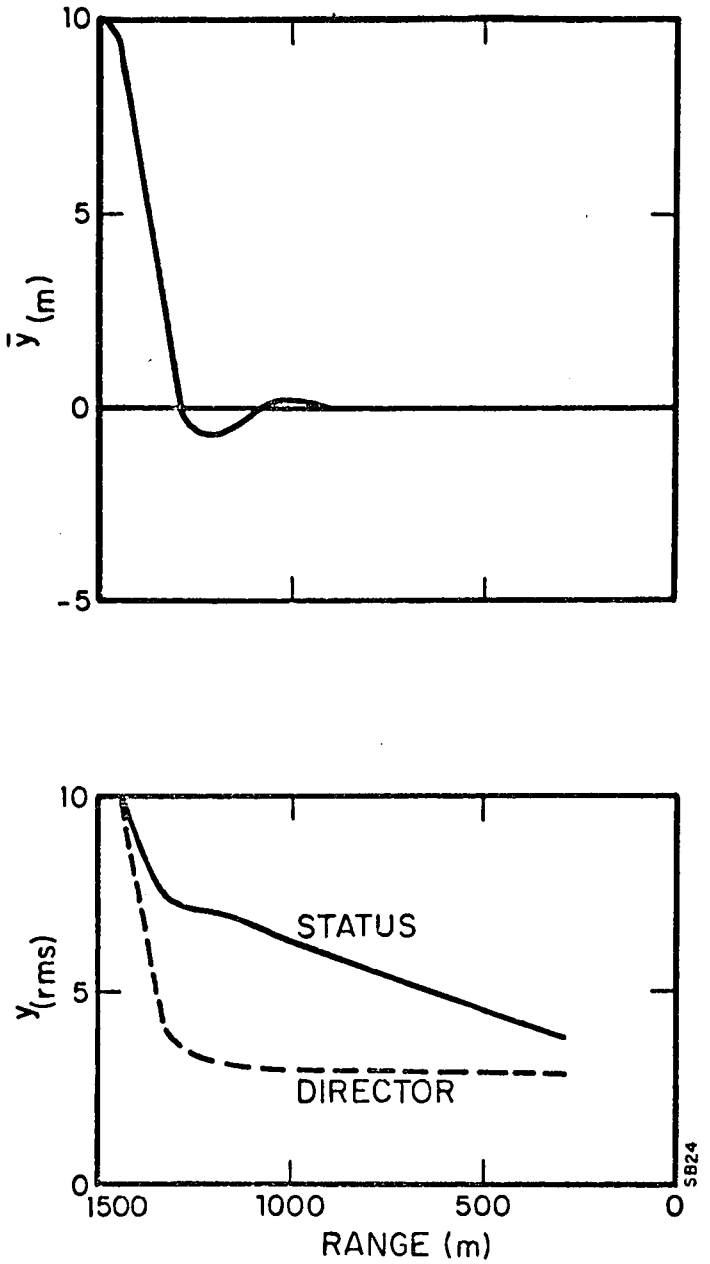

FIGURE 31. Localizer Capture Response for Status and Director Displays

Table 25

EFFECT OF NOISE RATIO ON APPROACH PERFORMANCE IN WIND-SHEAR

	Status		Status-Director	
Variable	P_o = -20dB	P_o = -11dB	P_o = -20dB	P_o = -11dB
$\bar{y}$	.73	1.73	.73	1.58
σ_y (m)	4.13	8.47	3.77	6.29
$\bar{\dot{y}}$ (m/s)	-.045	-.09	-.047	-.08
$\sigma_{\dot{y}}$ (m/s)	1.61	2.63	1.47	1.96
$\bar{\phi}$ (deg)	-1.58	-1.56	-1.59	-1.58
σ_ϕ (deg)	4.36	7.0	3.90	5.01
δ_w (deg)	-.4	-.39	-.40	-.39
σ_{δ_w} (deg)	9.2	14.9	8.21	10.8

SUMMARY

Some aspects of the STOL approach in a mean-wind with shear-variation have been analyzed with the pilot-vehicle-display model. Results were obtained for longitudinal control with the status display and for lateral control with the status display and the status-interim-director combination. In general, the wind-shears degrade

performance by producing both mean errors and increased variability in the response, with the increased variability appearing to be the major effect.

Two wind profiles were considered in the analysis of longitudinal control, a decreasing and an increasing tailwind. Relatively good performance at the window was obtained in both cases. However, for the decreasing tailwind, the results showed that with the throttle fixed, excessive nozzle-control was required for wind compensation. When the nozzle control was limited (indirectly, by penalizing control motions subsequent to shear-onset), the height errors increased significantly. The relatively good performance for the increasing tailwind was achieved with control requirements that were not so excessive and, consequently, represent a more reliable result. The better performance is undoubtedly due to the additional time available for error compensation and is, of course, to be expected.

The results for lateral control were about as expected. Specifically, the status-director combination performed better in terms of response to shears both from an absolute standpoint and in terms of sensitivity to observation noise/signal ratio. Beam capture response was also better for the configuration that included the director.

To the extent that they were investigated, the wind-shear responses tended to confirm essentially the steady-state results (albeit that performance was worse in the wind-shear). With regard to the details of the transient responses, it may be said that the behavior is easily explained. The transient response depends very much on the specific assumptions about initial

conditions and pilot strategy, which is not the least bit surprising. If one is interested in reproducing or predicting a particular time history (ensemble) then it is essential that conditions used in the model match those of the experiment.

CONCLUSION

This chapter is comprised of two parts: for the convenience of the reader, we summarize the key results of the study and provide references to supporting data contained in the main body of the text; then we suggest areas for further work.

Summary of Main Results

A. With respect to the status displays of the STOLAND-EADI:

(i) Steady-state analysis indicates that high levels of pilot workload (probably unacceptable) will be required to achieve a 95% approach-success probability (Category II - window specifications) in median-turbulence conditions. When all turbulence levels are considered a 95% success probability is not possible with reasonable workload levels (Figure 13).

(ii) Even with stability augmentation, the lateral-directional control task is more difficult than longitudinal control. To achieve a 95% probability of being within the lateral-"window" requires approximately three times the "work-load" necessary to attain the same success-level for the height-airspeed window (Figures 6, 10).

(iii) Comparison of proposed status displays with idealized status displays shows that the principal limitations imposed by the status display are the (a) the failure to provide adequate information on glide-path and localizer error rates (i.e., vertical and horizontal flight path angles) and (b) the requirement to share attention among the display elements (Figure 8, Table 8).

(iv) Wind-shears, as expected, tend to degrade performance. They introduce mean-errors and increase response variability (Tables 22, 24). A decreasing tailwind with 2m/s / 30m (4KTS/100') shear-variation appears to exceed the rate-of-descent capability of the aircraft with throttle-fixed (Figures 27, 28).

B. With respect to proposed display augmentation:

(i) The proposed interim -flight directors provide improvement in performance at substantially reduced workload (Figures 17, 19, 20). When the average of all-winds is considered, the addition of the flight directors reduces the miss-probability by about a factor of two at all levels of pilot attention (Figure 20). To achieve a given probability of success for the median wind-condition, requires about a third the workload with the directors as without them (Table 16).

(ii) Best performance on the longitudinal axis is obtained with attention shared roughly equally between director and status displays (Table 11). On the other hand, best lateral performance is obtained with an 80%-20% division of attention in favor of the director display (Table 15). Thus, the lateral director appears to provide a better "mix" of signals than does the longitudinal director, at least for the conditions analyzed.

(iii) The longitudinal director does not yield performance as good as that predicted by the idealized display (Table 12), which fact suggests that the director laws could be further optimized. The lateral director, however, does lead to performance levels very close to those associated with the idealized display.

(iv) Missed approaches with the directors, as without them, are primarily due to lateral errors (Figure 20). Insofar as the lateral director appears to yield performance close to that obtained with an idealized display, further improvement in performance via optimization of lateral displays will be very difficult using the feedbacks currently proposed for the status and director displays. Although improvements in longitudinal performance will not increase approach success-probabilities appreciably, further reduction in longitudinal workload via display design will allow more attention to the lateral task, thus increasing the overall success probability or reducing the overall workload.

(v) Response to cross-winds is improved by the lateral director, at least for the wind investigated (Table 24). The lateral director reduces the sensitivity of both mean and rms errors to attention-levels and will, therefore, reduce workload (Table 25).

C. With regard to the pilot-vehicle-display analysis procedure.

(i) The "optimal-control model" for the pilot (with its interference and workload sub-models) in conjunction with modern systems analysis techniques, provides a powerful means for analyzing displays and their effect on system performance and reliability.

(ii) The procedure may be used to determine bounds on expected display improvements via analysis of "idealized" displays (Table 5, 8).

(iii) The model for task interference and workload permits linearized analysis of combined longitudinal and lateral performance in a rational and consistent manner. Interaction between axes is introduced via the limited capacity of the pilot and not through any vehicle coupling.

(iv) The analysis techniques can serve as a basis for director design. Such a (preliminary) procedure for design of a longitudinal director system, that considered only the gust-regulation problem, yielded a configuration that resulted in substantially reduced workload (Figure 23).

Further Work

As is customary, we conclude this report with suggestions for additional work and research. First, it is important that the results of this analysis be confirmed by simulation experiments. Beyond this validation, experimentation and data

analysis are needed to solidify the basis for choosing cost functional weightings when flight directors are being used. Additional approach data are needed to pin-down details of the pilot's time-varying adaptation. "Transient" data in the form of ensemble averages and variability would be most helpful.

Further display analysis seems warranted. For example, a more thorough model-analysis of wind-shear response with the director configurations is desirable. An interesting and relatively minor extension, that could not be accomplished within the constraints of this program, would be to take the estimation data from this study and analyze pilot decision-making with regard to missed approaches [12]. Display performance in curved approaches is also an important area for investigation that is amenable to the techniques employed here.

It appears that the approach to flight-director design suggested in Section 5 has much merit and is worthy of continued investigation. It became apparent in that analysis that the facility for ignoring certain model feedbacks would be useful and the programs should be modified accordingly.

Finally, it is important to take cognizance of the changing role of the pilot from one of active controller to monitor and manager. Analysis procedures such as those employed here are necessary for investigating and understanding this role. It is our conviction that the models and techniques used here can serve as a basic building block for the development of models for flight management and that such development should be addressed vigorously.

E.

REFEPENCES

1. Baron, S., and D. L. Kleinman, "The Human as an Optimal Controller and Information Processor", IEEE Trans. Man-Machine Systems, Vol. MMS-10, No. 1 (March 1969).

2. Kleinman, D. L. and S. Baron, "Manned Vehicle Systems Analysis by Means of Modern Control Theory", NASA CR-1753 (June 1971).

3. Levison, W. H., S. Baron, and D. L. Kleinman, "A Model for Human Controller Remnant", IEEE Trans. Man-Machine Systems, Vol. MMS-10, No. 4 (December 1969).

4. Levison, W. H., J. I. Elkind, and J. L. Ward, "Studies of Multivariable Manual Control Systems: A Model for Task Interference", NASA CR-1746 (May 1971).

5. Kleinman, D. L., S. Baron, and W. H. Levison, "An Optimal-Control Model of Human Response, Part 1: Theory and Validation", Automatica, Vol. 6, pp. 357-369 (1970).

6. Kleinman, D. L. and S. Baron, "Analytic Evaluation of Display Requirements for Approach to Landing", NASA CR-1952 (November 1971).

7. Decker, D. W., "Display Requirements Specification for STOLAND EADI Display System".

8. Bryson, A. E. and Y. C. Ho, "Applied Optimal Control", Blaisdell Publishing Co., Waltham, Massachusetts (1969).

9. Vinje, E. W., "An Analysis of Pilot Adaptation in a Simulated Multiloop VTOL Hovering Task", IEEE Trans. on Man-Machine Systems", Vol. MMS-9, No. 4 (December 1968).

10. McRuer, D., D. Graham, E. Krendel, and W. Reisener, "Human Pilot Dynamics in Compensatory Systems", AFFDL TR 65-15 (July 1965).

11. Jex, H. R., R. W. Allen, and R. E. Magdaleno, "Display Format Effects on Precision Tracking Performance, Describing Functions and Remnant", USAF Aerospace Medical Division, AMRL-TR-71-63 (August 1971).

12. Levison, W. H. and R. B. Tanner, "A Control-Theory Model for Human Decision Making", Bolt Beranek and Newman Inc., Report No. 2119 (June 1971).

13. Baron, S., D. L. Kleinman et al., "Application of Optimal Control Theory to the Prediction of Human Performance in a Complex Task", AFFDL-TR-69-81 (March 1970).

14. Johnson, W. A. and D. T. McRuer, "A Systems Model for Low Level Approach", AIAA Guidance, Control and Flight Mechanics Conference, Santa Barbara, California, AIAA Paper No. 70-1034 (August 1970).

15. Levison, W. H., "The Effects of Display Gain and Signal Bandwidth on Human Controller Remnant", Wright-Patterson Air Force Base, AMRL-TR-70-93 (March 1971).

16. Chalk, C. R., T. P. Neal, T. M. Harris, and F. E. Prichard, "Military Specifications – Flying Qualities of Piloted Airplanes", AFFDL-TR-69-72 (August 1969).

17. Klein, R. H., "AWJSRA Flight Director Simulation Program", Systems Technology, Inc., Working Paper No. 1015-8 (March 1972).

18. Craig, S. J. and Klein, R. H., "Preliminary Longitudinal Flight Director Laws and Simulator Experimental Plans, Systems Technology, Inc., Quarterly Progress Report No. 1015-3 (February 1972).

19. Johnson, C. D., "Accommodation of External Disturbances in Linear Regulator and Servomechanism Problems", IEEE Trans. on Automatic Control, Vol. AC-16, No. 6 (December 1971).

20. Anderson, B.D.O. and J. B. Moore, "Linear Optimal Control", Prentice Hall, Edgewood Cliffs, New Jersey (1971).

21. Teper, G. L., "Aircraft Stability and Control Data", Systems Technology Report STI 176-1 (April 1969).

APPENDIX A

Modification for Time-Varying Input Disturbances

In Reference 6, procedures for modifying our model of the human operator to account for constant mean disturbance inputs were developed. Here, we consider a wider class of inputs, viz those that have a time-varying mean. Specifically, we consider the class of disturbances that may be modelled as the state (or output) of a linear dynamic system:

$$\dot{\underline{z}} = \underline{A}_z \underline{z} \quad ; \quad \underline{z}(t_o) = \underline{z}_o \tag{A.1}$$

where $\underline{A}_z$, a constant, and $\underline{z}_o$ are assumed known[+]. Various disturbance inputs may be generated from such a model. For a detailed discussion, see Ref.19. The results we present appear in various forms in the literature [Ref.19, 20] and are developed here for completeness and convenience.

The disturbance state is assumed to enter the system linearly, so the system state equations are

$$\dot{\underline{x}} = \underline{A}\,\underline{x} + \underline{B}\,\underline{u} + \underline{E}\,\underline{w} + \underline{F}\,\underline{z} \tag{A.2}$$

The problem is to choose $\underline{u}$ to minimize

$$J = \lim_{T\to\infty} E\{\frac{1}{T}\int_o^T [\underline{x}'\,\underline{Q}\,\underline{x} + \underline{u}'\,\underline{R}\,\underline{u}]dt\} \tag{A.3}$$

where $\underline{Q} \geq 0$, $\underline{R} > 0$.

[+]Thus, the state $\underline{z}(t)$ is known for all t. In applying the model, $\underline{z}(t)$ will have to be estimated from available, noisy outputs, as are other system states.

To solve this problem, we define an augmented state $\tilde{x}' = [z' \mid x']$ satisfying

$$\dot{\tilde{x}} = \begin{bmatrix} \dot{z} \\ \hline \dot{x} \end{bmatrix} = \left[\begin{array}{c|c} A_z & 0 \\ \hline F & A \end{array}\right] \begin{bmatrix} z \\ \hline x \end{bmatrix} + \begin{bmatrix} 0 \\ \hline B \end{bmatrix} u + \begin{bmatrix} 0 \\ \hline E \end{bmatrix} w \qquad \text{(A.4a)}$$

$$= \tilde{A}\,\tilde{x} + \tilde{B}\,u + \tilde{w}\,, \qquad \text{(A.4b)}$$

an augmented weighting matrix

$$\tilde{Q} = \left[\begin{array}{c|c} Q & Q \\ \hline Q & Q \end{array}\right]$$

and consider the minimization of (A.3) for fixed T. This is a well-defined problem whose solution is given by

$$u^*(t) = -R^{-1}\,\tilde{B}'\,\tilde{K}(t)\,\tilde{x}(t) \qquad \text{(A.5)}$$

where

$$-\dot{\tilde{K}} = \tilde{A}'\,\tilde{K} + \tilde{K}\,\tilde{A} + \tilde{Q} - \tilde{K}\,\tilde{B}\,R^{-1}\,\tilde{B}'\,\tilde{K}\;; \quad t \leq T$$
$$\tilde{K}(T) = 0 \qquad \text{(A.6)}$$

Letting $\tilde{K}$ be partitioned conformally with A, viz.

$$\tilde{K} = \left[\begin{array}{c|c} K_{11} & K_{21}' \\ \hline K_{21} & K_{22} \end{array}\right] \qquad \text{(A.7)}$$

we find that

$$\underline{u}^*(t) = -\underline{P}^{-1}\ \underline{B}'\ (\underline{K}_{21}(t)\underline{z} + \underline{K}_{22}(t)\underline{x}) \qquad (A.8)$$

and

$$-\dot{\underline{K}}_{11} = \underline{K}_{11}\ \underline{A}_z + \underline{A}_z'\ \underline{K}_{11} + \underline{K}_{21}'\ \underline{F} + \underline{F}'\ \underline{K}_{21} - \underline{K}_{21}'\ \underline{B}\ \underline{R}^{-1}\ \underline{B}'\ \underline{K}_{21}\ ;$$

$$\underline{K}_{11}(T) = \underline{O} \qquad (A.9a)$$

$$-\dot{\underline{K}}_{21} = \underline{K}_{21}\ \underline{A}_z + \underline{K}_{22}\ \underline{F} + (\underline{A}' - \underline{K}_{22}\ \underline{B}\ \underline{R}^{-1}\ \underline{B}')\underline{K}_{21}\ ;$$

$$\underline{K}_{21}(T) = \underline{O} \qquad (A.9b)$$

$$-\dot{\underline{K}}_{22} = \underline{K}_{22}\ \underline{A} + \underline{A}'\ \underline{K}_{22} + \underline{Q} - \underline{K}_{22}\ \underline{B}\ \underline{R}^{-1}\ \underline{B}'\ \underline{K}_{22}\ ;$$

$$\underline{K}_{22}(T) = \underline{O} \qquad (A.9c)$$

Note that Eqn. (A.9c) is the Riccati Eqn. for the regulator problem without the time-varying mean disturbance. Also, since (A.9b, c) and (A.8) are independent of $\underline{K}_{11}$ the solution to (A.9a) is not needed in implementing the optimal control.

The structure of the controller implied by (A.8) and (A.9) is shown in Figure A1. The feedback structure of the controller is identical to that of the optimal linear regulator; the modification to the regulator is a set of feedforward gains operating on the disturbance(on the estimate of the disturbance, in practice).

We wish to explore conditions that lead to constant gains in (A.8) inasmuch as this simplifies the model implementation and interpretation considerably. Thus, we consider the case, $T \to \infty$.

It is well-known that the solution to (A.9c) yields

$$\lim_{T\to\infty} \underline{K}_{22}(t) = \underline{\bar{K}} = \text{constant} \tag{A.10a}$$

where

$$\underline{\bar{K}}\,\underline{A} + \underline{A}'\,\underline{\bar{K}} + \underline{Q} - \underline{\bar{K}}\,\underline{B}\,\underline{R}^{-1}\,\underline{B}'\underline{\bar{K}} = \underline{O} \tag{A.10b}$$

Using (A.10), it can be shown that

$$\lim_{T\to\infty} \underline{K}_{21}(t) = \underline{K}_z = \text{constant} \tag{A.11a}$$

satisfying

$$\underline{K}_z\,\underline{A}_z + \underline{\bar{A}}'\,\underline{K}_z = -\underline{\bar{K}}\,\underline{F} \tag{A.11b}$$

$$\underline{\bar{A}} = \underline{A} - \underline{B}\,\underline{R}^{-1}\,\underline{B}'\,\underline{\bar{K}} \tag{A.12}$$

if, and only if,

$$\text{Re}\,\{\lambda_i + \mu_j\} < 0 \qquad \forall\ i, j \tag{A.13}$$

where λ_i and μ_j are the eigenvalues of $\underline{\bar{A}}$ and $\underline{A}_z$, respectively. Inasmuch as $\text{Re}\,\{\lambda_i\} < 0\ \forall\ i$ by virtue of the stabilizing properties of the optimal regulator, a sufficient condition for (A.13) to hold is that

$$\text{Re}\,\{\mu_j\} \leq 0\ ,\ \forall\ j \tag{A.14}$$

The condition that the disturbance not have an exponentially growing component (which is the case if $\text{Re}\,\{\mu_j\} \leq 0$) is sufficient for the gains on the disturbance to be constant, but does not

guarantee the optimality of our solution. This is so because the cost functional may not be finite as $T\to\infty$. This would not seem to be a serious complication for our purposes. The upper limit T may be considered to be sufficiently large for the solution to the Riccati equation to converge: Once the gains have been computed, as constants, we evaluate the various scores by integrating appropriate equations forward in time. For realistic inputs and reasonable times, the scores will be reasonable. Of course, if the cost functional (A.3) is bounded as $T\to\infty$, then we have the optimal solution.

In the special case of a constant disturbance, $\underline{A}_z = 0$, and Eqn. (A.14b) yields

$$\underline{K}_z = -(\underline{\bar{A}})^{-1}\ \underline{\bar{K}}\ \underline{F} \qquad \text{(A.15a)}$$

and, substituting for $\underline{u}$ in (A.2) and setting $\underline{W} \equiv 0$, we find

$$\lim_{t\to\infty} \underline{x}(t) = -\underline{\dot{A}}^{-1}(\underline{F} - \underline{B}\ \underline{R}^{-1}\ \underline{B}'\ \underline{K}_z)\ \underline{z}_o = \text{constant} \qquad \text{(A.15b)}$$

Equations (A.15a) and (A.15b) verify the results obtained "directly" in Ref. 1.

APPENDIX B

Computation of System Response to Specific Initial Conditions

In this section we develop general expressions for computing model responses to specific initial conditions[+]. These formulae are needed to compute control and monitoring performance associated with specific time-varying disturbances, e.g., mean winds (see Chapter 6). For simplicity, we consider here the case where the human's time-delay is negligible (or may be accounted for by adjusting τ_N), i.e., $\tau = 0$.

We begin by assuming that, in general, the initial state $\underline{x}(t_o)$ is a gaussian random variable with mean $\underline{m}_o$ and covariance $\underline{X}_o$. The equations governing the motion of the optimal closed loop system are well known and given by [6].

$$\dot{\underline{x}} = \underline{A}\,\underline{x} - \underline{B}\,\underline{L}^*\,\hat{\underline{x}} + \underline{E}\,\underline{w}(t) \tag{B.1a}$$

$$\dot{\hat{\underline{x}}} = \underline{F}\,\hat{\underline{x}} + \underline{P}(t)\,[\underline{C}(t)\,\underline{e} + \underline{v}(t)] \quad ; \quad \hat{\underline{x}}(t_o) = \underline{m}_o \tag{B.1b}$$

$$\dot{\underline{e}} = \underline{G}(t)\,\underline{e} + \underline{E}\,\underline{w}(t) - \underline{P}(t)\,\underline{v}(t) \tag{B.1c}$$

where

$$\underline{F} \triangleq \underline{A} - \underline{B}\,\underline{L}^*$$

$$\underline{G}(t) \triangleq \underline{A} - \underline{\Sigma}(t)\underline{C}'(t)\,\underline{V}^{-1}(t)\,\underline{C}(t) \tag{B.2}$$

$$\underline{P}(t) \triangleq \underline{\Sigma}(t)\,\underline{C}'(t)\,\underline{V}^{-1}(t)$$

[+]These results are a generalization and amplification of those given in Appendix C of Ref. 6. In addition, the derivation is somewhat different and, hopefully, more straightforward.

and,[+]

$$\left.\begin{aligned} \underline{W}(t)\ \delta(t-\tau) &= \overline{\{\underline{w}(t)\underline{w}^T(\tau)\}} \\ \underline{V}(t)\ \delta(t-\tau) &= \overline{\{\underline{v}(t)\ \underline{v}^T(\tau)\}} \end{aligned}\right\} \quad (B.3)$$

$\underline{L}^*$ is the "optimal gain" matrix computed from the optimal linear regulator problem and $\underline{\Sigma}(t)$ is the solution to the variance equation.

$$\left.\begin{aligned} &\dot{\underline{\Sigma}} = \underline{A}\ \underline{\Sigma} + \underline{\Sigma}\ \underline{A}' - \Sigma\ C'(t)\ V^{-1}(t)\ C(t)\Sigma + \underline{E}\ \underline{W}(t)\ \underline{E}' \ ; \\ &\underline{\Sigma}(t_o) = \underline{X}_o \end{aligned}\right\} \quad (B.4)$$

which may also be written as

$$\left.\begin{aligned} &\dot{\underline{\Sigma}} = \underline{G}(t)\ \underline{\Sigma} + \underline{\Sigma}(t)\ \underline{G}' + \underline{P}(t)\ \underline{V}(t)\ \underline{P}'(t) + \underline{E}\ \underline{W}(t)\ \underline{E}' \ ; \\ &\underline{\Sigma}(t_o) = \underline{X}_o \end{aligned}\right\}$$

In most problems it is assumed that $\underline{V}(t)$ and $\underline{W}(t)$ are known a priori, so $\underline{\Sigma}(t)$ may be precomputed. In the case of the human-operator-model application, $\underline{V}(t)$ depends on the state and $\underline{\Sigma}(t)$ is computed on-line; this is possible because solution to (B.4) is carried out in the forward direction. In either instance, the optimal filter implementation involves solution to (B.1) and (B.4).

For convenience, we define the composite "state" and "input as

[+]Bar denotes expectation operator.

$$\tilde{\underline{x}} = \begin{bmatrix} \underline{x} \\ \hat{\underline{x}} \\ \underline{e} \end{bmatrix} \quad ; \quad \tilde{\underline{w}} = \begin{bmatrix} \underline{w} \\ \underline{v} \end{bmatrix} \tag{B.5}$$

Then, (B.1) may be written as

$$\dot{\tilde{\underline{x}}} = \tilde{\underline{A}}(t)\ \tilde{\underline{x}} + \tilde{\underline{E}}(t)\ \tilde{\underline{w}} \tag{B.6}$$

where

$$\tilde{\underline{A}}(t) = \begin{bmatrix} \underline{A} & -\underline{BL}^* & \underline{0} \\ \underline{0} & \underline{F} & \underline{P}(t)\ \underline{C}(t) \\ \underline{0} & \underline{0} & \underline{G}(t) \end{bmatrix} \quad ; \quad \tilde{\underline{E}} = \begin{bmatrix} \underline{E} & \underline{0} \\ \underline{0} & \underline{P}(t) \\ \underline{E} & -\underline{P}(t) \end{bmatrix} \tag{B.7}$$

We now consider the response of (B.6) to a <u>specific</u> initial condition $\underline{x}(t_o)$ drawn from the original distribution.

$$\underline{x}(t_o) = \underline{m}_o + \underline{e}_o \tag{B.8}$$

Thus,

$$\tilde{\underline{x}}(t_o) = \begin{bmatrix} \underline{m}_o + \underline{e}_o \\ \underline{m}_o \\ \underline{e}_o \end{bmatrix} \tag{B.9}$$

Then

$$\tilde{\underline{x}}(t) = \underline{\Psi}\ (t\ ,\ t_o)\ \tilde{\underline{x}}(t_o) + \int_{t_o}^{t} \underline{\Psi}(t,\tau)\ \tilde{\underline{E}}\ (\tau)\ \tilde{\underline{w}}(\tau)\ d\tau \tag{B.10}$$

where

$$\frac{d\,\underline{\Psi}}{dt}(t,t_o) = \tilde{\underline{A}}(t)\ \underline{\Psi}\ (t,t_o) \quad ; \quad \underline{\Psi}(t_o,t_o) = \underline{I} \tag{B.11}$$

Writing $\underline{\Psi}$ in partitioned form corresponding to $\tilde{\underline{A}}$,

$$\underline{\Psi} = \begin{bmatrix} \underline{\Psi}_{11} & \underline{\Psi}_{12} & \underline{\Psi}_{13} \\ \underline{\Psi}_{21} & \underline{\Psi}_{22} & \underline{\Psi}_{23} \\ \underline{\Psi}_{31} & \underline{\Psi}_{32} & \underline{\Psi}_{33} \end{bmatrix}$$

it is relatively straightforward to compute the sub-matrices $\underline{\Psi}_{ij}$, in terms of $\underline{\Psi}_{33}$ owing to the triangular form of $\tilde{\underline{A}}$. The results are presented in Table B1.

We are actually interested in the ensemble of responses, to this specific initial condition, that are generated by samples of the random processes $\underline{w}(.)$ and $\underline{v}(.)$. These are completely characterized, because of our assumptions, by the first- and second-order moments, i.e., the mean and variance.

The mean-response of (B.6) given (B.9) is readily calculated from (B.10)

$$\bar{\underline{\tilde{x}}}(t) = \underline{\Psi}(t,t_o)\ \bar{\underline{\tilde{x}}}(t_o) + \int_{t_o}^{t} \underline{\Psi}(t,\tau)\ \tilde{\underline{E}}(\tau)\ \bar{\underline{\tilde{w}}}(\tau)\,d\tau$$

If $\bar{\underline{\tilde{w}}}(.) \equiv 0$, as we will assume,

$$\bar{\underline{\tilde{x}}}(t) = \underline{\Psi}(t,t_o)\ \bar{\underline{\tilde{x}}}(t_o) \tag{B.12}$$

We note that starting from a specific initial condition $\underline{\tilde{x}}(t_o) = \bar{\underline{\tilde{x}}}(t_o)$. We have included the expectation on initial conditions for

TABLE B1

$\underline{\Psi}_{33}(t,\tau)$: Solution of $\frac{d\underline{\Psi}_{33}}{dt}(t,\tau) = \underline{G}(t)\ \Psi_{33}(t,\tau)$; $\underline{\Psi}_{33}(\tau,\tau) = \underline{I}$

$$\underline{\Psi}_{32}(t,\tau) = \underline{O}$$

$$\underline{\Psi}_{31}(t,\tau) = \underline{O}$$

$$\underline{\Psi}_{23}(t,\tau) = \int_{\tau}^{t} e^{\underline{F}(t-s)}\ \underline{P}(s)\ \underline{C}(s)\ \underline{\Psi}_{33}\ (s,\tau)ds$$

$$\underline{\Psi}_{22}(t,\tau) = e^{\underline{F}(t-\tau)}$$

$$\underline{\Psi}_{21}(t,\tau) = \underline{O}$$

$$\underline{\Psi}_{11}(t,\tau) = e^{\underline{A}(t-\tau)}$$

$$\underline{\Psi}_{12}(t,\tau) = -\int_{\tau}^{t} e^{\underline{A}(t-s)}\ \underline{BL}^{*}\ e^{\underline{F}(s-\tau)}ds$$

$$\underline{\Psi}_{13}(t,\tau) = -\int_{\tau}^{t} ds\ e^{\underline{A}(t-s)}\ \underline{BL}^{*}\ \left[\int_{\tau}^{s} e^{\underline{F}(s-\sigma)}\ \underline{P}(\sigma)\ \underline{C}(\sigma)\ \underline{\Psi}_{33}(\sigma,\tau)d\sigma\right]$$

generality. In cases where there may be step changes in disturbances, t_o could correspond to a time after the initial time and $\tilde{\underline{x}}(t_o)$ would be a random variable. A similar consideration will be necessary in computing the variances.

In order to compute the covariance of $\tilde{\underline{x}}(.)$, we define

$$\underline{\lambda} = \begin{bmatrix} \underline{\xi} \\ \underline{\eta} \\ \underline{\gamma} \end{bmatrix} = \tilde{\underline{x}} - \bar{\tilde{\underline{x}}} = \begin{bmatrix} \underline{x} - \bar{\underline{x}} \\ \hat{\underline{x}} - \bar{\hat{\underline{x}}} \\ \underline{e} - \bar{\underline{e}} \end{bmatrix} \tag{B.13}$$

It is easily seen that

$$\dot{\underline{\lambda}} = \tilde{\underline{A}}(t)\ \underline{\lambda} + \tilde{\underline{E}}(t)\ \tilde{\underline{w}}$$

and, moreover, that $E\{\underline{\lambda}\ \underline{\lambda}^T\} = \text{cov}\{\tilde{\underline{x}}\} \triangleq \underline{\Lambda}$, satisfies

$$\frac{d\underline{\Lambda}}{dt} = \tilde{\underline{A}}(t)\ \underline{\Lambda} + \underline{\Lambda}\ \tilde{\underline{A}}'(t) + \tilde{\underline{E}}(t)\ \underline{\Omega}(t)\ \tilde{\underline{E}}'(t) \quad ;\ \underline{\Lambda}(t_o) = \underline{\Lambda}_o \tag{B.14}$$

where

$$\underline{\Omega}(t) = \begin{bmatrix} \underline{W}(t) & \underline{O} \\ \underline{O} & \underline{V}(t) \end{bmatrix} \tag{B.15}$$

The solution to (B.14) may be written directly as

$$\underline{\Lambda}(t) = \underline{\Psi}(t,t_o)\ \underline{\Lambda}(t_o)\ \underline{\Psi}'(t,t_o) + \int_{t_o}^{t} \underline{\Psi}(t,\tau)\ \tilde{\underline{E}}(\tau)\ \underline{\Omega}(\tau)\ \tilde{\underline{E}}'(\tau) \cdot \underline{\Psi}'(t,\tau)\,d\tau \tag{B.16}$$

In practice, because of the triangular form of $\tilde{\underline{A}}$, it is not necessary to obtain all sub-matrices of $\underline{\Lambda}(t)$ to determine cov $\{\underline{x}\}$, cov $\{\hat{\underline{x}}\}$, and cov $\{\underline{e}\}$; indeed, the only additional computation

involves determining cov $\{\hat{\underline{x}}, \underline{e}^T\}$ and its transpose. Thus, (B.14) yields

$$\frac{d}{dt} \text{cov } \{\underline{e}\} = \frac{d\underline{\Lambda}_{33}}{dt} = \underline{G}(t)\ \underline{\Lambda}_{33} + \underline{\Lambda}_{33}\ \underline{G}'(t) + \underline{E}\ \underline{W}(t)\ \underline{E}' + \underline{P}(t)\ \underline{V}(t)\ \underline{P}'(t) \tag{B.17}$$

$$\frac{d}{dt} \text{cov } \{\hat{\underline{x}},\underline{e}\} = \frac{d\underline{\Lambda}_{23}}{dt} = \underline{F}\ \underline{\Lambda}_{23} + \underline{\Lambda}_{23}\ \underline{G}'(t) + \underline{P}(t)\ \underline{C}(t)\ \underline{\Lambda}_{33}(t) - \underline{P}(t)\ \underline{V}(t)\ \underline{P}'(t) \tag{B.18a}$$

$$\underline{\Lambda}_{32} = \text{cov } \{\underline{e}, \hat{\underline{x}}\} = \underline{\Lambda}'_{23} \tag{B.18b}$$

$$\frac{d}{dt} \text{cov } \{\hat{\underline{x}}\} = \frac{d\underline{\Lambda}_{22}}{dt} = \underline{F}\ \underline{\Lambda}_{22} + \underline{\Lambda}_{22}\ \underline{F}' + \underline{P}(t)\ \underline{C}(t)\ \underline{\Lambda}_{32}(t) + [\underline{P}(t)\ \underline{C}(t)\ \underline{\Lambda}_{32}(t)]' + \underline{P}(t)\ \underline{V}(t)\ \underline{P}'(t) \tag{B.19}$$

$$\frac{d}{dt} \text{cov } \{\underline{x}\} = \frac{d\underline{\Lambda}_{11}}{dt} = \underline{A}\ \underline{\Lambda}_{11} + \underline{\Lambda}_{11}\ \underline{A}' - [\underline{B}\ \underline{L}^*\ \underline{\Lambda}_{22}(t)] - [\underline{B}\ \underline{L}^*\ \underline{\Lambda}_{22}(t)]' + \underline{E}\ \underline{W}(t)\ \underline{E}' \tag{B.20}$$

Comparing Eqns. (B.17)and (B.4), we find

$$\frac{d}{dt}(\underline{\Lambda}_{33} - \underline{\Sigma}) = \underline{G}(t)\ (\underline{\Lambda}_{33} - \underline{\Sigma}) + (\underline{\Lambda}_{33} - \underline{\Sigma})\ \underline{G}'(t)$$

thus

$$\underline{\Lambda}_{33}(t) = \text{cov } \{\underline{e}(t)\} = \underline{\Sigma}(t) + \underline{\Phi}(t,t_o)\ [\underline{\Lambda}_{33}(t_o) - \underline{\Sigma}(t_o)]\ \underline{\Phi}'(t,t_o) \tag{B.21}$$

where

$$\dot{\underline{\Phi}}(t,t_o) = \underline{G}(t)\ \underline{\Phi}\ (t,t_o)\ ;\ \underline{\Phi}\ (t_o,t_o) = \underline{I} \tag{B.22}$$

Eqns. (B.18) may be integrated directly to obtain

$$\underline{\Lambda}_{23}(t) = e^{\underline{F}(t-t_o)}\ \underline{\Lambda}_{23}(t_o)\ \underline{\Phi}'(t,t_o) + \int_{t_o}^{t} e^{\underline{F}(t-\tau)}\ \underline{P}(\tau)$$
$$[\underline{C}(\tau)\ \underline{\Lambda}_{33}(\tau) - \underline{V}(\tau)\ \underline{P}'\ (\tau)]\ \underline{\Phi}'(t,\tau)d\tau$$

or, using (B.2),

$$\Lambda_{23}(t) = e^{\underline{F}(t-t_o)}\ \underline{\Lambda}_{23}(t_o)\ \underline{\Phi}'(t,t_o) + \int_{t_o}^{t} e^{\underline{F}(t-\tau)}\ \underline{P}(\tau)\ \underline{C}(\tau)\cdot$$
$$[\underline{\Lambda}_{33}(\tau) - \underline{\Sigma}(\tau)]\ \underline{\Phi}'(t,\tau)d\tau \tag{B.23}$$

Substitution of (B.21) into (B.23), gives

$$\mathrm{cov}\{\hat{\underline{x}}(t),\underline{e}(t)\} = \underline{\Lambda}_{23}(t) = e^{\underline{F}(t-t_o)}\ \underline{\Lambda}_{23}(t_o)\ \underline{\Phi}'(t,t_o) + \underline{\Gamma}(t,t_o)$$
$$[\underline{\Lambda}_{33}(t_o) - \underline{\Sigma}(t_o)]\ \underline{\Phi}'(t,t_o) \tag{B.24}$$

where

$$\underline{\Gamma}(t,t_o) = \int_{t_o}^{t} e^{\underline{F}(t-\tau)}\ \underline{P}(\tau)\ \underline{C}(\tau)\ \underline{\Phi}(\tau,t_o)d\tau \tag{B.25}$$

In a similar fashion, we obtain+

+Alternative expressions are, of course, possible. For example one can solve for cov $\{\underline{x}\}$ = cov $\{\hat{\underline{x}}\}$ + cov $\{\underline{e}\}$ + cov $\{\hat{\underline{x}},\underline{e}\}$ + cov $\{\underline{e},\hat{\underline{x}}\}$, as was done in Ref. 6.

$$\text{cov}\{\hat{\underline{x}}(t)\} = \underline{\Lambda}_{22}(t) = e^{\underline{F}(t-t_o)}\ \underline{\Lambda}_{22}(t_o)\ e^{\underline{F}'(t-t_o)} + \int_{t_o}^{t} e^{\underline{F}(t-\tau)}\ [\underline{P}(\tau)\ \underline{C}(\tau)\ \underline{\Lambda}_{32}(\tau) + \underline{\Lambda}_{23}(\tau)\ \underline{C}'(\tau)\cdot \underline{P}'(\tau) + \underline{P}(\tau)\ \underline{V}(\tau)\ \underline{P}'(\tau)]\ e^{\underline{F}'(t-\tau)}\,d\tau \quad \text{(B.26)}$$

and

$$\text{cov}\{\underline{x}(t)\} = e^{\underline{A}(t-t_o)}\ \underline{\Lambda}_{11}(t_o)\ e^{\underline{A}'(t-t_o)} + \int_{t_o}^{t} e^{\underline{A}(t-\tau)}\ [\underline{E}\ \underline{W}(\tau)\ \underline{E}' - (\underline{B}\ \underline{L}^*\ \underline{\Lambda}_{22}(\tau)) - (\underline{B}\ \underline{L}^*\underline{\Lambda}_{22}(\tau))']\ e^{\underline{A}'(t-\tau)}\,d\tau \quad \text{(B.27)}$$

Eqns. (B.21) and (B.24) are especially revealing. We see from (B.21) that if

$$\underline{\Lambda}_{33}(t_o) = \underline{\Sigma}(t_o) = \underline{X}_o \quad \text{(B.28)}$$

then $\underline{\Sigma}(t)$ is the actual covariance. Also, referring to (B.24), if $\underline{\Lambda}_{23}(t_o) = 0$ and (B.28) holds then the estimate and the error are uncorrelated for all t. When $\underline{x}(t_o)$ is considered as a random variable the above conditions hold and the filter is optimal with respect to the given data.

For a sample path corresponding to a specific initial condition (or for the ensemble of paths corresponding to that condition), $\underline{\Lambda}_{33}(t_o) = 0$ because $\underline{e}(t_o)$ is fixed. Thus, (B.28) does not generally hold, the actual error covariance differs from $\underline{\Sigma}$ and the error and the estimate are correlated. The filter is optimal in the same sense as before, i.e., based on the prior knowledge of the random variable $\underline{x}(t_o)$. However, one could of course do better, if the initial condition were known exactly.

The above results are interesting from another standpoint. It is possible that $\underline{\Lambda}_{33}(t_o) \neq \underline{\Sigma}(t_o)$ even though we are not considering a specific initial condition. Such would be the case, e.g., if the pilot did not know the initial state covariance perfectly, as is most certainly the case. Equation (B.21) then reveals the sensitivity of the solution to this type of error.

APPENDIX C
Vehicle Dynamics

In this Appendix, we present longitudinal and lateral dynamics that were used in the analyses described in the report. The basic equations were linearized perturbation equations of standard form [21].

Longitudinal Dynamics

In vector-matrix notation, the longitudinal dynamics are

$$\left.\begin{aligned} \dot{\underline{x}} &= \underline{A}\,\underline{x} + \underline{B}\,\underline{\delta} + \underline{E}\,\underline{w} \\ \underline{y} &= \underline{C}\,\underline{x} + \underline{D}\,\underline{\delta} \end{aligned}\right\} \text{C-1}$$

The state, control and output vectors for longitudinal control were for the no-director case*

$$\left.\begin{aligned} \underline{x}^T &= (u_g,\ w_g,\ u,\ w,\ \theta,\ \alpha,\ h) \\ \underline{\delta}^T &= (\delta_e,\ \delta_N) \\ \underline{y}^T &= (h,\ \dot{h},\ \theta,\ \alpha,\ u) \end{aligned}\right\} \text{C-2}$$

where superscript T denotes transpose.

Two sets of longitudinal dynamics were investigated in this report because of a change in stability derivatives and trim-conditions that was made in the course of the effort. Initial values for the system matrices as provided by Ames personnel

*When a director is used that has dynamics (from filtering, e.g.) additional states are needed. The additions are not shown here.

were used for the analysis of the STOLAND DISPLAY (ALONE) and the "model-based" director. These dynamics are given by the computer printout labeled STL3 (pp4-5).The second set of dynamics were used to analyze the "interim" director (because the interim director was designed for these dynamics. These dynamics are given by the computer printout labeled STL9.

It is of interest to compare performance for the two sets of dynamics. This was done for the 1%-wind using nominal conditions (the STOLAND display; the resulting rms performance scores are shown in Table C1. The differences are clearly minor.

Table C1

COMPARISON OF PERFORMANCE SCORES FOR TWO SETS OF LONGITUDINAL DYNAMICS

Variable	STL3	STL9
h(m)	2.3	2.2
$\dot{h}$	.68	.65
θ	1.8	1.5
α	1.2	1.08
u	1.3	1.33
δ_e	2.1	1.85
δ_N	12.	12.

Lateral Dynamics

Simplified lateral dynamics illustrated in the block diagram of Figure 18, were used. The lateral states; controls, and outputs are

$$\underline{x}^T = (v_g,\ p,\ \phi,\ \psi,\ y)$$

$$\delta = \delta_w$$

$$\underline{y}^T = (y,\ \dot{y},\ \phi,\ \dot{\phi})^*$$

The values for A, B, C, E in the lateral case are given by LAT1 for the SAS-off case (p. 8) and LAT3 for the SAS-on dynamics (p. 9).

*The vector $\underline{y}$ is used to denote, generically, the display vector whereas the scalar y is the lateral error.

FILE NAME: STL3

TOTAL NO. OF NOISE STATES= 2

A MATRIX:

-1.500E-01	0.000E-01	0.000E-01	0.000E-01	0.000E-01
0.000E-01	0.000E-01			
0.000E-01	-1.000E+00	0.000E-01	0.000E-01	0.000E-01
0.000E-01	0.000E-01			
-3.600E-02	1.600E-01	-3.600E-02	1.600E-01	-1.700E-01
0.000E-01	0.000E-01			
-2.870E-01	-4.860E-01	-2.870E-01	-4.860E-01	1.030E-02
5.320E-01	0.000E-01			
0.000E-01	0.000E-01	0.000E-01	0.000E-01	0.000E-01
1.000E+00	0.000E-01			
4.360E-01	-2.230E-01	4.360E-01	-2.230E-01	-7.580E-03
-1.280E+00	0.000E-01			
0.000E-01	0.000E-01	-6.120E-02	-1.000E+00	5.340E-01
0.000E-01	0.000E-01			

B MATRIX:

0.000E-01	0.000E-01
0.000E-01	0.000E-01
0.000E-01	-2.860E-02
-2.390E-02	6.670E-04
0.000E-01	0.000E-01
-1.120E+00	-9.170E-02
0.000E-01	0.000E-01

E MATRIX:

5.500E-01	0.000E-01
0.000E-01	1.414E+00
0.000E-01	0.000E-01
0.000E-01	0.000E-01
0.000E-01	0.000E-01
0.000E-01	0.000E-01
0.000E-01	0.000E-01

C MATRIX:

0.000E-01	0.000E-01	0.000E-01	0.000E-01	0.000E-01
0.000E-01	1.000E+00			
0.000E-01	0.000E-01	-6.100E-02	-1.000E+00	5.330E-01
0.000E-01	0.000E-01			
0.000E-01	0.000E-01	0.000E-01	0.000E-01	1.000E+00
0.000E-01	0.000E-01			
0.000E-01	0.000E-01	0.000E-01	0.000E-01	0.000E-01
1.000E+00	0.000E-01			
1.000E+00	0.000E-01	1.000E+00	0.000E-01	0.000E-01
0.000E-01	0.000E-01			

D MATRIX:

0.000E-01	0.000E-01
0.000E-01	0.000E-01
0.000E-01	0.000E-01
0.000E-01	0.000E-01
0.000E-01	0.000E-01

FILE NAME: STL9

TOTAL NO. OF NOISE STATES= 2

A MATRIX:

-1.500E-01	0.000E-01	0.000E-01	0.000E-01	0.000E-01
0.000E-01	0.000E-01			
0.000E-01	-1.000E+00	0.000E-01	0.000E-01	0.000E-01
0.000E-01	0.000E-01			
-5.200E-02	1.230E-01	-5.200E-02	1.230E-01	-1.700E-01
0.000E-01	0.000E-01			
-2.760E-01	-5.220E-01	-2.760E-01	-5.220E-01	1.740E-02
5.300E-01	0.000E-01			
0.000E-01	0.000E-01	0.000E-01	0.000E-01	0.000E-01
1.000E+00	0.000E-01			
5.020E-01	-2.040E-01	5.020E-01	-2.040E-01	-1.200E-02
-1.350E+00	0.000E-01			
0.000E-01	0.000E-01	2.270E-02	-1.000E+00	5.370E-01
0.000E-01	0.000E-01			

B MATRIX:

0.000E-01	0.000E-01
0.000E-01	0.000E-01
0.000E-01	-2.880E-02
-2.400E-02	2.220E-03
0.000E-01	0.000E-01
-1.280E+00	-5.630E-02
0.000E-01	0.000E-01

E MATRIX:

5.500E-01	0.000E-01
0.000E-01	1.414E+00
0.000E-01	0.000E-01
0.000E-01	0.000E-01
0.000E-01	0.000E-01
0.000E-01	0.000E-01
0.000E-01	0.000E-01

C MATRIX:

0.000E-01	0.000E-01	0.000E-01	0.000E-01	0.000E-01
0.000E-01	1.000E+00			
0.000E-01	0.000E-01	2.270E-02	-1.000E+00	5.370E-01
0.000E-01	0.000E-01			
0.000E-01	0.000E-01	0.000E-01	0.000E-01	1.000E+00
0.000E-01	0.000E-01			
0.000E-01	0.000E-01	0.000E-01	0.000E-01	0.000E-01
1.000E+00	0.000E-01			
1.000E+00	0.000E-01	1.000E+00	0.000E-01	0.000E-01
0.000E-01	0.000E-01			

D MATRIX:

0.000E-01	0.000E-01
0.000E-01	0.000E-01
0.000E-01	0.000E-01
0.000E-01	0.000E-01
0.000E-01	0.000E-01

FILE NAME: LAT1

TOTAL NO. OF NOISE STATES= 1

A MATRIX:

-1.500E-01	0.000E-01	0.000E-01	0.000E-01	0.000E-01
8.540E-02	-5.964E-01	2.500E-01	0.000E-01	0.000E-01
0.000E-01	1.000E+00	0.000E-01	0.000E-01	0.000E-01
0.000E-01	0.000E-01	3.160E-01	0.000E-01	0.000E-01
0.000E-01	0.000E-01	0.000E-01	5.410E-01	0.000E-01

B MATRIX:

0.000E-01
6.115E-01
0.000E-01
0.000E-01
0.000E-01

E MATRIX:

5.500E-01
0.000E-01
0.000E-01
0.000E-01
0.000E-01

C MATRIX:

0.000E-01	0.000E-01	0.000E-01	0.000E-01	1.000E+00
0.000E-01	0.000E-01	0.000E-01	5.410E-01	0.000E-01
0.000E-01	0.000E-01	1.000E+00	0.000E-01	0.000E-01
0.000E-01	1.000E+00	0.000E-01	0.000E-01	0.000E-01

D MATRIX:

0.000E-01
0.000E-01
0.000E-01
0.000E-01

)

FILE NAME: LAT3

TOTAL NO. OF NOISE STATES= 1

A MATRIX:

-1.500E-01	0.000E-01	0.000E-01	0.000E-01	0.000E-01
0.000E-01	-1.620E+00	0.000E-01	0.000E-01	0.000E-01
0.000E-01	1.000E+00	-9.600E-02	0.000E-01	0.000E-01
0.000E-01	0.000E-01	3.210E-01	0.000E-01	0.000E-01
1.000E+00	0.000E-01	0.000E-01	5.320E-01	0.000E-01

B MATRIX:

0.000E-01
6.230E-01
0.000E-01
0.000E-01
0.000E-01

E MATRIX:

5.500E-01
0.000E-01
0.000E-01
0.000E-01
0.000E-01

C MATRIX:

0.000E-01	0.000E-01	0.000E-01	0.000E-01	1.000E+00
1.000E+00	0.000E-01	0.000E-01	5.320E-01	0.000E-01
0.000E-01	0.000E-01	1.000E+00	0.000E-01	0.000E-01
0.000E-01	1.000E+00	-9.600E-02	0.000E-01	0.000E-01

D MATRIX:

0.000E-01
0.000E-01
0.000E-01
0.000E-01